CONTRACT NAS10-1108

Martin CR-64-6

DETERMINATION OF ROCKET ENGINE NOISE DAMAGE TO COMMUNITY DWELLINGS NEAR LAUNCH SITES (FINAL REPORT)

DECEMBER 1964

prepared by

MARTIN COMPANY
DENVER DIVISION
DENVER, COLORADO

prepared for

NATIONAL AERONAUTICS AND SPACE ADMINISTRATION
J. F. KENNEDY SPACE CENTER, FLORIDA

Martin CR-64-65 (Vol I) Copy No. 35

Contract NAS10-1108

DETERMINATION OF ROCKET ENGINE NOISE DAMAGE TO COMMUNITY DWELLINGS NEAR LAUNCH SITES

(Final Report)

December 1964

Prepared by

R. W. Peverly

Approved

L. F. Nichalson, Manager
Advanced Ground Systems Department

MARTIN COMPANY
Denver, Colorado
Aerospace Division of Martin-Marietta Corporation

FOREWORD

This report is submitted in accordance with Contract NAS10-1108, Determination of Rocket Engine Noise Damage to Community Dwellings Near Launch Sites. This report is presented in two volumes. Volume I contains a concise discussion of the study, including the test and analytical work. Volume II, appendix material, is a more detailed presentation of data.

Customer Changes requested by P. V. King's letter, dated November 25, 1964 (Martin Ref 4-W-25595), have been incorporated in this final report.

The following Martin Company personnel assisted in the analysis, testing, and were responsible for the preparation of the final report:

R. W. Peverley	Project Manager
John R. Baratono	Acoustic Testing
William Lees Brown	Community Survey and Graphs
Dr. S. P. Chan	Dynamic Analysis
Charles L. Pullen	Focusing Analysis
E. B. Smith	Acoustic Prediction
N. I. Stephenson	Film Script

Acknoweledgment is made of the following Martin Company personnel who assisted in the testing.

Raymond Pitsker	Field Testing
H. N. McGregor	Laboratory Testing
William Moore	Martin-Canaveral Facilities

Without the support of the following NASA personnel, this study would not have been possible:

Paul V. King	S. Perlman
A. H. Moore	Col. P. Siebeneichen
Dr. P. Ricca	J. P. Nelson
Dr. R. H. Burns	L. F. Keene

CONTENTS

Figure

SUMMARY

A sound pressure level criterion of 120 db has been established for rocket engine noise intrusion into communities near the John F. Kennedy Space Center. This criterion is partially based on suspected damage thresholds of buildings such as homes, stores, etc. Normally, the noise produced during the launch of a Saturn V or Post-Saturn booster would not exceed the established sound pressure level. During adverse weather conditions, however, acoustic energy may be focused into community areas producing a noise environment in excess of 120 db. Unfortunately, there were not sufficient data on acoustically-induced structural damage to community dwellings to define how far the criteria could be exceeded. This study was conducted for the Director of Safety, National Aeronautics and Space Administration, John F. Kennedy Space Center to evaluate the rocket engine damage thresholds near the John F. Kennedy Space Center.

The study was conducted in four phases. Phase I was a study phase which consisted of a literature survey, prediction of noise environments, and community survey. During the second phase, a sinusoidal siren and its associated equipment was transported to the John F. Kennedy Space Center and acoustic tests were conducted on abandoned dwellings on the Merritt Island Annex. Tests were also conducted on a NASA test wall which is instrumented during Saturn I flights. Laboratory tests using a random siren and sinusoidal siren were conducted on a replica of the NASA wall during the third phase. During the fourth phase the data were analyzed and reported. A 12-minute movie was also produced.

The results of this study showed that window damage in the Titusville area produced as a result of a post Saturn booster flight would be negligible except during extreme focusing conditions. Even then, the amount of breakage would be small. Damage to plaster, however, could occur during minor focusing but is unlikely during standard atmospheric conditions. The plaster damage should be minor, such as small cracks, etc. The only feasable control is to launch during atmospheric conditions which are not conducive to intense focusing.

I. INTRODUCTION

A. STATEMENT OF THE PROBLEM

The intrusion of rocket engine noise into community areas was one of the safety hazards considered in the planning of the Post-Saturn launch sites at the John F. Kennedy Space Center. A sound pressure level of 120 db (re 0.0002 dynes/cm^2) was established as the maximum allowable noise intrusion level. The subsequent location of these launch sites provided sufficient separation distance to conform to the noise criterion during standard atmospheric conditions. It was found, however, that some nonstandard atmospheric conditions could produce focusing of this acoustic energy back to the earth, resulting in sound pressure levels in excess of the 120-db level. Thus, it became important to determine how far this criterion could be safely exceeded.

Rocket engine noise intrusion into community areas has not been considered a problem at the Kennedy Missile Test Center in the past. The comparatively low acoustic yield of the booster engines in the 10^5-lb-thrust class and the remote distances from the communities to the launch sites precluded the occurrence of a community problem. The higher acoustic power generated by the Post-Saturn booster engines and the shorter distances from the Post-Saturn launch sites to communities obviously created a more intense noise environment. There is still another factor that could compound this problem. The acoustic spectrum of the large diameter Post-Saturn booster engine peaks at very low frequencies. Thus, less atmospheric attenuation could be expected and an intense amount of energy would be present at the resonant frequency of community dwellings.

The 120-db-noise criterion was established as a safe level based on experience with jet engines and lower thrust booster engines. The criterion, however, has several shortcomings. Any evaluation of noise must consider time of exposure and frequency content of the noise source. These parameters are extremely important in examining the Post-Saturn noise problem. Potential hazards to the community exist in physiological damage to the occupants of a community, damage to public relations, and damage to community dwellings. For example, jet aircraft noise and sonic boom have recently received considerable publicity. Jet aircraft noise is lower in amplitude than rocket noise but

the occurrence rate is higher by significant orders of magnitude. Sonic boom is of a different frequency content, shorter time exposure, higher amplitude, and higher occurrence rate. Another example is the noise resulting from the Saturn engine static firings at the Marshall Space Flight Center (MSFC) being focused into the city of Huntsville, Alabama. This noise problem was more acute than the one of the Kennedy Space Center because of the longer time exposure and lack of visible association that occurs during a flight. The problem at MSFC could be solved, however, by expedient scheduling and ground suppressors. These solutions obviously could not be applied at the Kennedy Space Center. The low frequency content of the Post-Saturn noise field should preclude hearing damage. The possibility of physiological damage is somewhat controversial. The limited data that are available on the physiological response of human beings to low frequency noise does not appear conclusive. Because of the range of sound pressure levels considered (below 135 db), the low occurrence rate and the short time exposure, it seems reasonable, however, to assume that the possibility of physiological damage is somewhat remote. Structural damage resulting from acoustic loading, however, may not necessarily be time dependent. If the acoustic force produces deflections, which in turn produce stress levels above the yield stress, failure can be instantaneous. Such failures have been produced in missile and space booster skin tests. Because the rocket engine noise community problem has not been serious in the past, insufficient data are available on the fragility of walls and glass under acoustic loading to accurately predict damage thresholds. Thus, the need for a test program to acquire such data is apparent.

To acquire such data, the test conditions require reasonable duplication of the intense low frequency noise that would be characteristic of the Post-Saturn engines. In addition, duplication of the edge conditions of windows is also important. Such duplication can not be guaranteed under laboratory conditions with new windows because of dried putty, stress due to foundation settling, etc. To satisfy these conditions, acoustic tests were made on abandoned houses on the Merritt Island Launch Area (MILA) using a sinusoidal siren. Once the effect of boundary conditions were determined, tests were conducted on new windows under laboratory conditions where the acoustic spectrum could be more accurately duplicated.

B. OBJECTIVES

The overall objective of the study was to determine rocket engine noise damage thresholds of community buildings near the John F. Kennedy Space Center. This objective was satisfied in six steps.

Literature Survey - Existing literature, including research papers, journals, industrial reports, etc, were studied. The pertinent information was cataloged for use during the study.

Community Survey - A cross section of the structures in the community of Titusville, Florida, and the surrounding area was surveyed to determine the type, number, and susceptibility category. The survey was made on the site and from data obtained from such sources as the NASA Community Relations Office, building inspectors, aerial observations, etc.

Noise Level Survey - The noise levels in the areas surrounding MILA were predicted. Weather effects were considered. State-of-the-art knowledge was applied.

Field Tests - Tests were conducted in the field on abandoned houses on the Merritt Island Launch Area and on the NASA test wall. Sinusoidal acoustic energy was used and the effect of field boundary conditions on window and wall response determined.

Laboratory Tests - Tests were conducted at the Martin-Denver Acoustic Laboratory to simulate rocket engine acoustic loading. A replica of the NASA test wall was used.

Data Analysis - Test data were analyzed and plate vibration theory used to determine damage thresholds.

C. SCOPE

The study was conducted in four phases:

Phase I - literature survey, community survey, and noise level survey; Phase II - field test and data analysis; Phase III - laboratory test and data analysis; and Phase IV - threshold predictions, report, and film.

The study was limited to those types of structures typical of the Titusville area. The data should also be applicable, however, to structures in other areas. Data were analyzed by conventional methods and no new theory was used or resulted.

II. TEST PROGRAM

A. FIELD TESTS

1. Test Equipment

A field test unit was assembled and checked out at the Martin-Denver Acoustic Test Facility. The unit was designed to be self-contained, portable, and capable of operation in the sandy soil off existing Florida roads. The equipment consisted of a sinusoidal siren, pneumatic control system for the air source, electrical control system for speed control, diesel driven power supply, and associated instrumentation. Portable air compressors and the diesel power supply were obtained by the Martin Company at the test area. The field test unit itself was shipped to Florida from Denver. The composite test unit is shown in Fig. II-1.

2. Test Specimen Description

Tests were performed on 17 test windows and test walls, with approximately 2700 accelerometer, acoustic, and strain data points acquired. A description of the test specimens is given in Table II-1.

3. Florida Layout

A typical test equipment layout is shown in Fig. II-2 and II-3. Figure II-2 shows the acoustic test fixture adjacent to a test specimen. The air compressors are to the right of the test fixture, and are shown in Fig. II-3. The panel truck in the left foreground of Fig. II-3 houses the instrumentation and acoustic siren controls. The panel truck was parked approximately 200 ft from the acoustic siren for each test, due to the high acoustic levels generated.

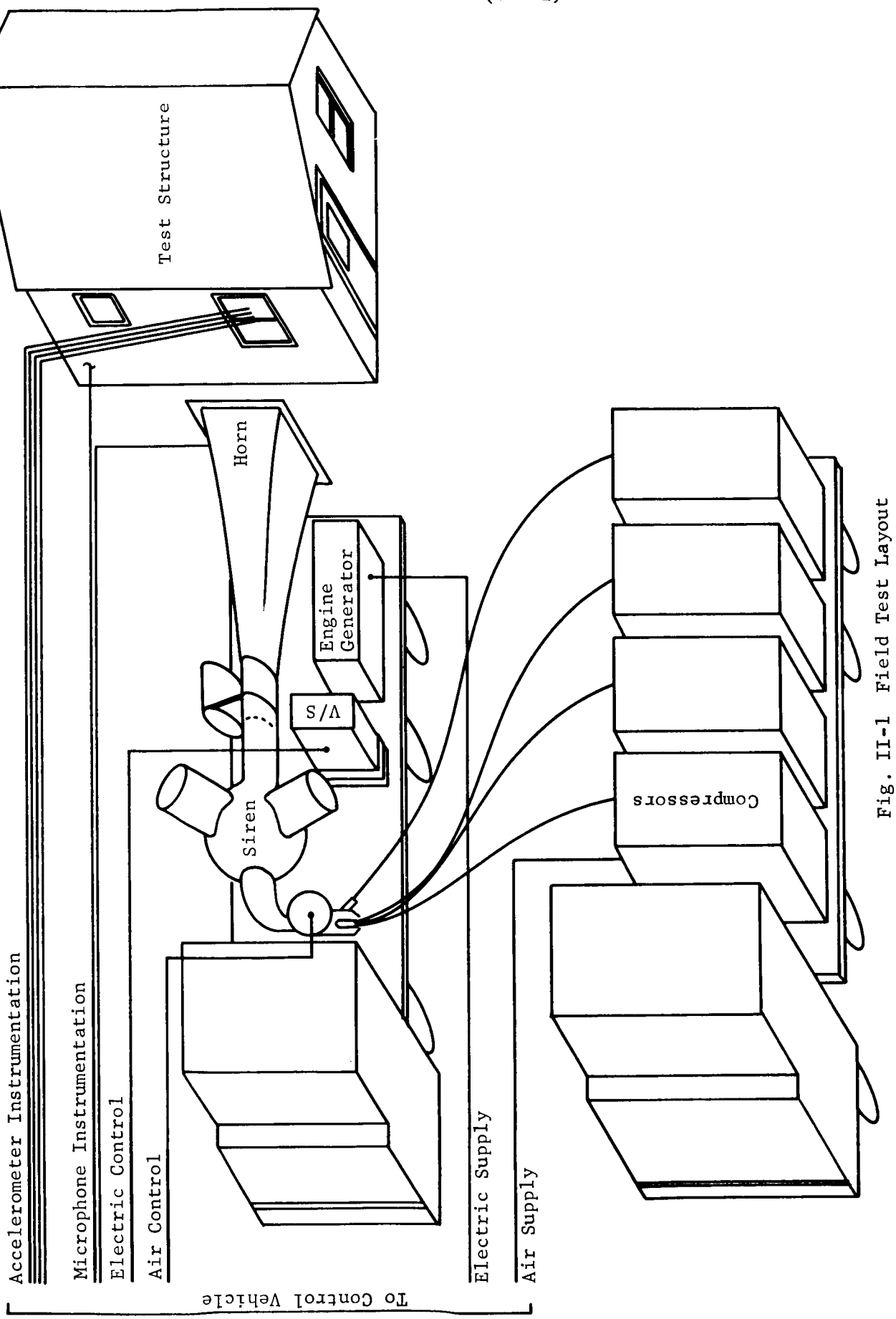

Fig. II-1 Field Test Layout

Table II-1 Description of Test Specimens

Item	Location	Use	Wall Construction	Glass Size (in.)	Window Type
1	K8-989	Residence	Block w/Stucco	4 x 34	Jalousies
2	NASA Test Wall	Complex 37	Frame	24 x 24	Double Hung
3	NASA Test Wall	Complex 37	Frame	14 x 33	Awning
4	NASA Test Wall	Complex 37	Frame	30 x 13	Double Hung
5	K8-988	Shopping Center	Block	89 x 61	Fixed (Plate)
6	K8-988	Shopping Center	Block	89 x 86	Fixed (Plate)
7	K8-991	Store	Block	37 x 56	Fixed
8	K8-991	Store	Block	12 x 16	Casement
9	K8-985	Residence	Block	11 x 34	Awning
10	1 mi N of Dummit Grove, W Side AIA	Residence	Frame and block	12¼ x 16¼	Casement
11	1 mi N of Dummit Grove, W Side AIA	Residence	Frame and block		Wood Wall
12	1/4 mi S Old Canal, W Side AIA	Residence	Frame	32 x 22	Fixed
13	1/4 mi S Old Canal, W Side AIA	Residence	Frame		Wood Wall
14	1-1/8 mi N of Dummit Grove, W Side AIA	Residence	Frame	14 x 33	Casement
15	1 mi W of Wilson, N Side 402	Store	Block w/Stucco	83 x 51½	Fixed (plate)
16	K8-990	Residence	Block w/Stucco	4 x 34	Jalousies
17	NASA Test Wall	Complex 37	Block	48 x 60	Fixed
18	Martin Test Wall	Test	Wood w/Stucco	23-5/8 x 13-5/8	Wood Double Hung (4 Panes)
19	Martin Test Wall	Test	Wood w/Stucco	33 x 14-3/8	Awning
20	Martin Test Wall	Test	Wood w/Stucco	21-3/4 x 19-3/4	Wood Double Hung (2 Panes)

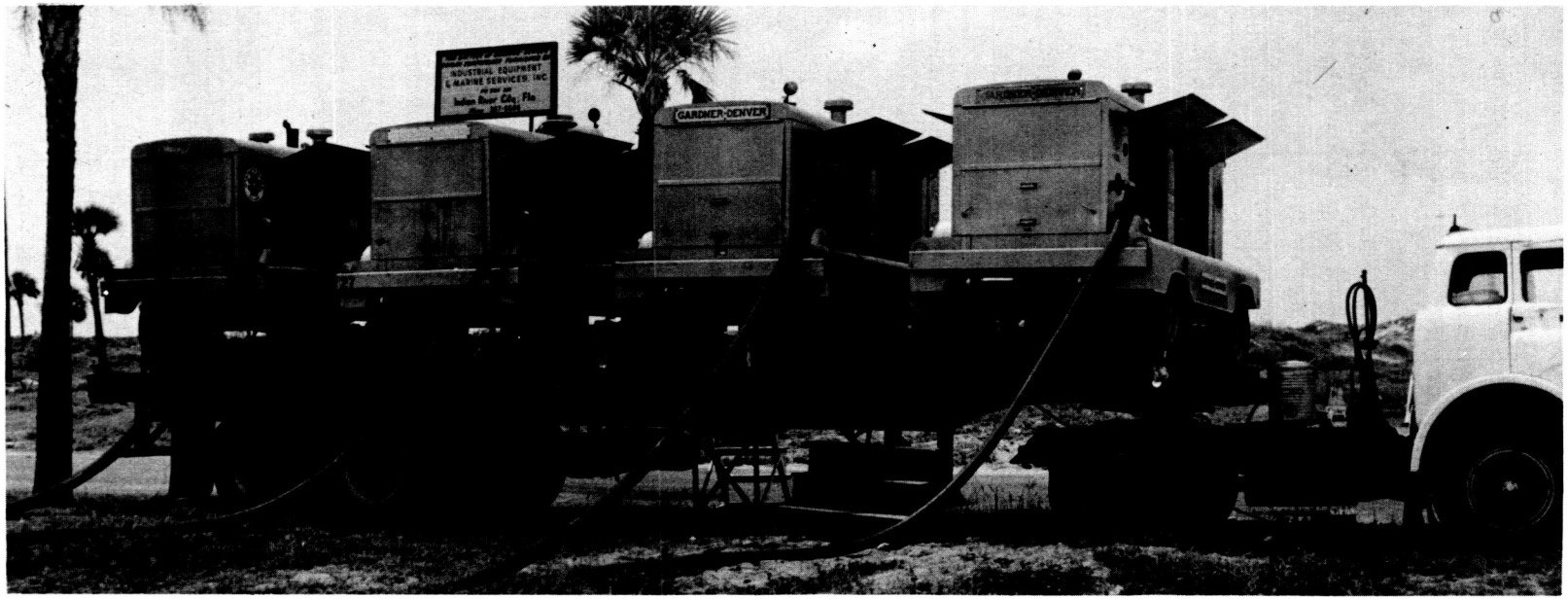

Fig. II-2 Acoustic Test Fixture

Fig. II-3 Test Equipment Arrangement

4. Instrumentation

At least one microphone was used during each test run. Acoustic levels were measured at discrete frequencies, at each test window and/or wall. The microphone was capable of measuring acoustic levels from 20 cps to 10,000 cps. Three or four accelerometers were attached to each test specimen for each test run. The accelerometers used were Clevite, type 2E-5, and did not contribute significantly to the mass of each test specimen. A maximum of two strain gages were also attached to some of the test windows. A Bruel and Kjaer (B&K) narrow band analyzer was used to monitor the sound pressure level existing at each test specimen, for each test run. The analyzer was capable of monitoring both overall and discrete frequency acoustic levels.

Two methods of obtaining data at the test site were used. A B&K microphone amplifier unit was used to obtain a tabulation of the accelerometer data. A switching unit made it possible to quickly obtain all accelerometer readings during each test run. In addition to the tabulated data obtained indirectly from the B&K narrow band analyzer and microphone amplifier, a Minneapolis-Honeywell Visicorder was also used to obtain a permanent record of the data. Figure II-4 shows the instrumentation in the truck van.

5. Typical Test Run Description

The acoustic test fixture was backed up to the test window. A typical setup is shown in Fig. II-5. Figure II-6 shows the actual mounting of four accelerometers on the test window. The microphone used to monitor the window acoustic environment was attached to the bungee cord, as shown in the figure. In addition, two strain gages were attached to the center of the glass as shown. Figure II-7 is a sketch showing typical accelerometer locations for a jalousie-type window. After the instrumentation was installed and calibrated, three runs were made to cover the frequency range of interest (approximately 20 cps to 550 cps). Belts controlling siren speed (and thus frequency) were changed twice for each window. During each run, data were taken at each frequency at a constant acoustic level, whenever possible. Accelerometer, acoustic, and strain data were normally obtained during each run.

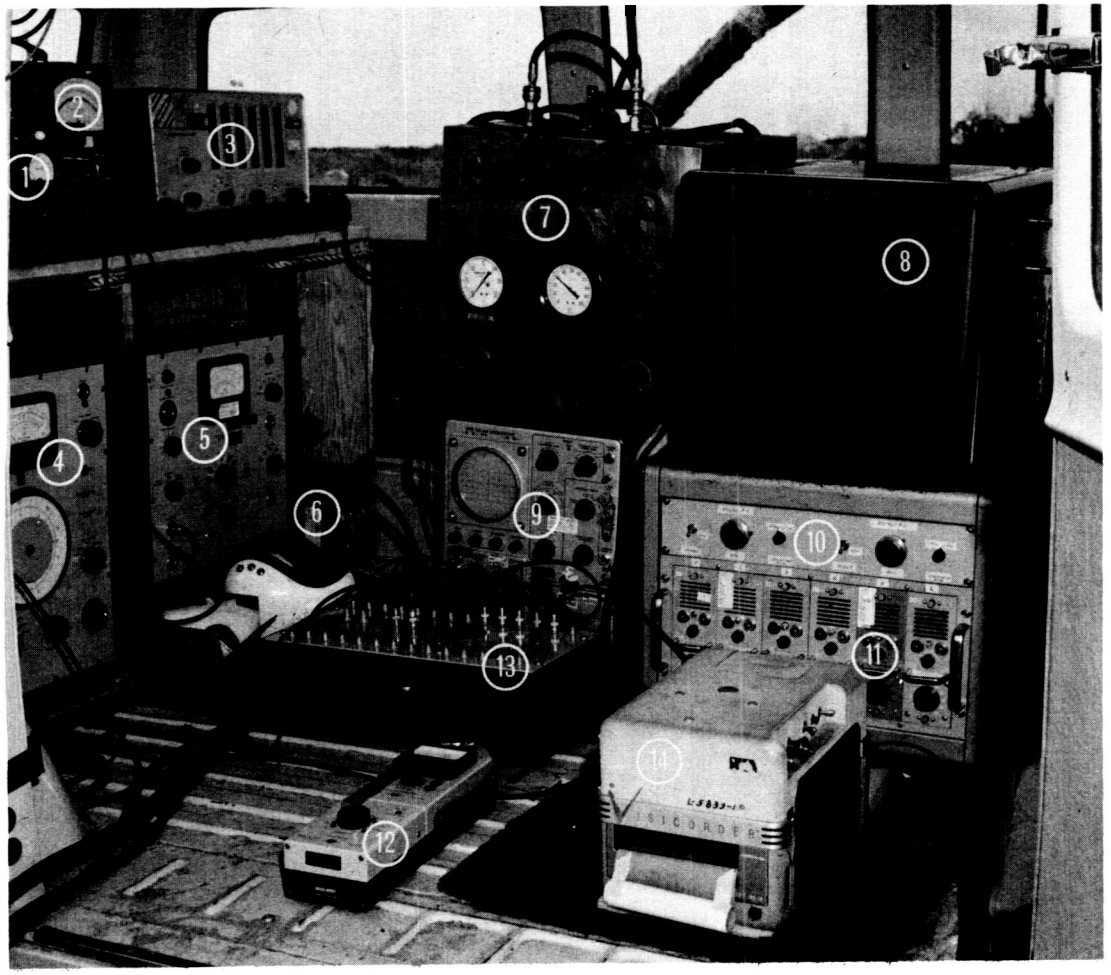

Legend:

1. Signal Generator
2. VTVM
3. EPUT
4. B&K Narrow Band Analyzer
5. B&K Microphone Amplifier (True rms)
6. Microphone Power Supplies
7. Siren Control Console
8. Accelerometer Power Supplies and Blower
9. Tektronix Oscilloscope
10. Strain Gage Power Supply and Calibrator
11. Kintel Amplifier (Signal Conditioning)
12. B&K Sound Level Meter
13. Switching Box
14. Visicorder

Fig. II-4 Instrumentation Mounted in Truck

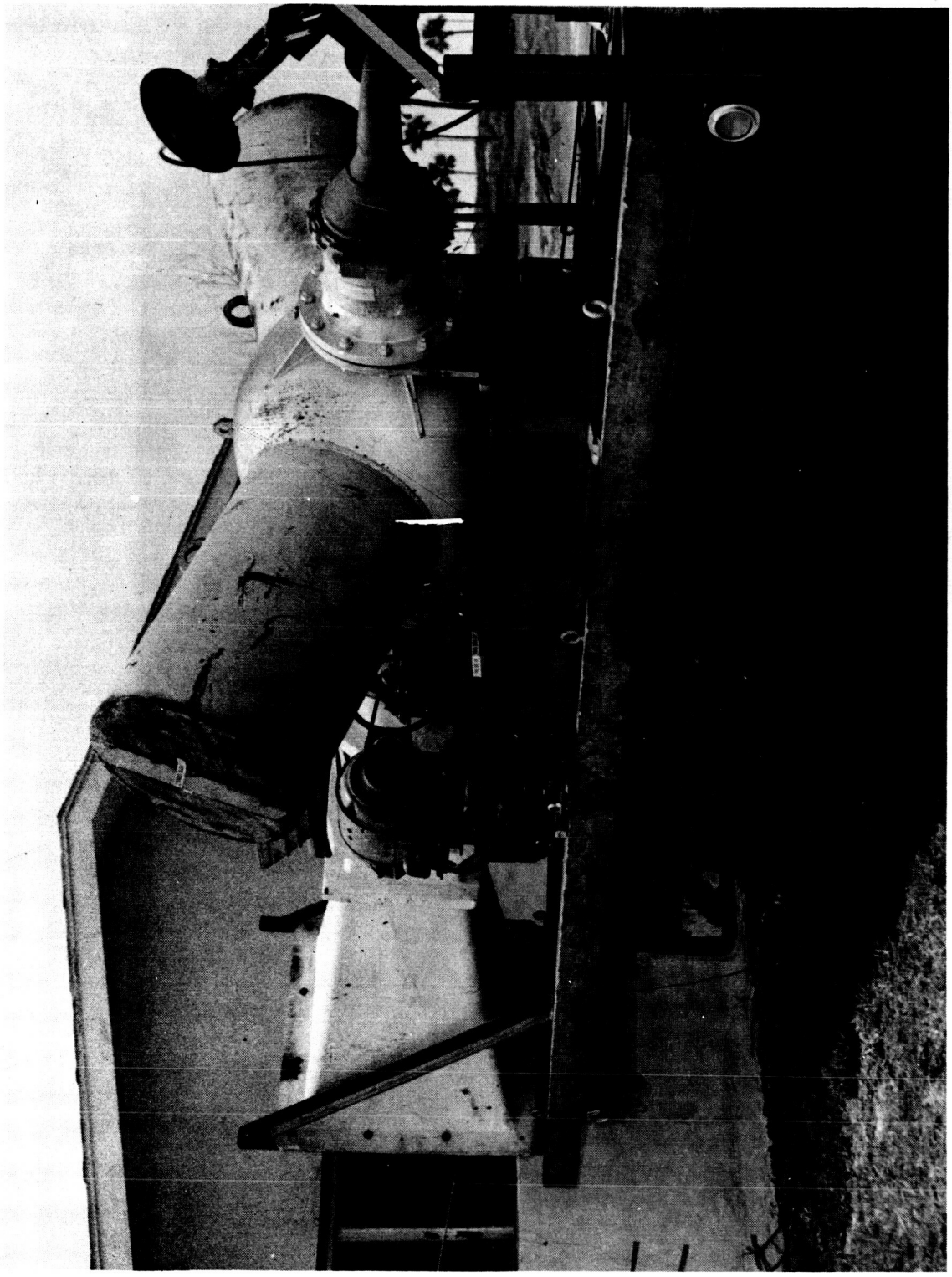

Fig. II-5 Test Fixture Backed Up to Test Window

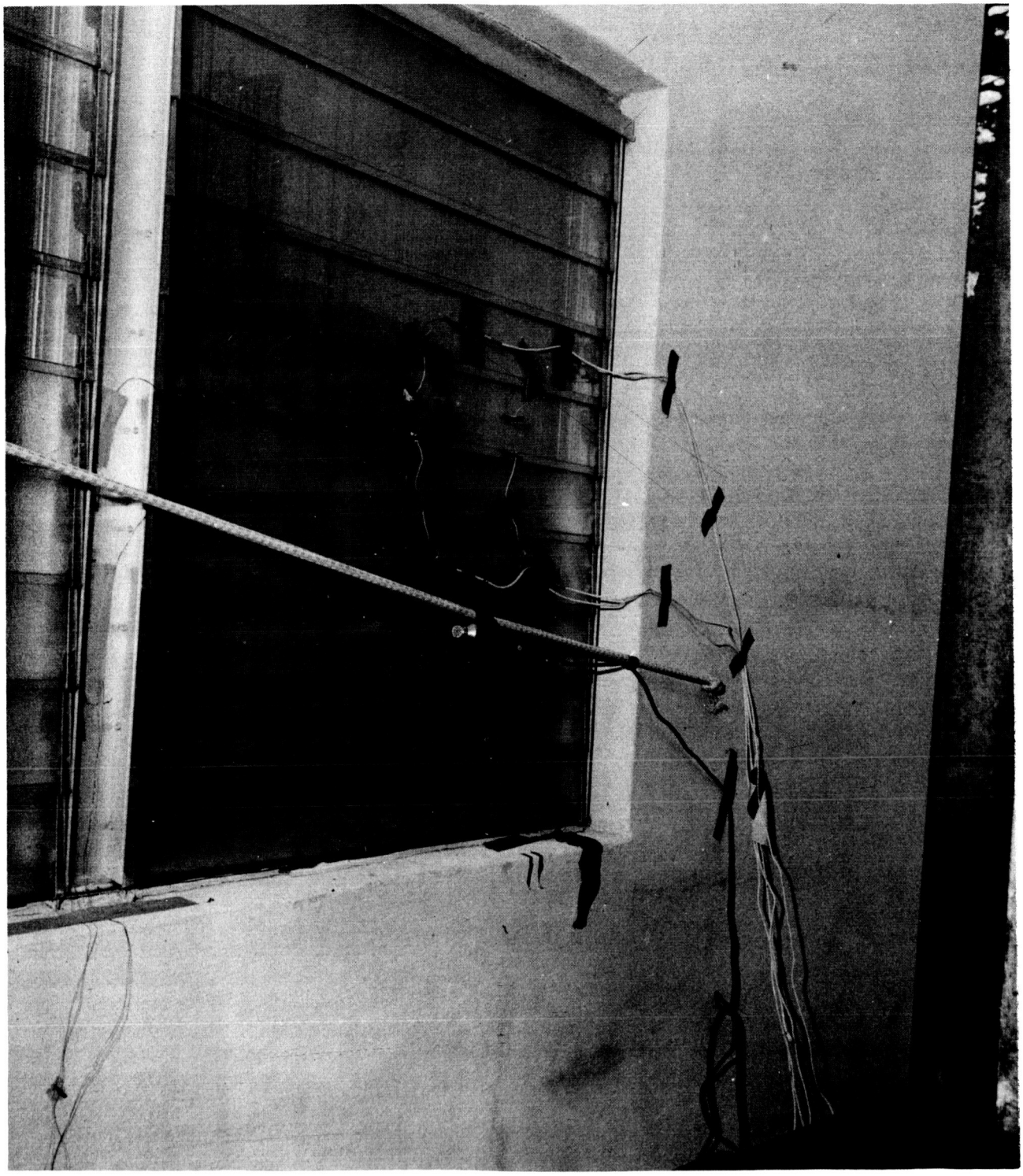

Fig. II-6 Four Accelerometers Mounted on Test Window

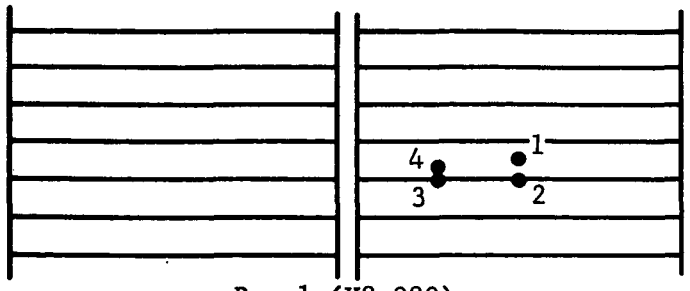

Run 1 (K8-989)

Note: 1. Pane size: 34x4x3/16 in.
2. Aluminum sash.

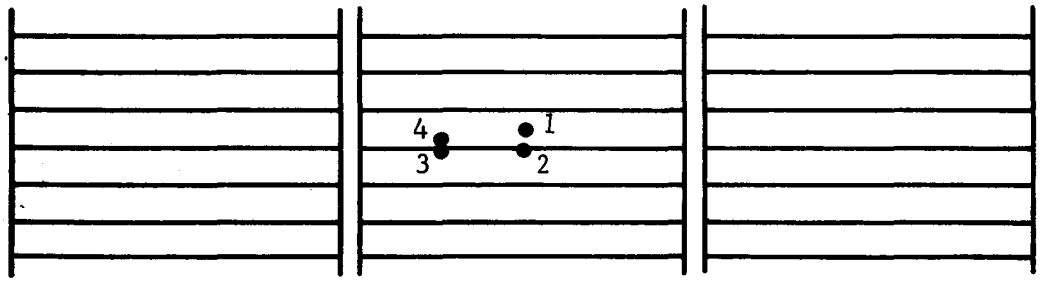

Run 16

Fig. II-7 Typical Jalousie-Type Window Accelerometer Locations

6. NASA Wall Tests

Acoustic tests were also conducted on the two NASA walls, which are normally located in the near vicinity of Saturn I launch stands. A sketch of this wall is shown in Fig. II-8 and a photograph in Fig. II-9. The wall was relocated near the test buildings for these tests. Figure II-10 is a drawing of the second NASA wall tested in Florida. This wall was constructed with concrete block. The test equipment was moved directly onto Saturn Complex 37 for purposes of testing this wall. Acoustic, accelerometer, and strain data were taken on both walls.

7. Test Results and Data Analysis

The data obtained during a typical test run are shown in tabulated form in Table II-2. Unless otherwise noted the data are related to an acoustic level of 135 db. Figure II-11 shows the scatter of accelerometer data points for the composite test runs. An analysis of the data is presented in further detail in Chap. III of this report.

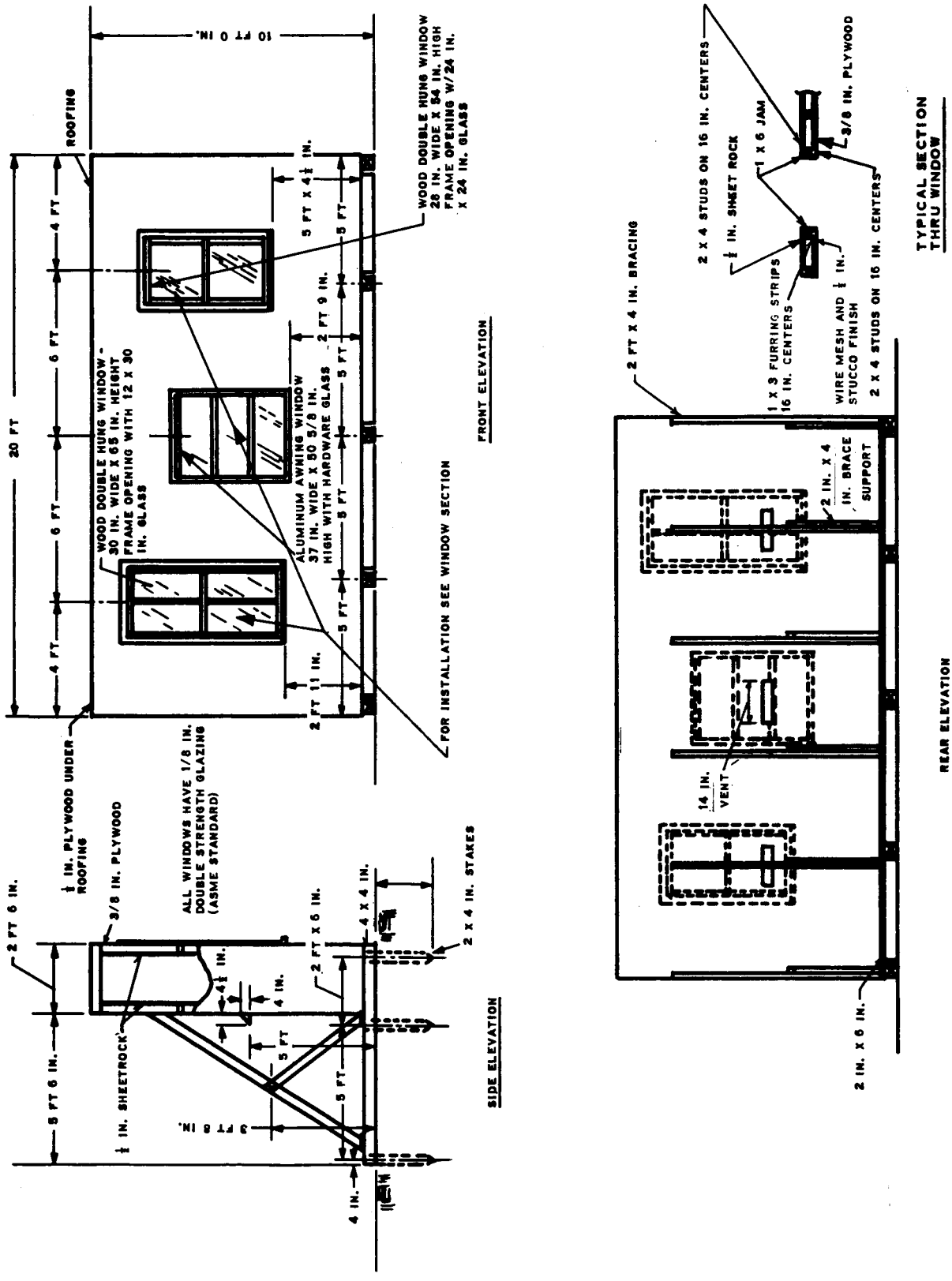

Fig. II-8 NASA Wooden Wall

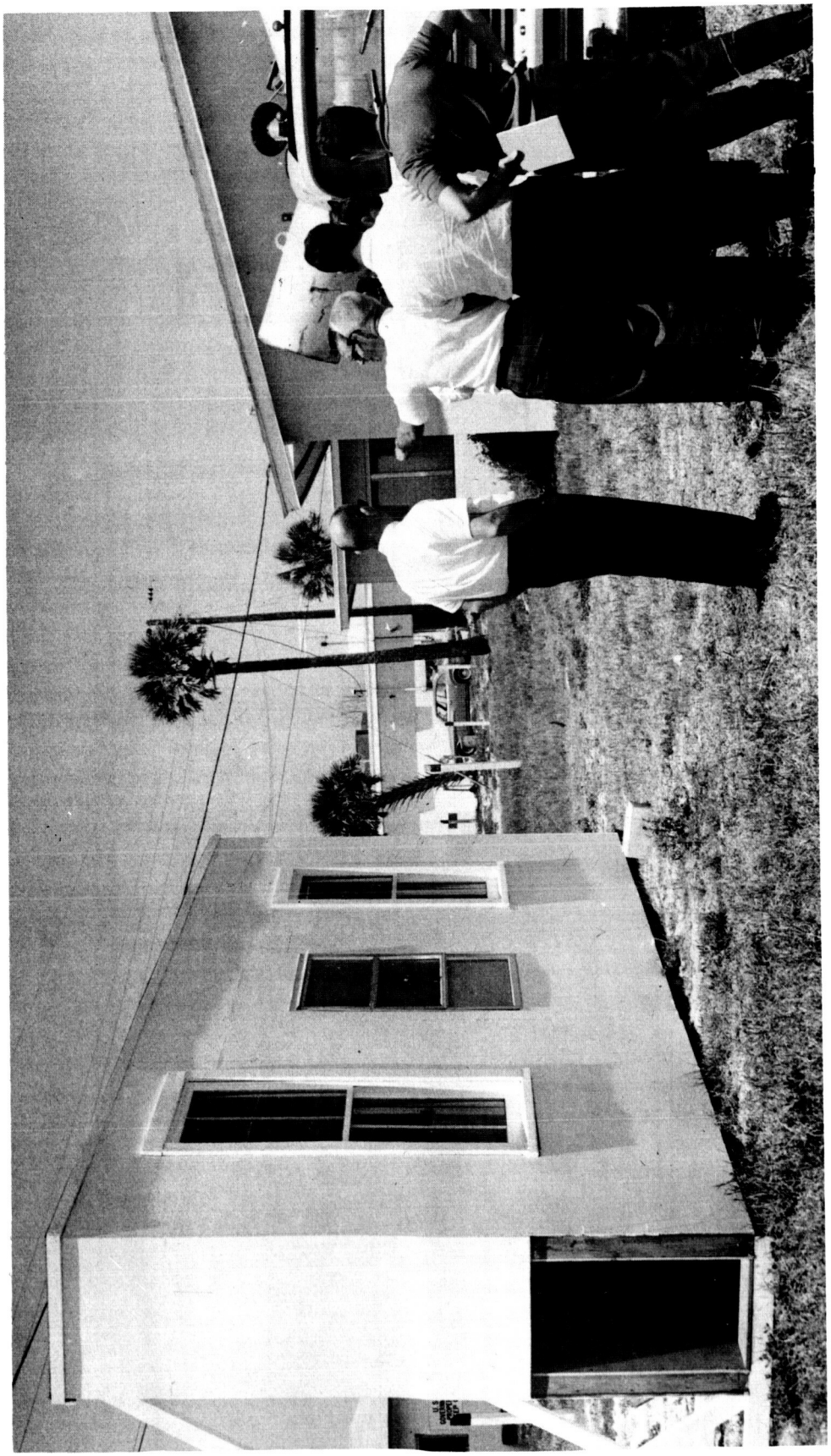

Fig. II-9 Photograph of NASA Wooden Wall

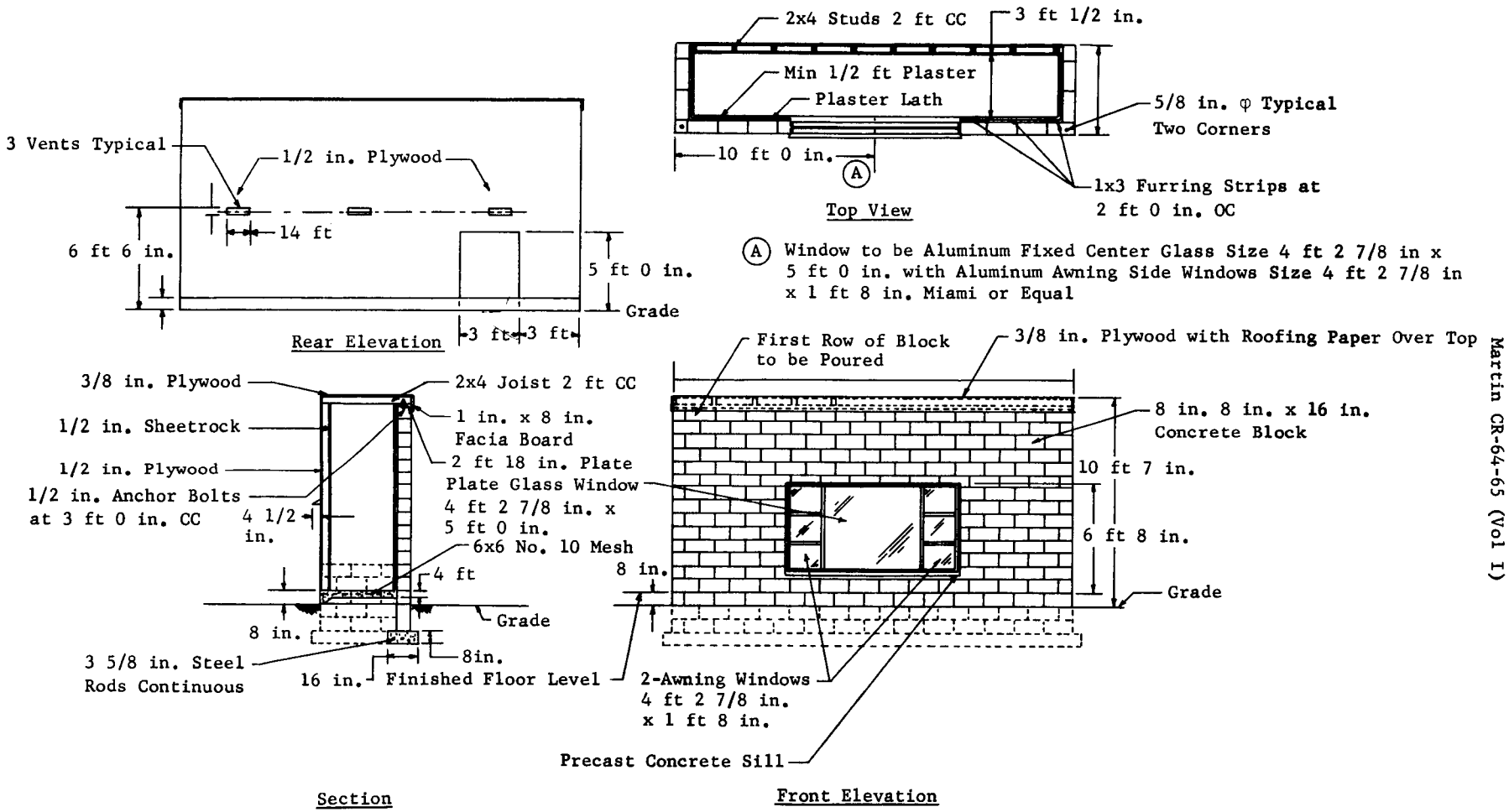

Fig. II-10 NASA Concrete Block Wall

Table II-2 Sample Data Sheet, Florida Tests

(Test Run 6 - 1, 2, 3 - Fixed-Plate Window)

Frequency (cps)	Accelerometer 1 (g peak)	Accelerometer 2 (g peak)	Accelerometer 3 (g peak)	Accelerometer 4 (g peak)	SPL (db)	Strain μ in./in.
550	3.4	3.6	2.7	1.6	135	24
520	4.2	2.5	2.8	1.4	136	24
450	3.0	1.6	2.5	1.2	135	24
400	3.7	2.2	2.6	1.6	135	25
360	2.8	1.4	1.8	1.0	135	24
280	1.7	1.2	1.6	1.0	134	24
240	4.7	3.2	5.2	2.6	136	24
160	3.9	3.2	3.4	2.7	135	26
140	3.4	2.9	3.0	2.4	135	26
120	3,2	2.2	2.7	1.8	135	26
100	4.5	3.0	4.4	2.6	135	26
80	5.1	2.8	3.3	2.5	135	26
80	8.6	4.7	5.2	4.1	141	29
80	12.3	5.6	6.0	4.3	146	35
80	17.3	6.4	6.6	4.6	150	44
76	5.0	2.8	3.5	2.6	135	26
68	5.0	3.6	4.4	3.0	135	40
50	5.9	4.2	5.4	3.7	135	43
35	7.0	5.0	6.8	4.7	135	30
33	6.7	5.0	6.5	4.8	135	30
30	7.1	5.0	6.9	4.8	135	41
26.8	13.5	8.5	12.6	7.5	131	78
25	5.5	4.5	6.4	4.6	129	42

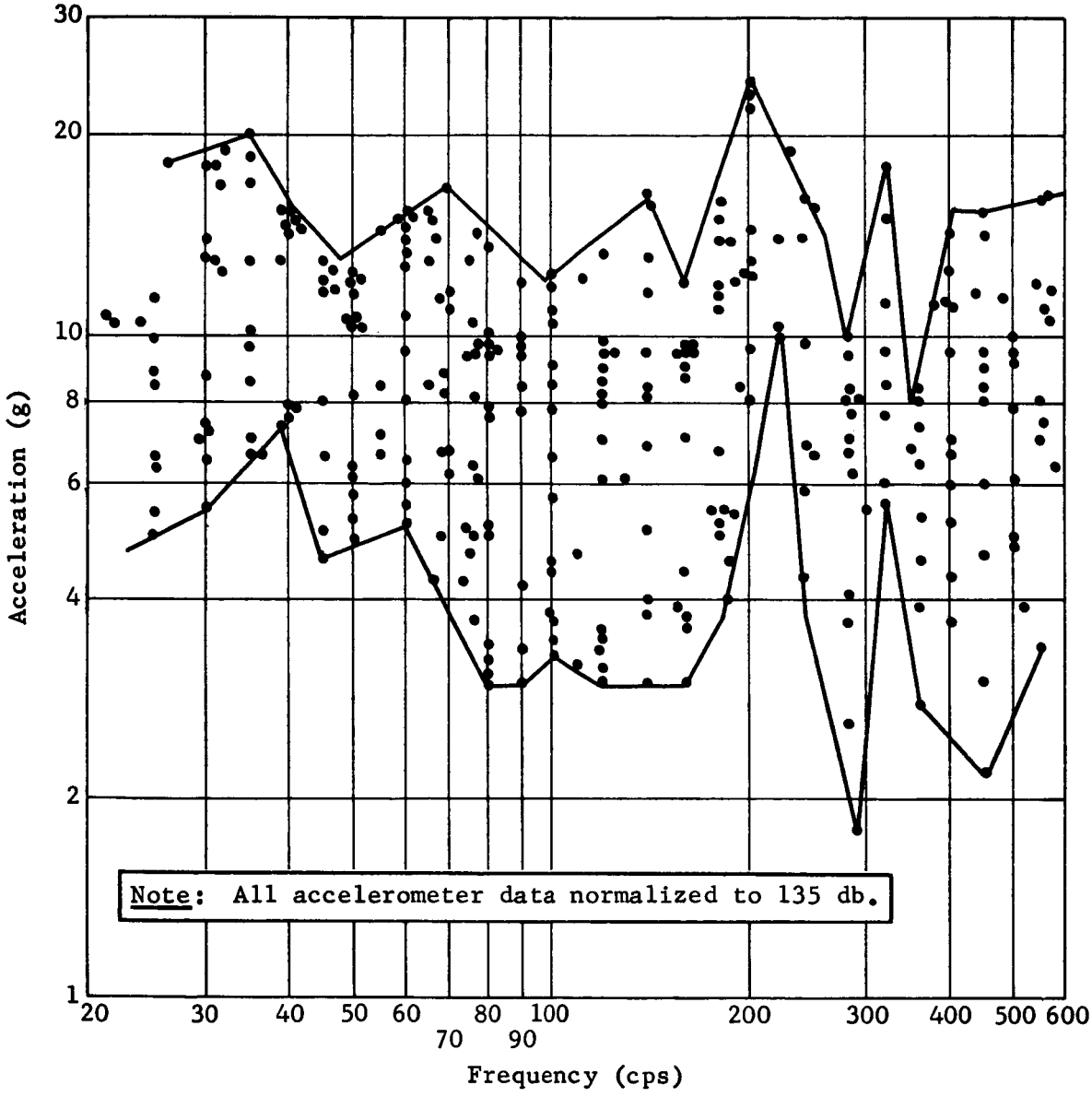

Fig. II-11 Scatter of Data from Florida Tests, Center Accelerometer

B. LABORATORY TESTS

1. Test Specimen

A test panel was constructed at the Martin-Denver Acoustic Facility. This panel was designed after the drawing shown in Fig. II-9 to simulate the NASA test wall. The Denver test panel is shown in Fig. II-12. The random siren is shown in position for a test on the left window. The mouth of the exponential horn was placed 3 ft from the window. The Denver test panel was similar to the Florida panel, except it was covered with stucco.

2. Instrumentation

Random Tests - Acceleration and strain data were acquired from the window tests. Sound-pressure levels were measured 2 in. from the windows. The microphone used in these measurements was also used to control the siren output. The accelerometer and strain gage measurement systems were the same as used in the Florida tests. The standard acoustic monitoring system, which has been used at the Martin Acoustics Laboratory for several years, was used for sound-pressure-level measurements. This system is made up of Altec Lansing components. The frequency response of all systems was flat (±2 db) within the range of interest. Single-point, end-to-end calibrations were used to establish system gain before each test. Accelerometer channel gain was established relative to peak calibration levels. All data were recorded on magnetic tape. Accelerometer and strain gage locations duplicated those of the Florida tests.

Sinusoidal Tests - Acceleration and sound-pressure-level measurements were acquired using the same measurement systems, except for the recorder. Accelerometers were located in the center of at least two panes in each window. The output of the microphones was monitored on a B&K audio frequency spectrometer and oscilloscope while the accelerometer output was monitored on the rms meter of a B&K microphone amplifier and an oscilloscope.

3. Test Procedure

Random Tests - Following calibration, the windows were tested at overall sound-pressure levels of 135, 140, 145, and 150 db. All data were recorded on magnetic tape for later analysis. During the recording, the overall sound-pressure level was monitored to maintain ±1 db maximum fluxuation. An example of the siren output is shown in Fig. II-13.

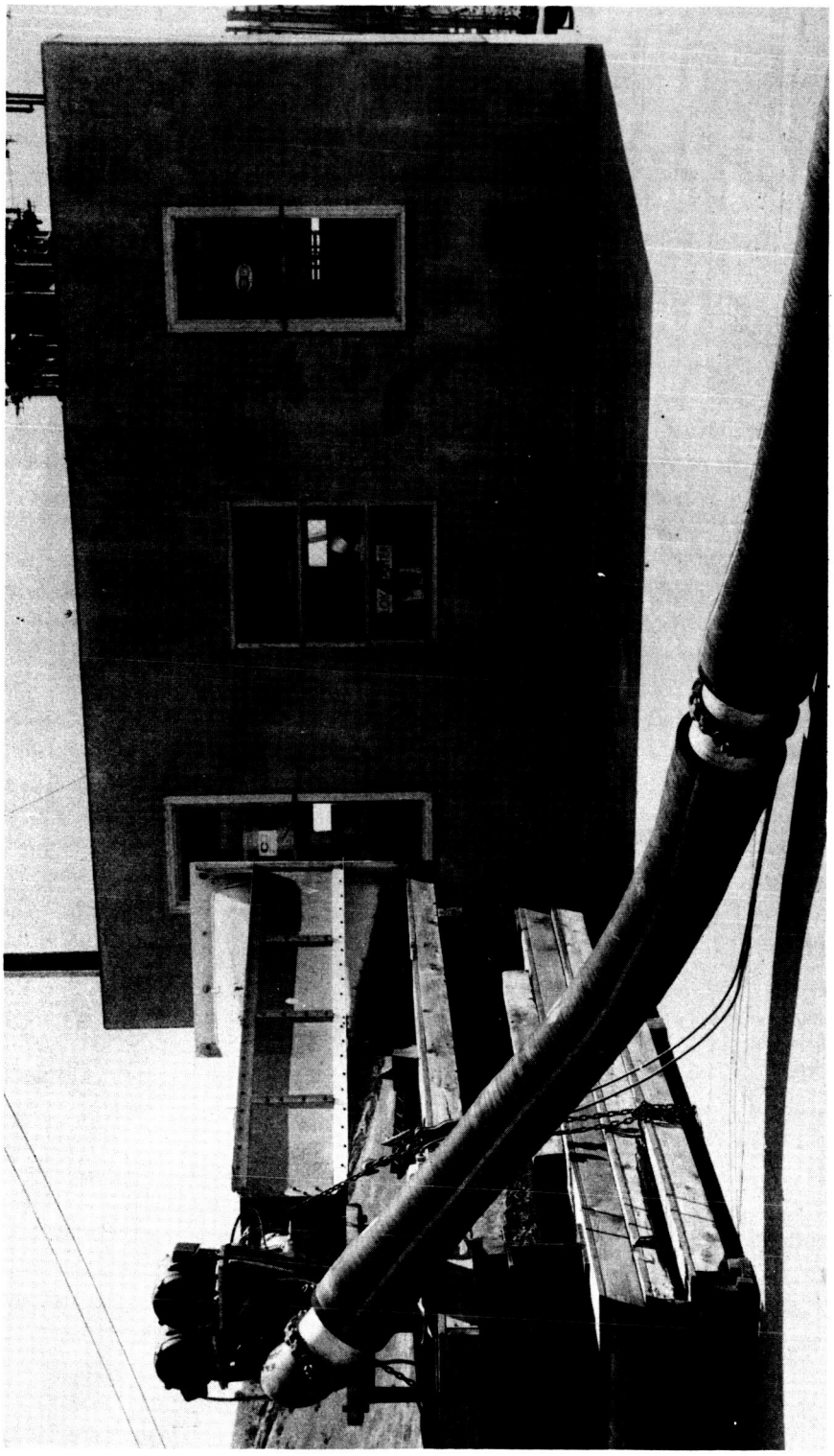

Fig. II-12 Denver Test Wall Unit

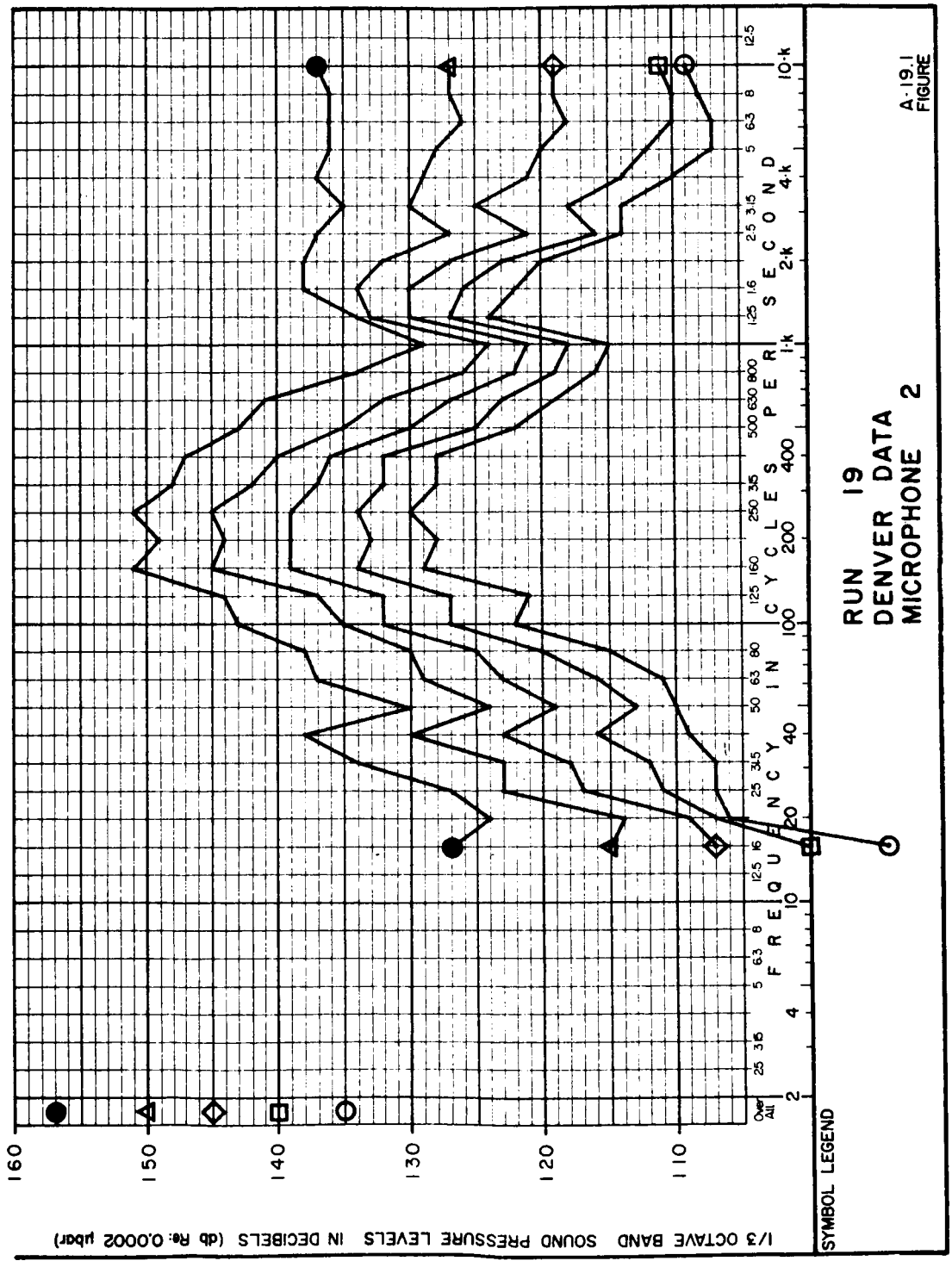

Fig. II-13 Typical Acoustic Test Levels, Center Window, Denver Tests

Sinusoidal Tests - The windows were tested at sound-pressure levels of 135 db at frequencies corresponding to the center 1/3-octave filter frequencies (i.e., 25, 31.5, 40, ...615 cps) in a frequency band ranging from 25 to 615 cps. Once the resonant frequency was established, the sound-pressure level was increased in 3-db steps from 130 to 154 db. Because the resonant frequency generally occurred in the 25-cps band, it was not possible to test higher than 154 db.

4. Test Results

Random Tests - No failures occurred during the random tests. An example of the accelerometer output for the excitation levels in Fig. II-13 is shown in Fig. II-14.

Sinusoidal Tests - Substantial damage was inflicted on windows and walls. Window failures are tabulated below.

	SPL (db)	Acceleration (g)
Left Window	143	34
	151	40
Center Window	147	64
	148.5	No Data
Left Window	147	76

Data from these tests are shown in Fig. II-15 thru II-17. The spread of acceleration data is shown in Fig. II-18. Photographs of window damage are shown in Fig. II-19 and II-20. In addition to window glass breakage, some damage to casements and metal stripping also occurred. This damage was observed on the television monitor, at or just before glass breakage. Following the first test, drywall plaster board was loosened. The wall was renailed and observations made between tests where amplitude was increased 3 db. No loosening was observed below 147 db. Above 147 db, the drywall became loose as a function of time. Since approximately 3 minutes was spent on each dwell, the wall was exposed to sound-pressure levels above 147 db, for slightly over 9 minutes. The damage from the first test consisted of nails pulled from the studs. Following the tests on the other windows, however, the drywall had broken around the nails. Photographs of wall board damage are shown in Fig. II-21. No obvious cracks were produced in the stucco. Immediately after the window behind the control microphone broke, the sound pressure level, as measured by this microphone, was found to have decreased approximately 6 db.

5. Test Environments

The random siren produces a continuous random noise and is very repeatable. No attempt was made to analyze the random noise in filters narrower than 1/3 octave, since such accuracies were not warranted. Previous 5-cps band analysis, however, did not show any "holes" in the spectrum. The random spectrum is reasonably representative of a rocket engine noise spectrum.

The sinusoidal siren was designed to operate at higher air pressures than were required to produce 135 db. As a result, a pure tone wave was not always produced and some harmonics were present. When these distortions were present, the data at these frequencies were not used. No definite criteria were used. The decision to include data was left to the test conductor. No attempt was made to salvage vibration data by filtering. The frequency of the siren was set by searching in a narrow band at a constant amplitude, until the filter output was maximum. This technique has been used in the past and has produced accuracies greater than $\pm 3\%$. The unfiltered waveform was monitored on an oscilloscope. When the filter output changed more than 1/2 db, the frequency and amplitude were both reestablished.

A complete description of the acoustic test facilities is contained in the appendix (Vol II).

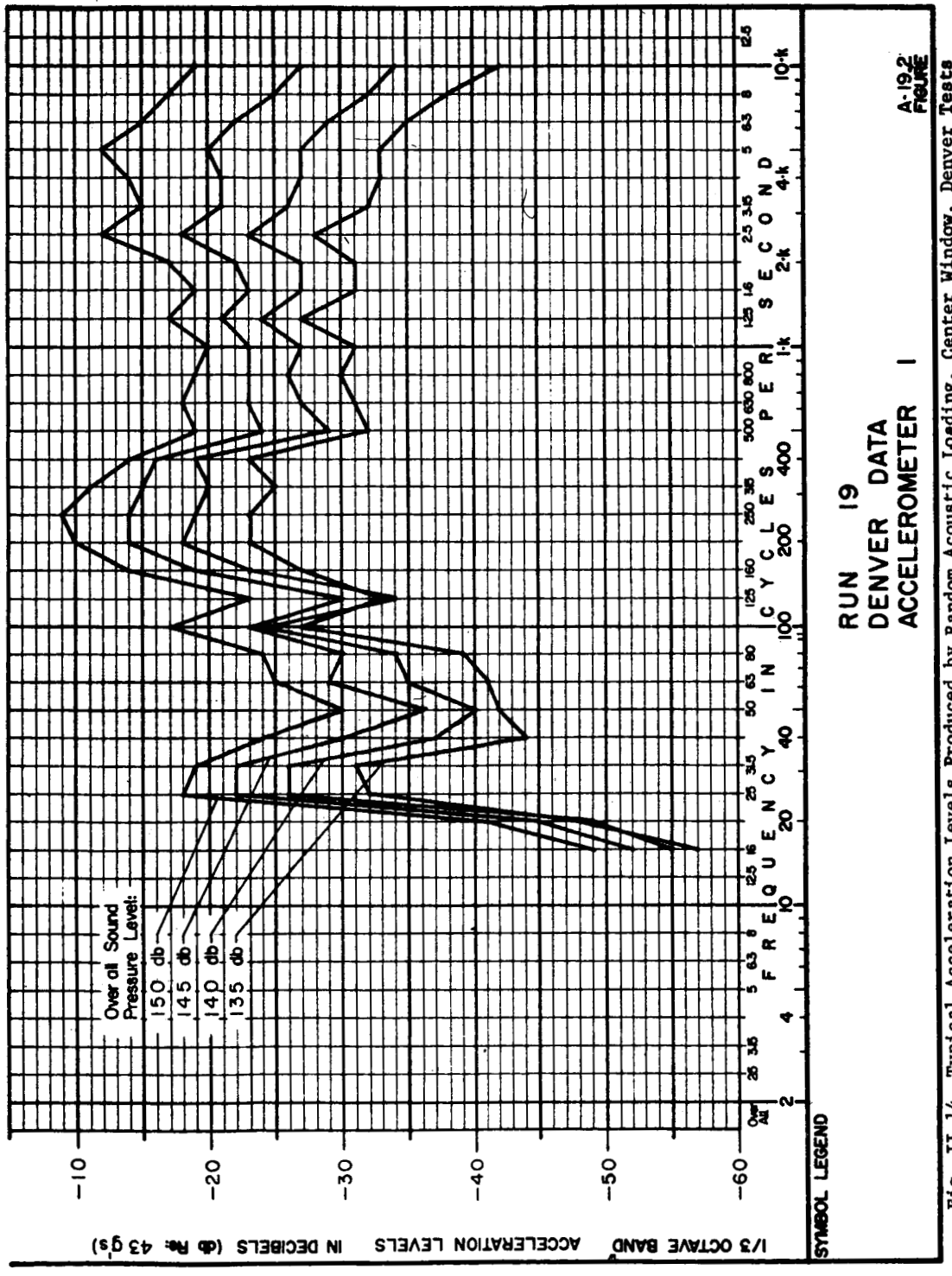

Fig. II-14 Typical Acceleration Levels Produced by Random Acoustic Loading, Center Window, Denver Tests

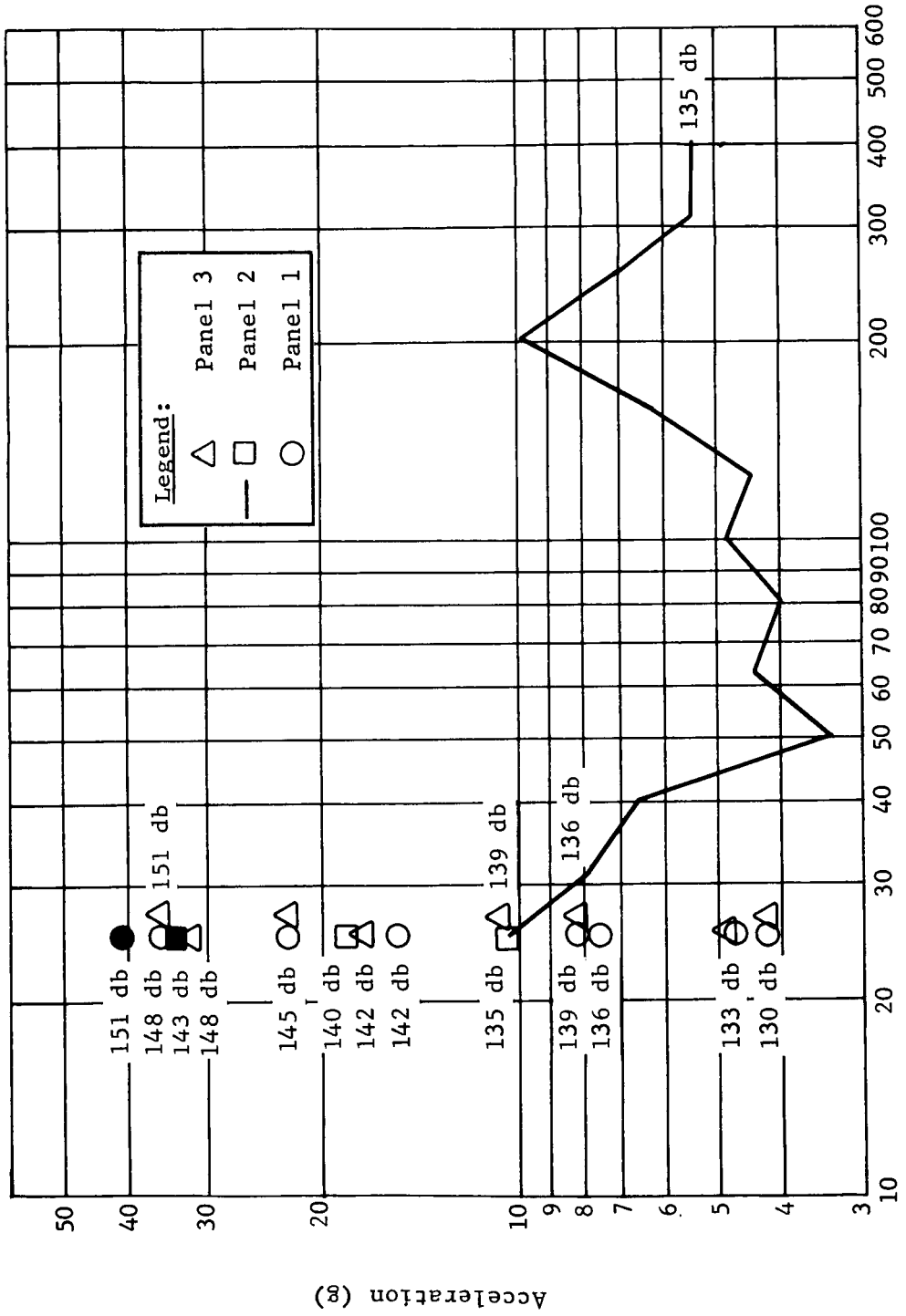

Fig. II-15 Measured Acceleration Levels, Center Accelerometer, Left Window, Denver Test Panel, Sinusoidal Excitation

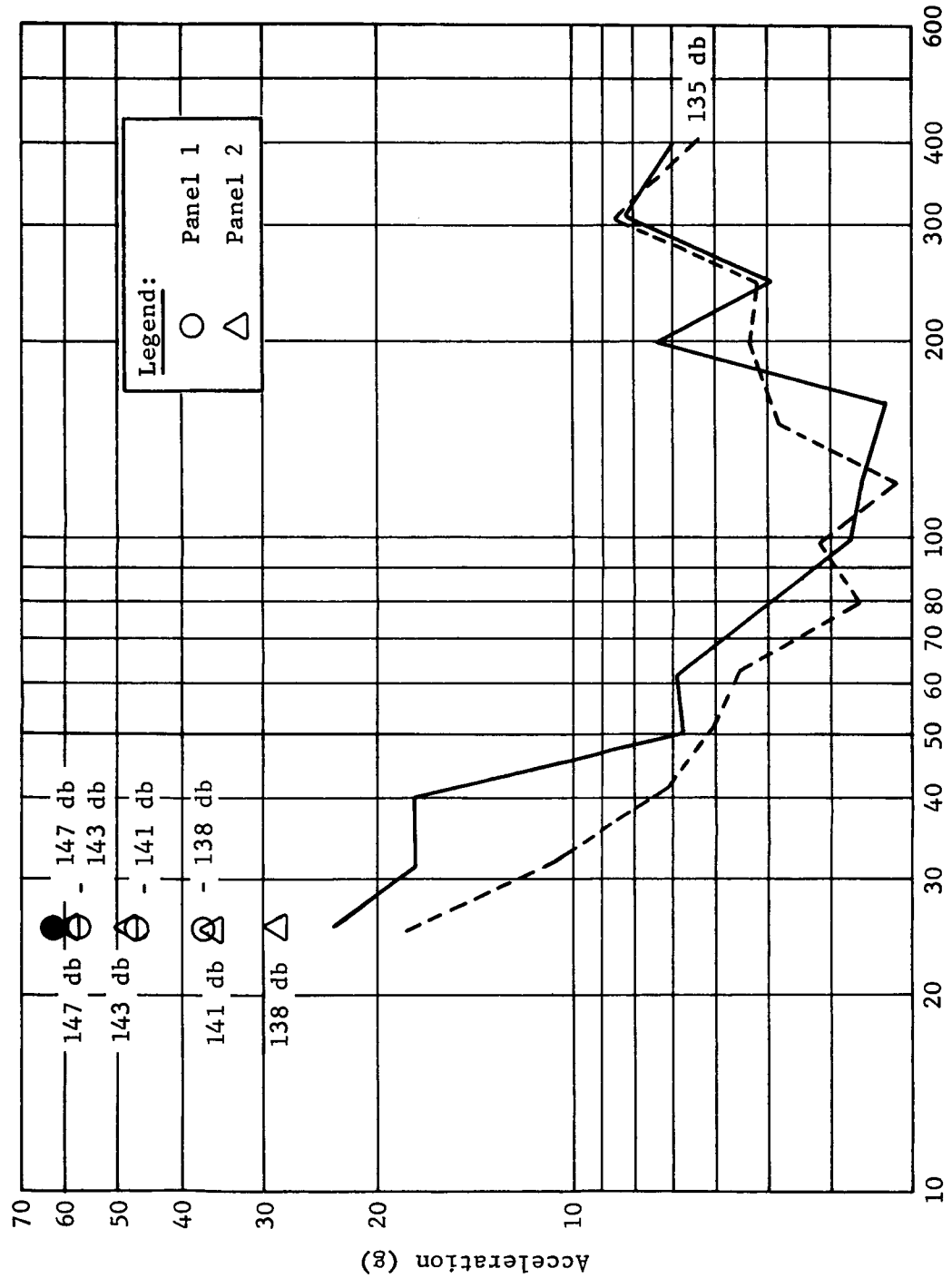

Fig. II-16 Measured Acceleration Levels, Center Accelerometer, Center Window, Denver Test Panel, Sinusoidal Excitation

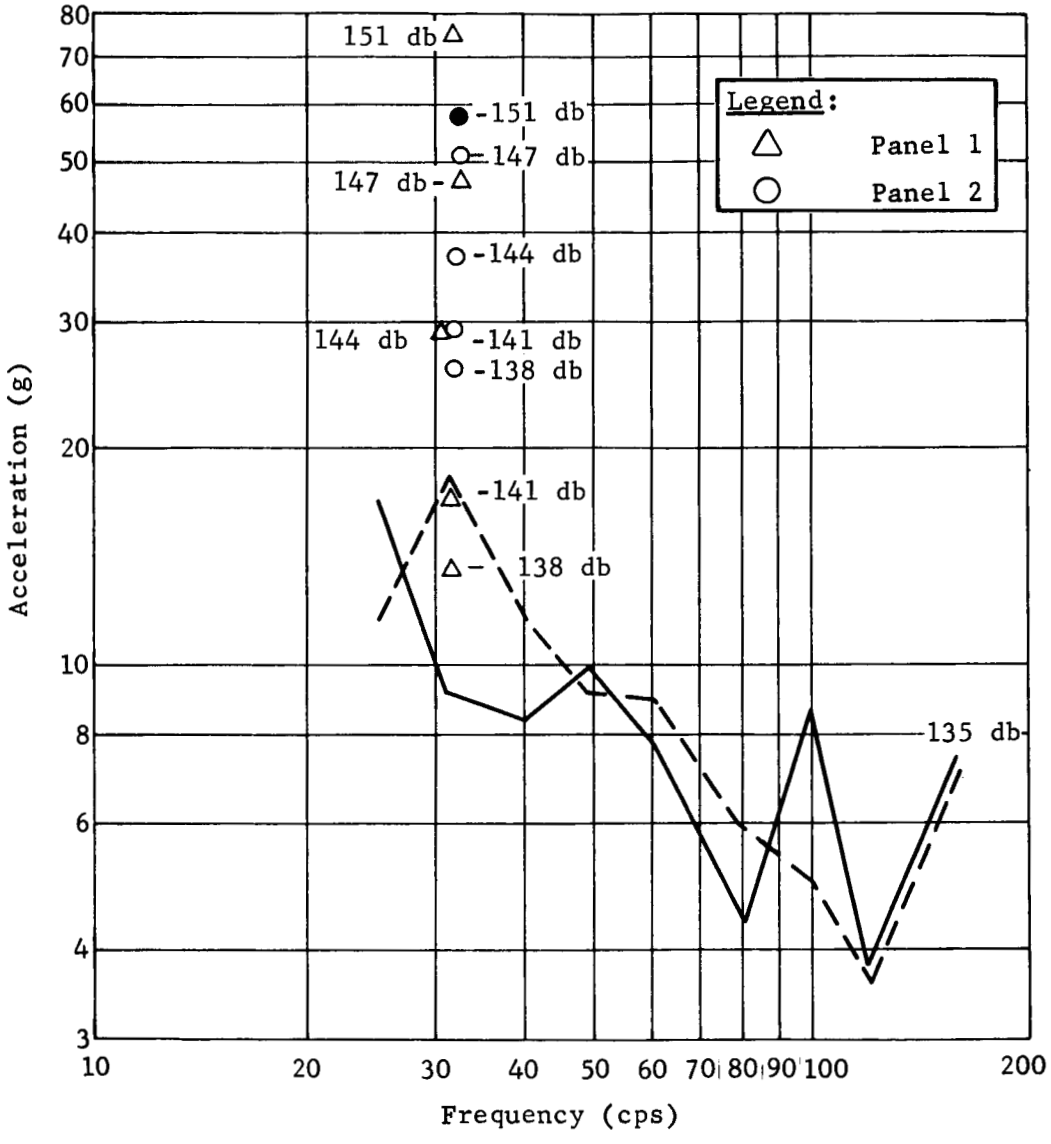

Fig. II-17 Measured Acceleration Levels, Center Accelerometer, Right Window, Denver Test Panel, Sinusoidal Excitation

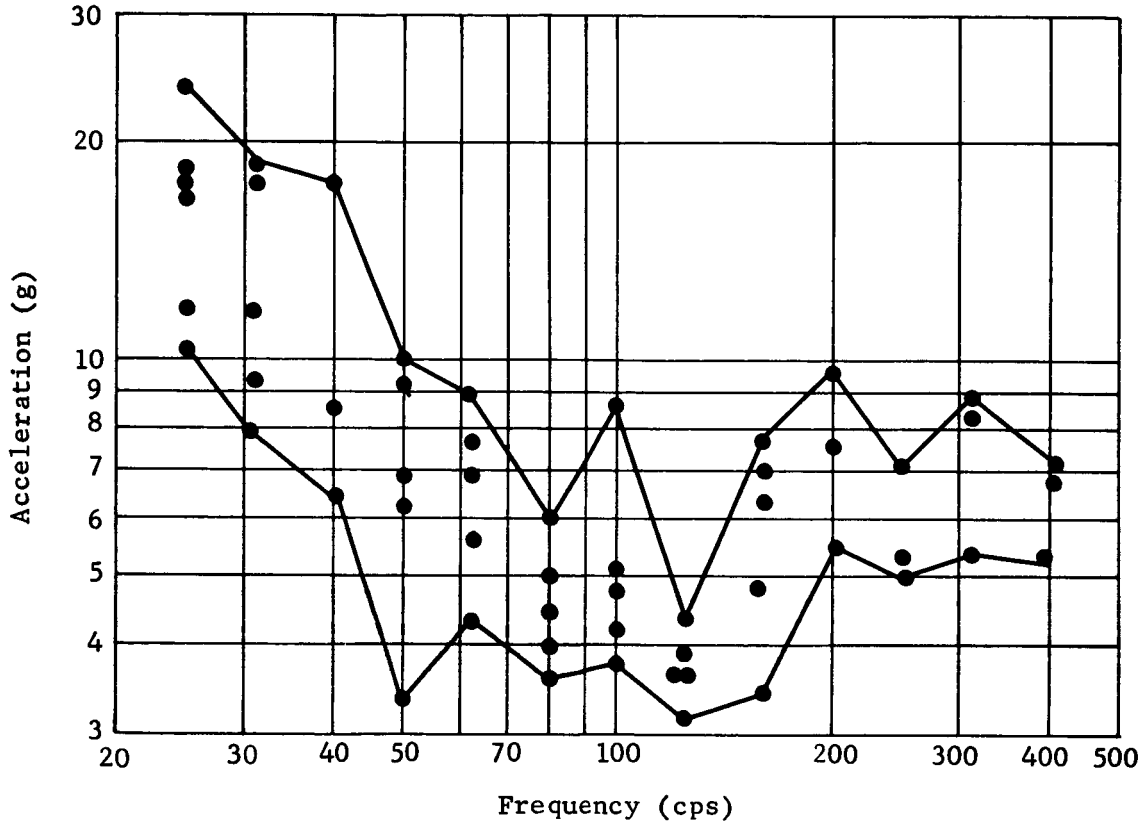

Fig. II-18 Spread of Data Points from Center Accelerometer for Denver Panel Sinusoidal Tests

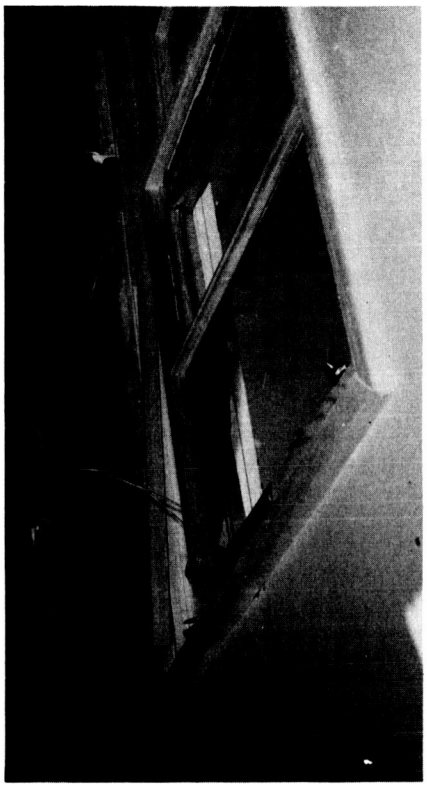

Fig. II-19 Window Breakage Due to Sinusoidal Excitation on Left Window of Denver Test Panel

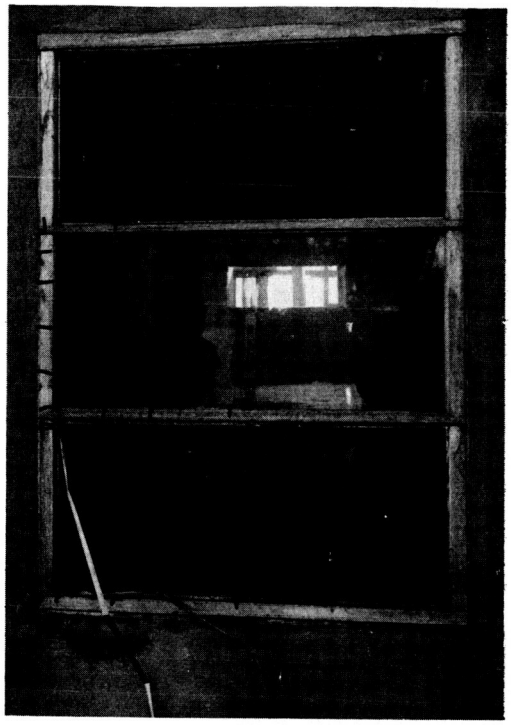

(a) Center Window

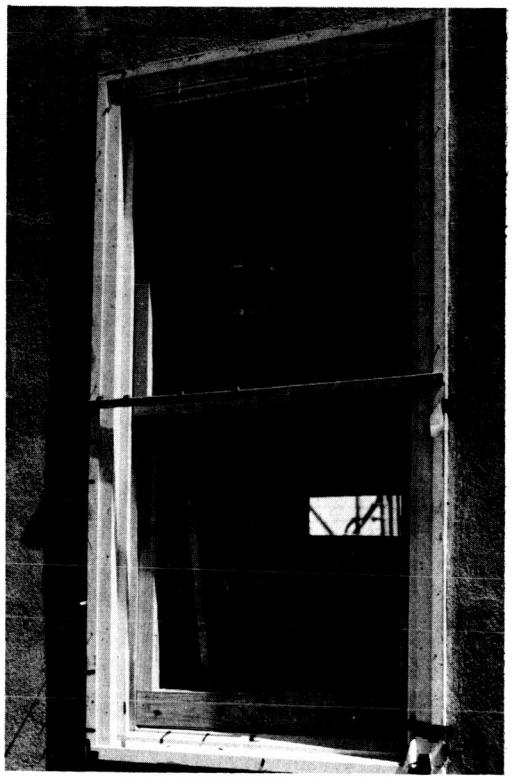

(b) Right Window

Fig. II-20 Window Breakage Due to Sinusoidal Excitation on Center and Right Windows of Denver Test Panel

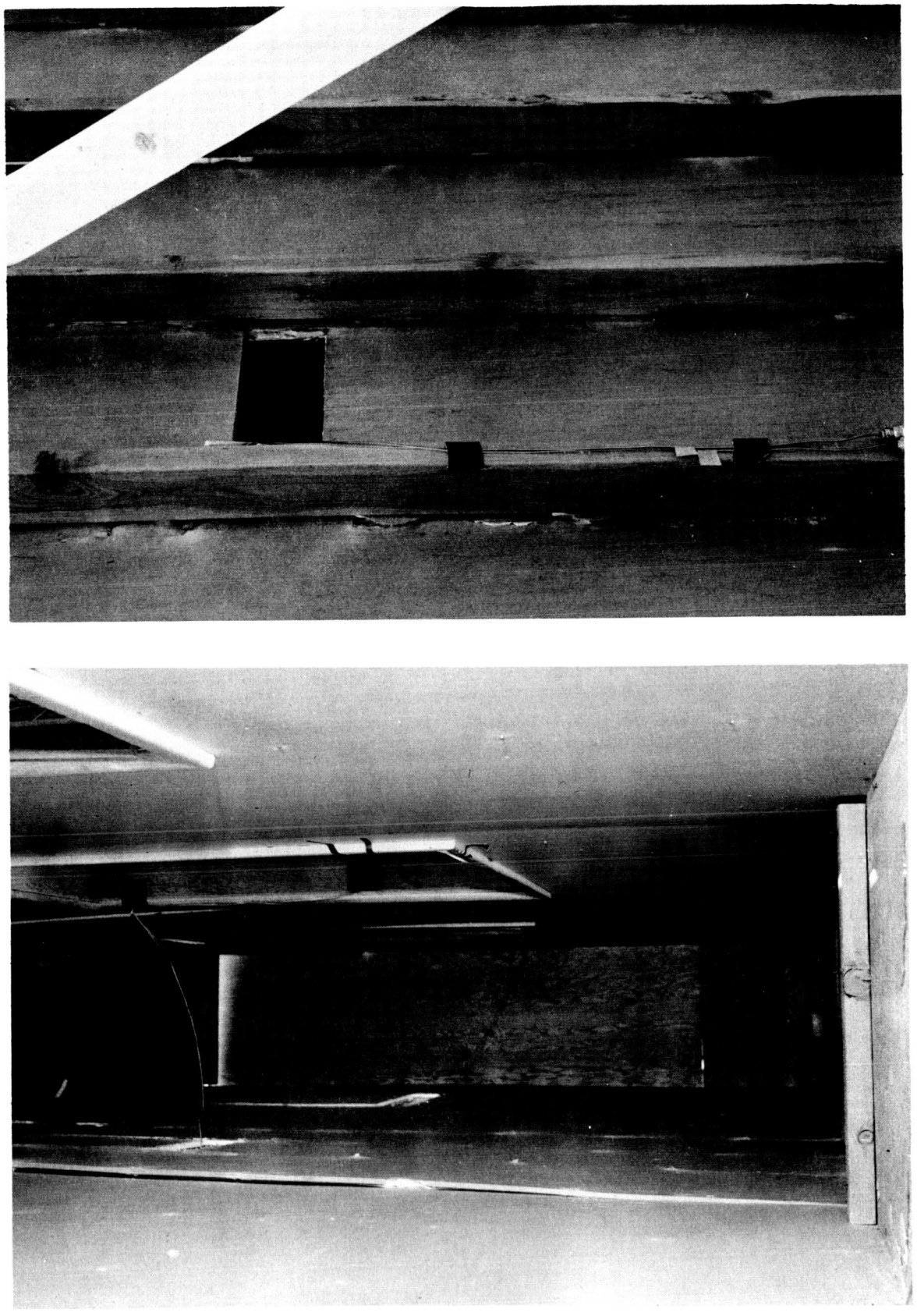

Fig. II-21 Wallboard Damage Due to Sinusoidal Excitation, Denver Test Panel

III. ANALYSIS

This chapter describes the analytical techniques that were used to determine the noise hazard potential, evaluate the test results, and formulate the conclusions. The information is contained in three sections; community survey, noise level predictions, and dynamic analysis of windows. The evaluation of the results is contained in Chap. IV.

A. COMMUNITY SURVEY

This survey was conducted in the Titusville area during February 1964. The survey was conducted by a helicopter survey, conference with local and county officials, and a building count. The survey included a definition of communities, type of buildings, and placement in susceptibility categories within the area shown in Fig. III-1. None of the buildings within the J. F. Kennedy Space Center are considered.

1. Survey

Figure III-1 shows that the communities closest to the Post-Saturn launch sites include Titusville, Mims, Scottsmoor, and Oak Hill, Florida. This general area is now predominantly agricultural with three exceptions:

1) The area northwest of Titusville, almost reaching Mims, is suburban with the majority of the population housed in small subdivisions. The land between subdivisions is farmed with strip development along State Highway 405.

2) The sparsely developed areas along Highway US 1 consists of commercial and residential structures, the majority of which are in fair to poor maintenance and paint condition.

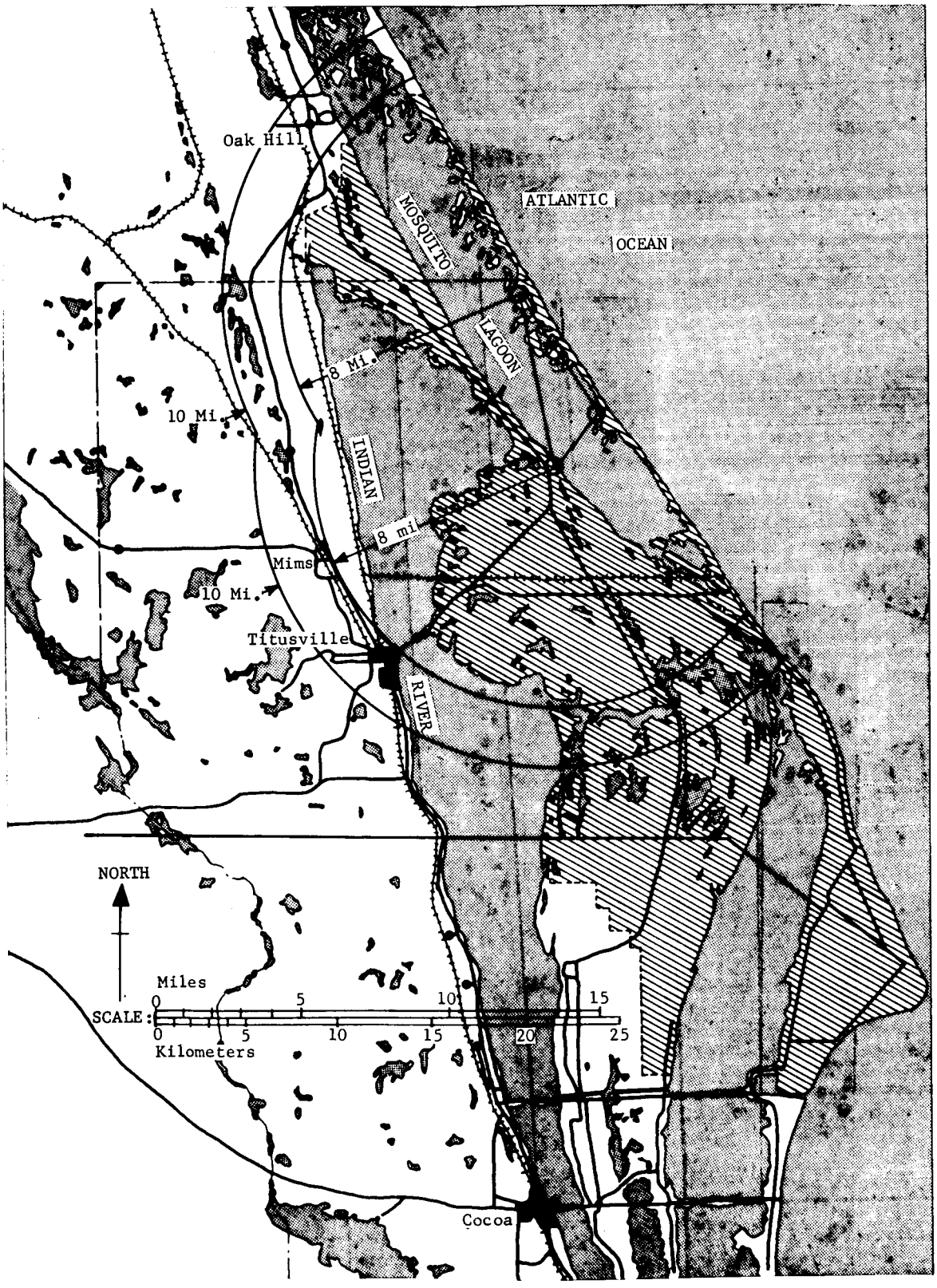

Fig. III-1 Communities Adjacent to John F. Kennedy Space Center

3) Mims, Florida, is a small unincorporated community, supported by agriculture, and showing none of the rapid growth that has developed a few miles to the south. A predominant feature of Mims is the economically depressed neighborhood. Ranging from one to three blocks wide and over a mile in length, this community of shacks, shanties, small homes, churches, and a school is the nearest to the launch sites.

Future development of MILA will undoubtedly cause extensive changes in this area. The land between Highway US 1 and the Indian River is now, and should remain, in groves. The area west of Highway US 1 will become island after island of subdivision housing between the swamps and lakes.

The survey to determine construction of the individual structures and the material used was performed in three parts:

1) A helicopter trip over the area revealed the overall pattern. It also helped locate hidden areas which lie beyond the edge of the road, and the patterns of past and possible future growth, including the problems solved and those to be encountered;

2) A series of conferences with NASA personnel and citizens of the community known to be knowledgable in the problem produced the specific information on construction methods and materials, both as to description and periods of use;

3) The final phase was the actual structure count. Sample areas were chosen and 1200 human shelters were classified as to use, construction, roofing material, window sizes and material, age, maintenance, etc.

The results of the survey are listed in the order they were obtained; however, information from all phases influenced matters of judgment throughout the survey.

Helicopter Results - The greater portion of the population surrounding the John F. Kennedy Space Center is housed south of the area of interest. Currently the major growth around Titusville is to the west and south. New building to the north is scattered and small by comparison. Though the area involved is largely rural now, the indicated growth of the Center will make it suburbia in the immediate future. It is estimated that 70 percent of the future residential structures in this area will be built of:

1) Concrete block walls that may or may not have exterior stucco finish;

2) Asphalt shingle or builtup roof with prefabricated roof trusses supporting sheathing;

3) Aluminum awning-type windows (15 per structure);

4) Interior finish of drywall to furring.

The majority of the remaining 30 percent will be economical construction of concrete block walls, same roof as above, aluminum framed jalousie windows, and interior finish of thin plaster coat applied directly to block.

Conference Results - Construction and material information obtained from conferences included:

1) The hurricane-proof construction has become part of the building code requirements of the area. It requires a continuous bond beam around the perimeter and caping the masonry walls of all structures; further all roof members shall have specified minimum ties to this beam. The prefabricated light king post truss with sheet metal gussets and strap steel anchors has become a standard;

2) The locally manufactured concrete block differs considerably from that generally found in other locations. It is practically impervious to moisture, and should have acoustic transmission loss superior to other concrete block;

3) The introduction of drywall interior finish was wholly accepted about 15 years ago; and, since then, has been exclusively used in the low-medium to most expensive dwellings. Plaster has retained its place in commercial and institutional structures, and has been modified to a putty coat applied directly to plaster for interior finish in the most economical housing.

Actual Count Results - The following statistics are based only on structures with foundations, with the exception of the first item, in which mobile houses are included.

1)	Structures on Foundations	96.2%
	Mobile (Trailers)	3.8%
2)	Type of Use -	
	Residential, Single Family	88.8%
	Residential, Multiple including Motels	3.7
	Commercial and Industrial	6.3
	Institutional	1.2
3)	Type of Construction -	
	Wood Frame (96% Siding, 4% Stucco)	27.7%
	Masonry (69% Block, 29% Stucco, 2% Brick)	71.8
	Curtain Wall Construction	0.5%
4)	Roof Finish -	
	Asphalt Shingles	16.9%
	Builtup	63.3
	Asphalt Plank	15.7
	Tile, Ceramic or Cement	2.5
	Metal	1.6
5)	Window Types -	
	Double Hung	26.3%
	Casement	2.5

Awning	53.8
Jalousies	12.6
Fixed	4.8
6) Window Material -	
Wood	24.9%
Steel	4.7
Aluminum	70.4
7) Number of Windows (Average) -	
Twelve Windows per Structure.	
8) Window Size -	
Small	5.9%
Medium	84.1
Large	10.0
9) Glazing Thickness -	
1/8 in.	82.5%
3/16 in.	1.3
1/4 in.	16.2
10) Glazing Stop Material	
Compound (Putty)	27.9%
Window Material	72.1
11) Maintenance -	
Good	16.3%
Average	66.4
Poor	17.3

12)	Condition of Paint -	
	Good	16.3%
	Average	65.9
	Poor	17.8
13)	Interior Finish -	
	Dry Wall	61.1%
	Plaster	37.6
	Other	1.3
14)	Age of Structures -	
	Less than 5 years	47.9%
	Between 5 and 10 years	21.0
	10 and 20 years	4.9
	20 and 30 years	6.5
	30 and 40 years	15.9
	Over 40 years	3.8

2. Conclusions

The community having the highest susceptibility to possible rocket engine noise damage is Mims, especially that slum area located even closer to the launch sites. It is possible, however, that should damage occur, the most vigorous complaints would come from outside this neighborhood.

The downtown section of Titusville and the community of Oak Hill are the next most susceptible with the exception of the individual structures scattered along the major highway and the rural farm houses. The proximity to the launch sites of the above two classifications is the primary cause for concern; however, they are almost wholly composed of prewar (Number 2) construction. The field and laboratory tests which are a part of this study may verify the contention that poorly maintained buildings will record damage before new and properly kept property.

B. NOISE LEVEL PREDICTION

This section contains three parts: a discussion of rocket engine noise generation and propagation in general; the effects of weather on noise propagation; and a specific description of Post-Saturn noise environments.

The scope of this work, as specified by contract, was to accumulate existing information. Thus, the work of others is used extensively. References are listed in Chap. VI.

1. Rocket Engine Noise Prediction

Considering the simple case of a sound radiating from a point source, the sound pressure at distance r can be shown to be:

$$p^2 \sim \frac{W_a \rho_o C_o}{4\pi r^2} \qquad \text{[III-1]}$$

where

p = sound pressure,

W_a = acoustic power,

ρ_o = density of air,

C_o = speed of sound in air.

This relationship has been used to derive an empirical method of determining rocket engine far field noise levels. Assuming the rocket engine to be a point noise source, Eq [III-1] would be valid, except that the directional characteristics of a rocket engine and the effects of excess attenuation must be considered. Thus,

$$p^2 \sim \frac{W_a \; G_1(\varphi)}{4\pi \; r^2 \; G_3(a)} \qquad \text{[III-2]}$$

where

G_1 (φ) = directivity factor,

G_3 (a) = excess attenuation,

and

$$SPL = PWL + DI - EA - RI \qquad [III-3]$$

where

SPL = sound pressure level (db re 0.0002 dynes/cm^2),

PWL = sound power level (db re 10^{-13} watts),

DI = directivity index (db),

EA = excess attenuation (db),

RI = radiation index (db = 10 log A).

Each of these terms must now be evaluated for the type of large booster engines to be used on Post-Saturn program.

The acoustic energy, produced by a rocket engine has been expressed in terms of total energy produced by the engines (Ref 1) as follows:

$$KE \text{ (acoustic)} \approx \eta \text{ KE (engine)} \approx \frac{\eta}{2} MV^2 \qquad [III-4]$$

where

KE = kinetic energy,

η = acoustic efficiency.

The value of η has been found to vary with the size of the engine. VonGierke, et al. (Ref 2) found the acoustic efficiency to vary, or

$$PWL = 78 + 13.5 \log W_{engine} \qquad [III-5]$$

for engines with thrust varying from 1000 to 130,000 lb. This relationship is shown as the straight line part of the curve of Fig. III-2. Obviously, this line cannot extend indefinitely. The curve was extended by Cole (Ref 3) beyond the 130,000-lb range. The overall acoustic power level as found from Titan (Ref 4) and Saturn (Ref 5, 6, and 7) measurements is also shown in Fig. III-2. The curve seems to indicate a decrease in conversion efficiency as the engine power level increases past 7×10^9 watts. The Saturn data lie below the curve, indicating that the slope of the curve may change sooner. The apparent decrease in conversion efficiency may be due to the fact that finite amplitude effects have not been considered in computing the acoustic power level from measured sound pressure levels. At the present time, there are insufficient data to provide a method of computing or allowing for the nonlinear damping of the high amplitude sound waves from such large power sources. Thus, the use of Fig. III-2 should provide some adjustment for finite amplitude losses until they may be computed. The finite amplitude index will therefore be included with the power level term.

In many previous documents, rocket engine jet stream power has been defined in terms of full rated thrust. On many future vehicles, however, engines that are overexpanded at liftoff may be used. Thus, it may be more meaningful to express the jet stream power in terms of specific impulse and thrust at liftoff:

$$PWL = 10 \log \frac{\eta W_m}{10^{-13}} = 10 \log \frac{0.676 \eta T \cdot I_{sp} \cdot g}{10^{-13}} \qquad [III\text{-}6]$$

$$= 10 \log \frac{0.676 \eta \left[\frac{V_e^2 \dot{w}}{g} + (P_e - P_o) A_e V_e \right]}{10^{-13}} \qquad [III\text{-}7]$$

where

W_m = mechanical power of the jet stream (watts),

T = thrust (lb),

I_{sp} = specific impulse (sec),

V_e = nozzle exit velocity (ft/sec),

w = weight flow (lb/sec),

g = gravitational constant,

p_e = exit pressure, absolute $(lb/in.^2)$,

p_o = ambient pressure, absolute $(lb/in.^2)$,

A_e = nozzle exit area $(in.^2)$.

A nondimensional power spectrum was also derived by VonGierke and is shown in Fig. III-3. This spectrum was derived from far field data acquired from rocket engines with thrusts up to 130,000 lb. The applicability of this spectrum for large booster engine midfield noise can be determined using Titan and Saturn data. The spread of these data is also shown in Fig. III-3. The Saturn data appear to agree more closely than Titan data. In general, the use of the generalized curve as recommended by Cole, et al., should be applicable to the far-field of large boosters.

When a large number of engines are used, multiple-nozzle effects may be observed. One may assume that two peaks in the sound pressure level produced by a multiple-nozzle booster may be measured. One peak would be produced by the combined effect of all engines, and the other peak produced by the single engines. The result would be a lower frequency peak produced by combined engines and a higher frequency peak produced by the single engines. An example of this effect is shown in Fig. III-4. The second peak in the Saturn data is much lower than would be predicted. In addition, not all the Saturn data show the higher frequency peak. More data are required on this phenomenon before an accurate prediction of its effects can be made. For the purpose of this report, it will be assumed that only one peak exists since the generalized spectrum includes both of the previously described peaks.

The present concepts for the Post-Saturn booster engine include such configurations as plug engines. Because of the differences in the exhaust jet produced by these and conventional engines, the noise spectrum produced may also differ. As an example, the effective diameter of the plug engine may be the jet diameter at the bottom of the plug and not at the nozzle exit. Thus, both the frequency and amplitude would change. A detailed study of these changes is beyond the scope of this report. More data from model studies are anticipated in the near future and may be compared to the predicted levels when available. The values used in this report should be slightly conservative and can be safely used.

The directivity index is defined as the deviation, in decibels, from spherical radiation. Rocket engines have produced a highly directive noise field as shown in Fig. III-5. An example of the effect of radiation patterns and the effect of a moving sound source, is shown from Saturn data in Fig. III-6. The radiation pattern and effect of a moving sound source for multimillion-pound thrust clustered engines was determined by Wilhold, et al. (Ref 8). The radiation index was combined with velocity (doppler frequency shift) effects to determine a distribution factor. The power level, radiation index, and excess attenuation terms were computed for Saturn I. Data from the SA-2 flight were then examined and the distribution factor determined by correlating the measured data with calculated levels. For convenience, the directivity index used in this document was derived from the distribution factor in Ref. 8.

Thus, the terms of Eq [III-3] have been evaluated and the acoustic levels produced by a Post-Saturn booster can be predicted.

The sound pressure levels for the community area surrounding MILA were predicted for Post-Saturn engines of the upper and lower thrust ratings shown in the following tabulation.

Item	T10RR-2	T10RR-3
Thrust (Total) $(lb \times 10^6)$	29.8	20.4
Type of Engine	Lox/RP-1 Cluster	Lox/LH_2 Plug
Number of Engines	4	18
Nozzle Diameter (ft)	30	9.4
Specific Impulse (sec)	278	373
Nozzle Velocity (fps)	8950	12,000

The predicted levels, for a standard day, are shown in Fig. III-7 thru III-10.

Post-Saturn predictions were made since they represent the worst case within present planning. Saturn V predicted levels are also shown in Fig. III-8 and III-9.

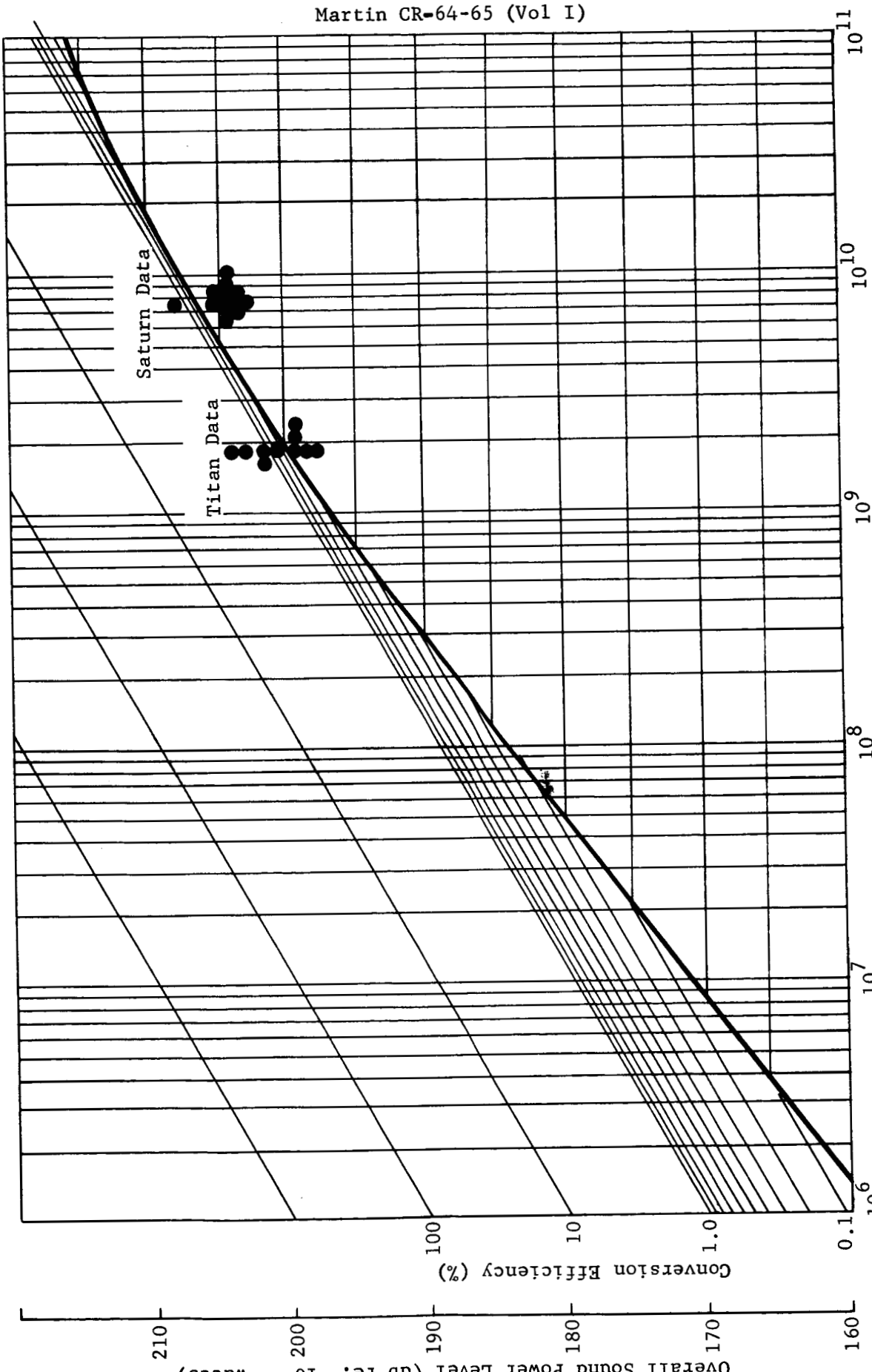

Fig. III-2 Overall Acoustic Power vs Jet Stream Mechanical Power

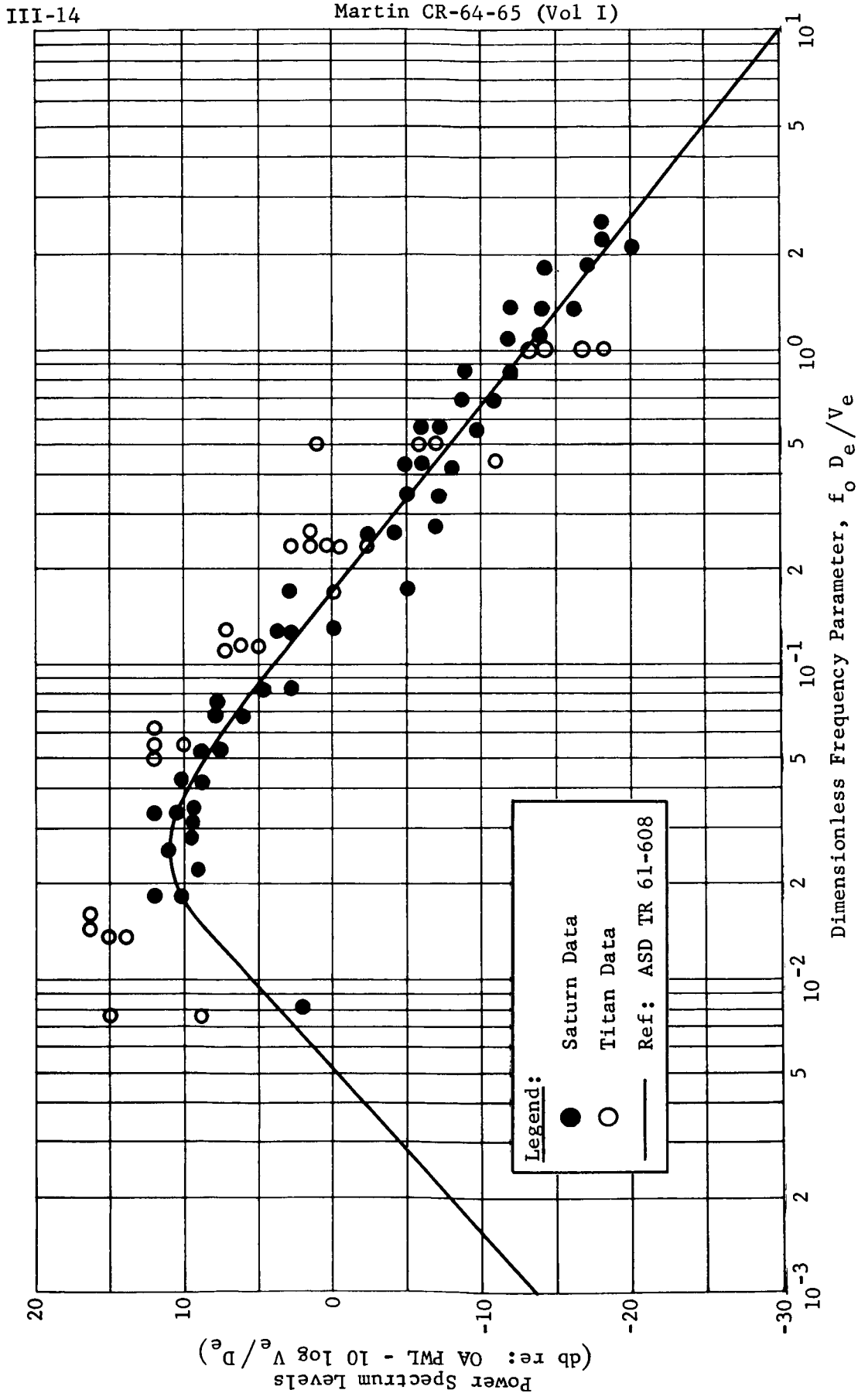

Fig. III-3 Generalized Power Spectrum of Rocket Noise Sources

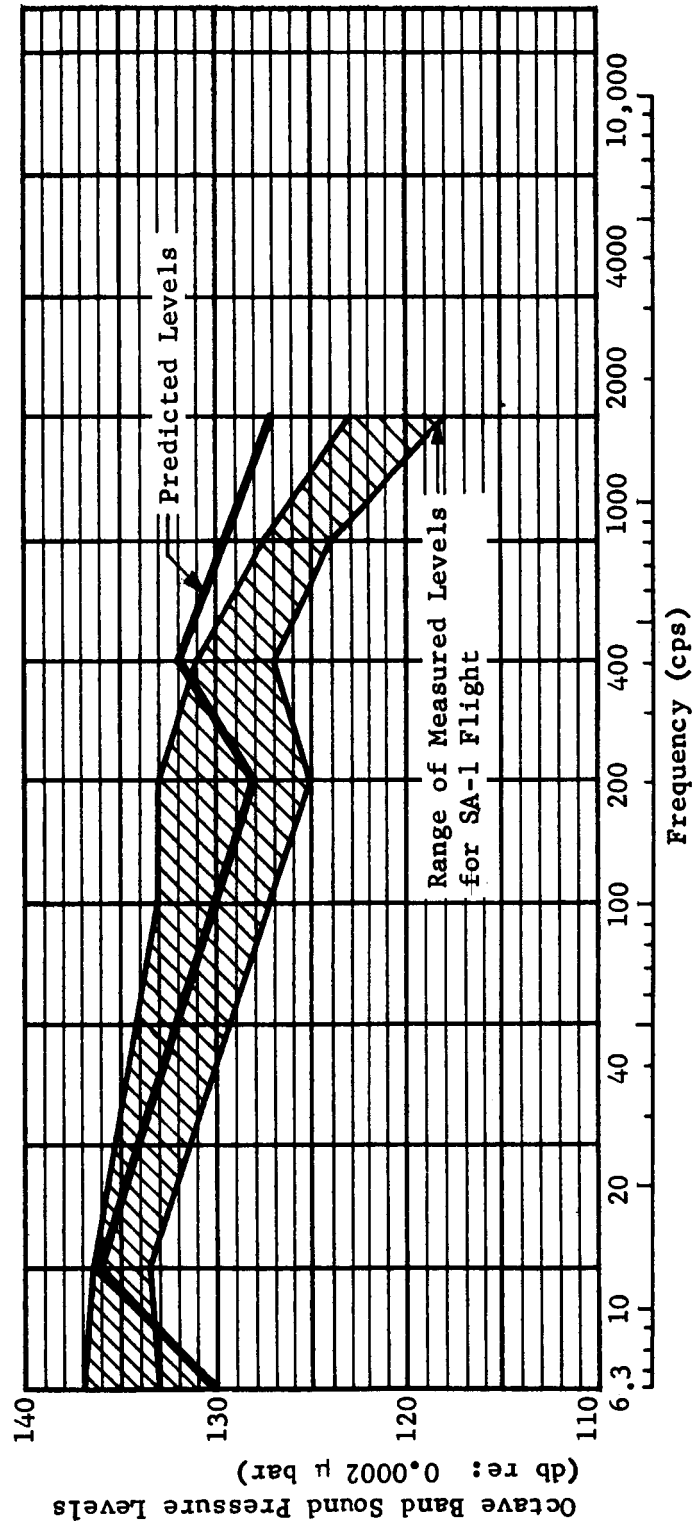

Fig. III-4 Apparent Multiple Nozzle Effect from Predicted and Measured Saturn Data

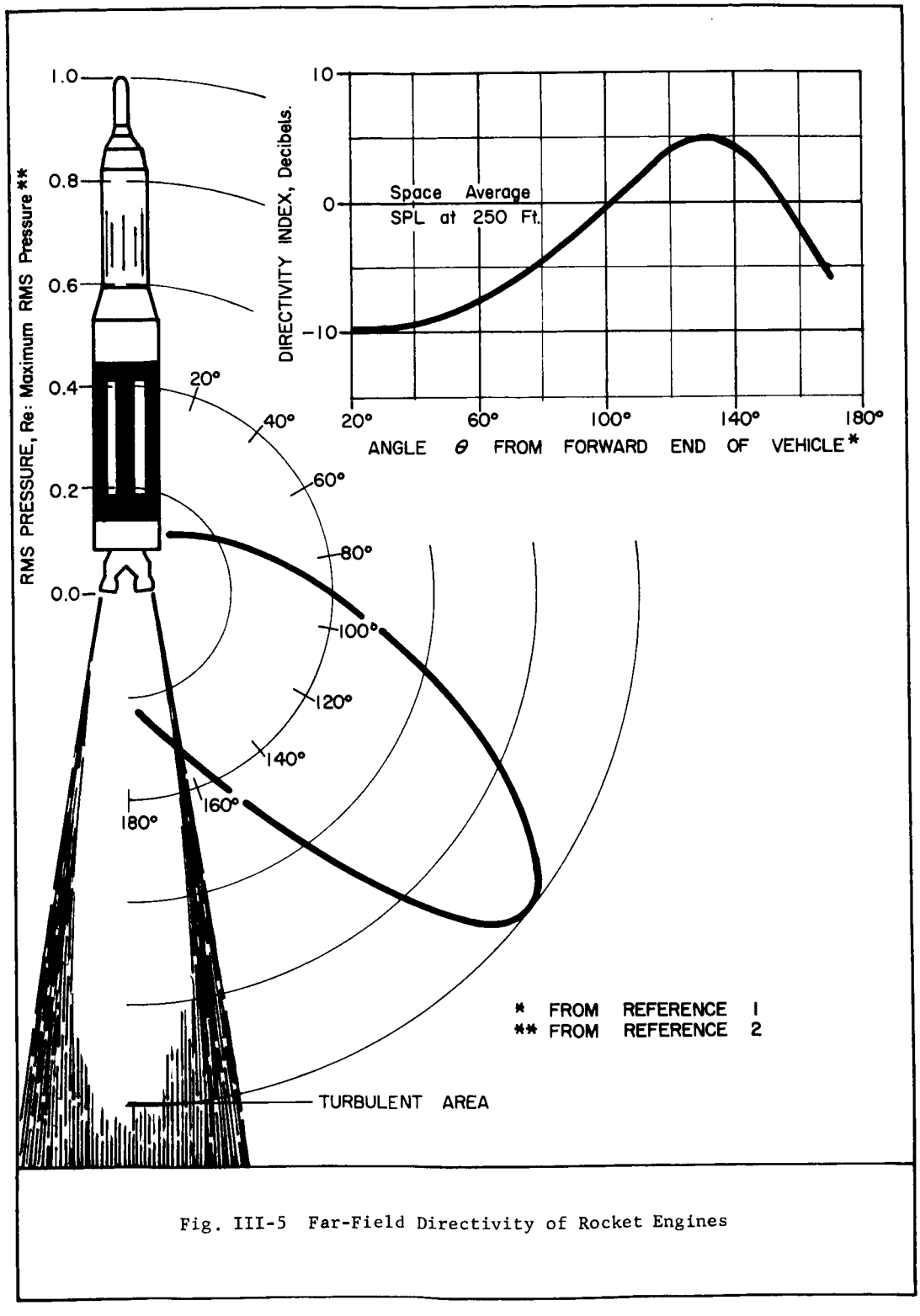

Fig. III-5 Far-Field Directivity of Rocket Engines

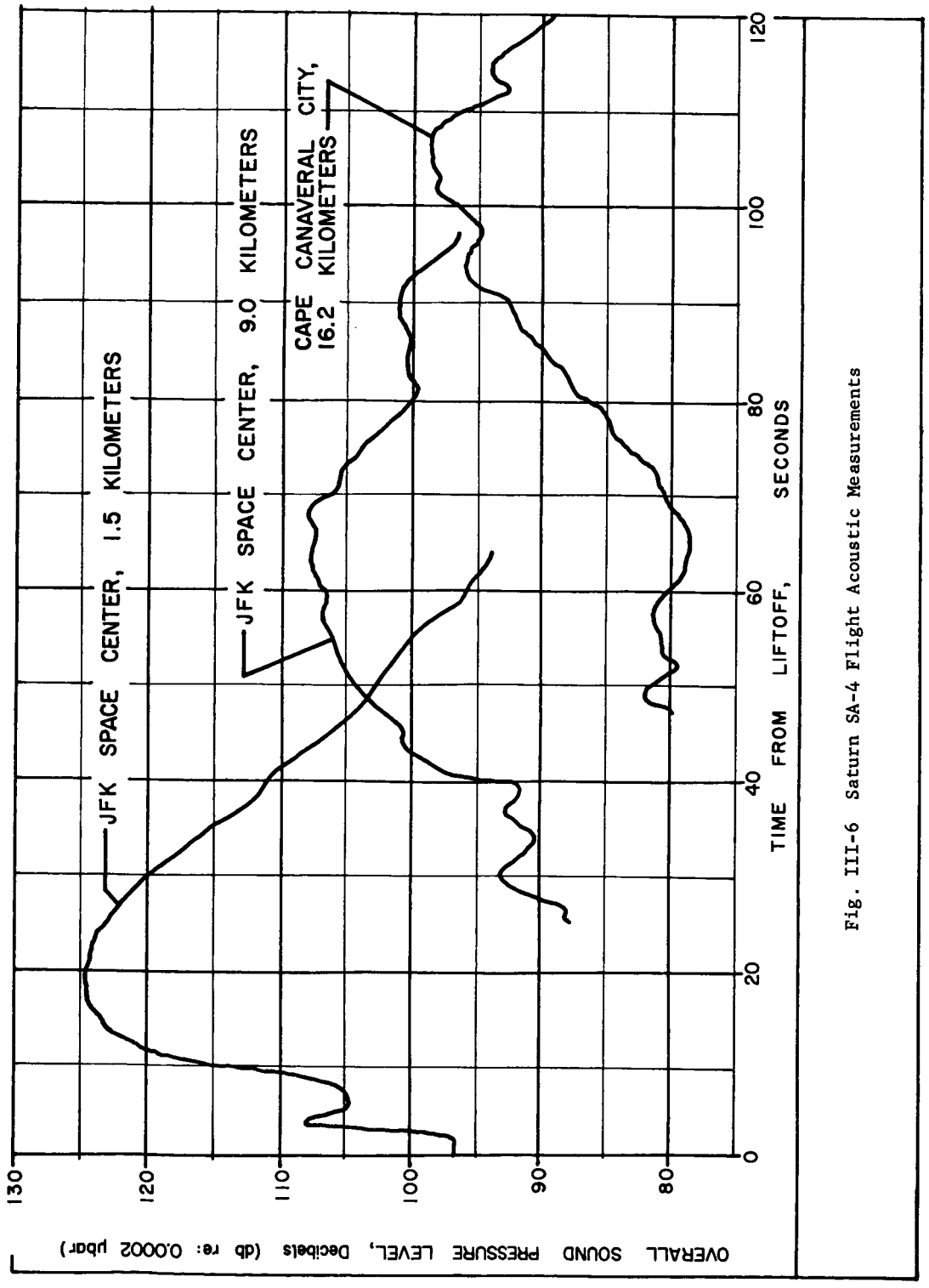

Fig. III-6 Saturn SA-4 Flight Acoustic Measurements

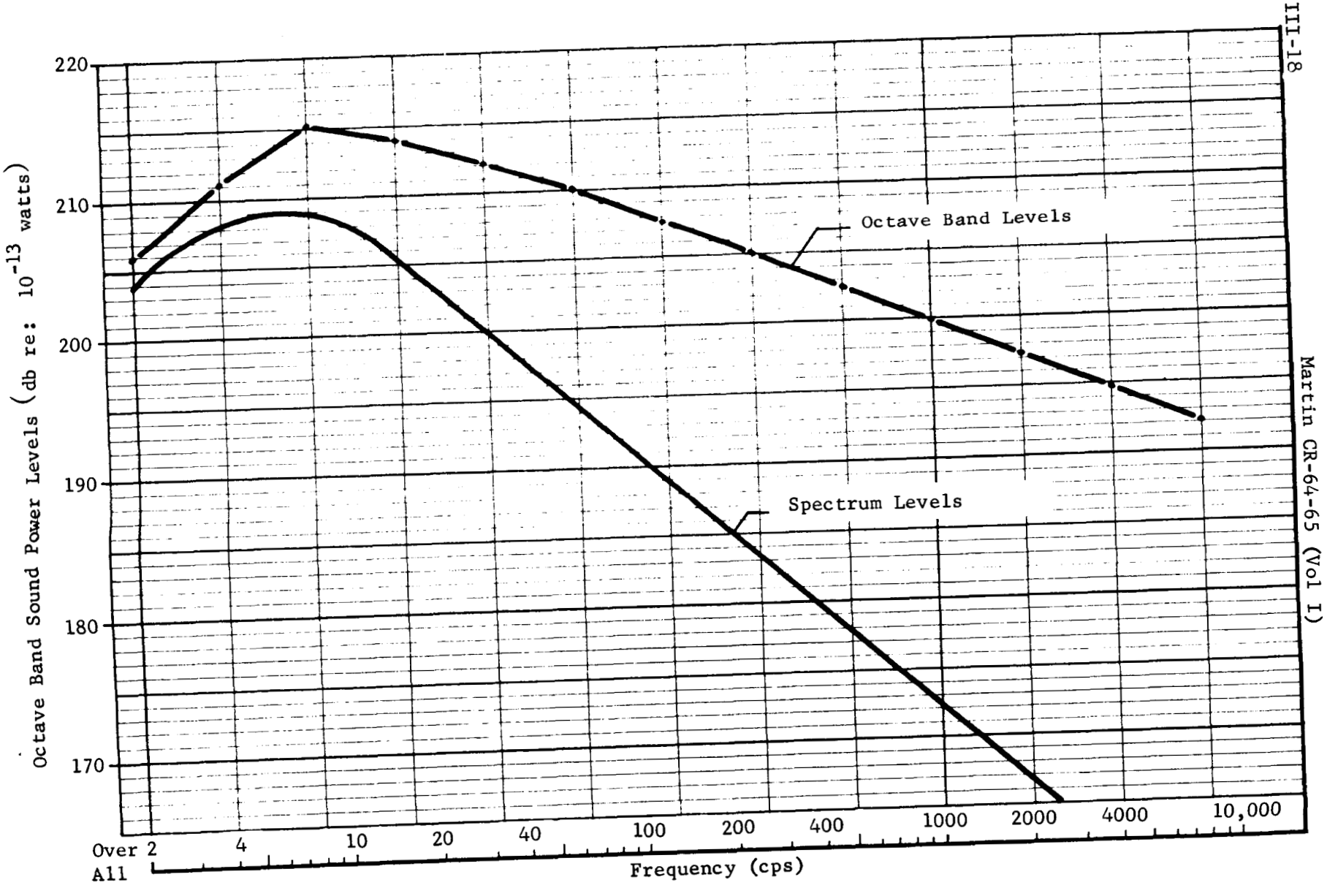

Fig. III-7 Post-Saturn Booster Engine Acoustic Power Levels, 20.4 to 29.8 x 10^6 lb of Thrust

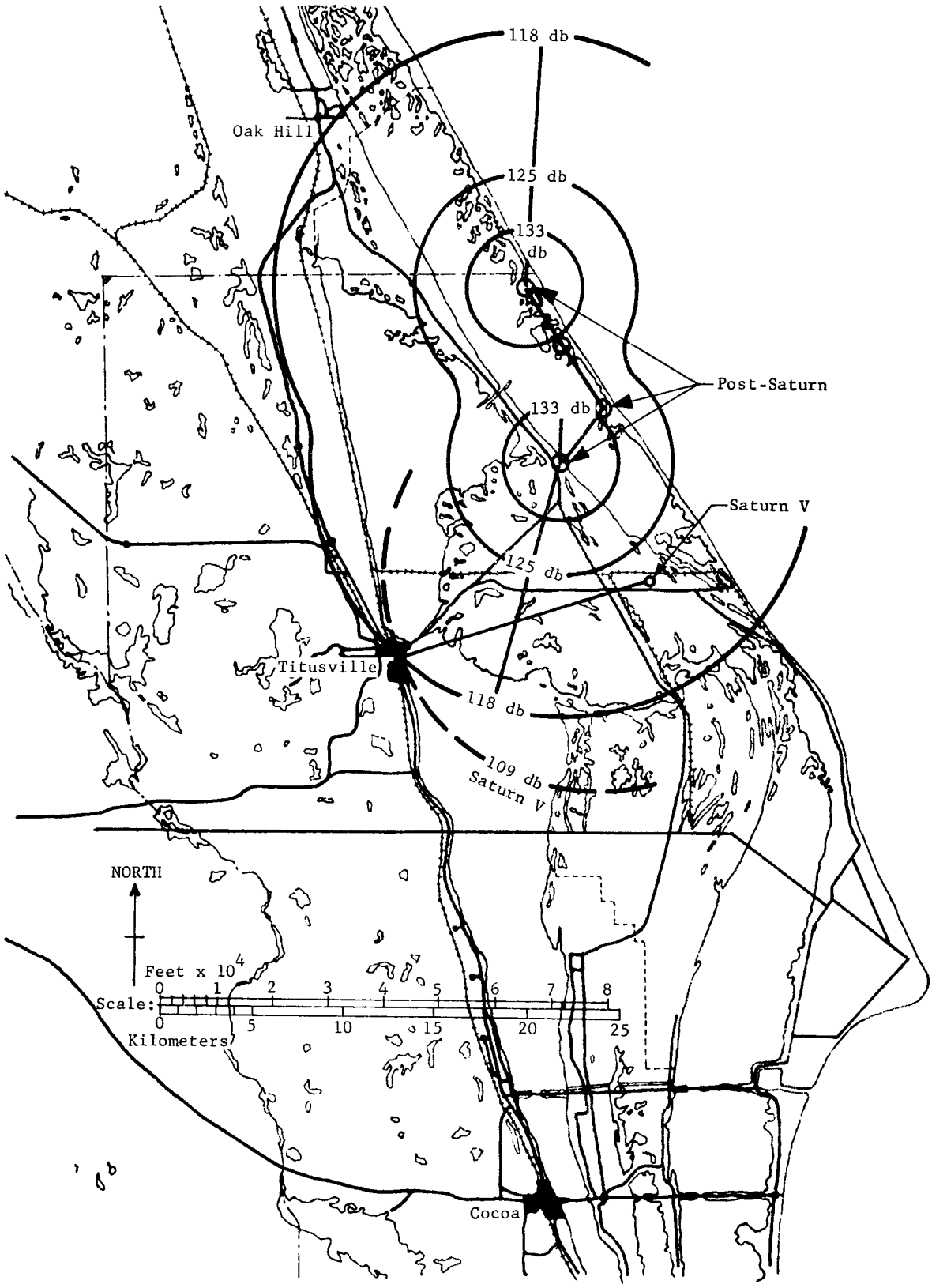

Fig. III-8 Predicted Post-Saturn and Saturn V Sound Pressure Levels

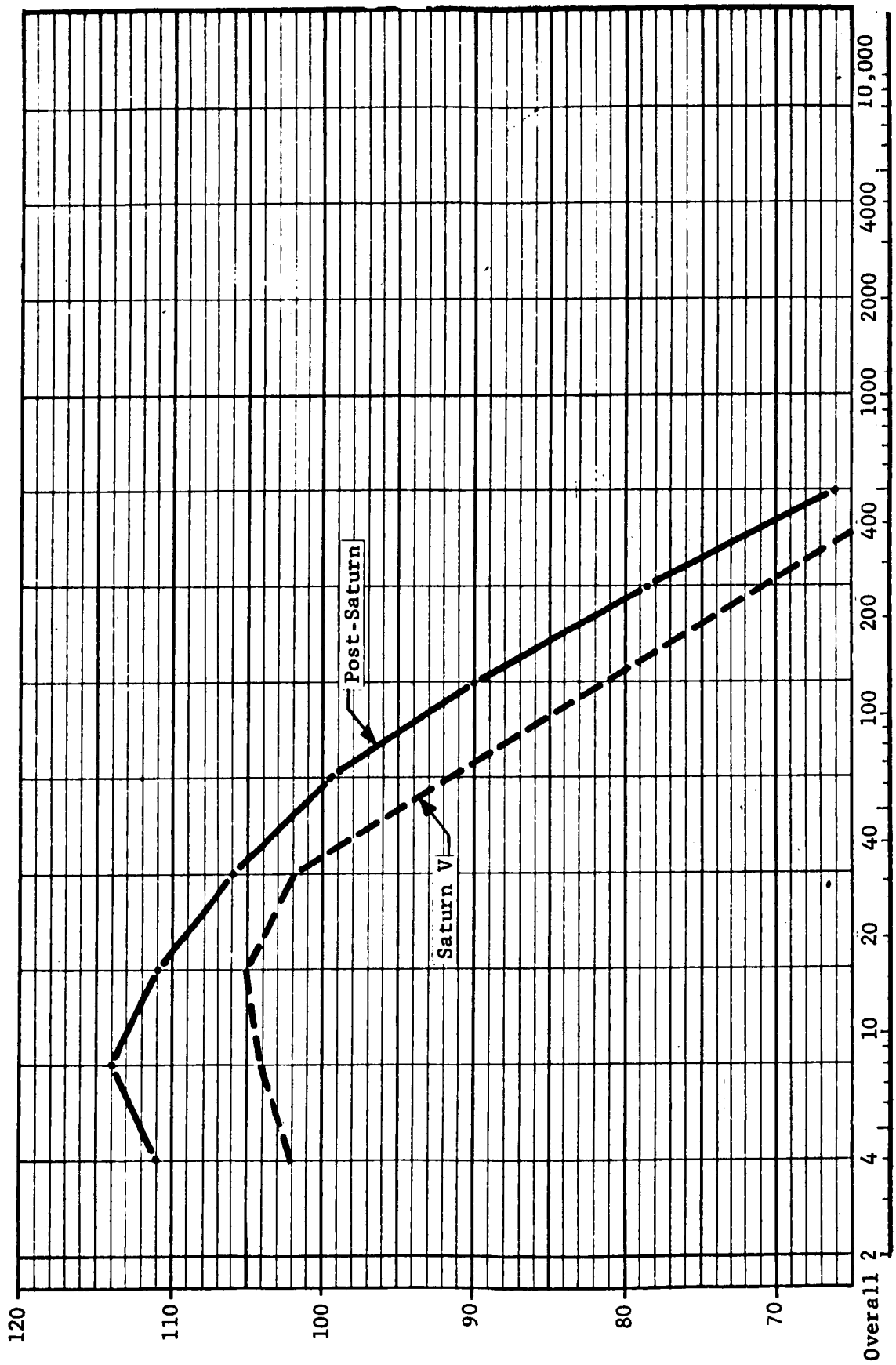

Fig. III-9 Post-Saturn and Saturn V Noise Levels in Titusville, Florida

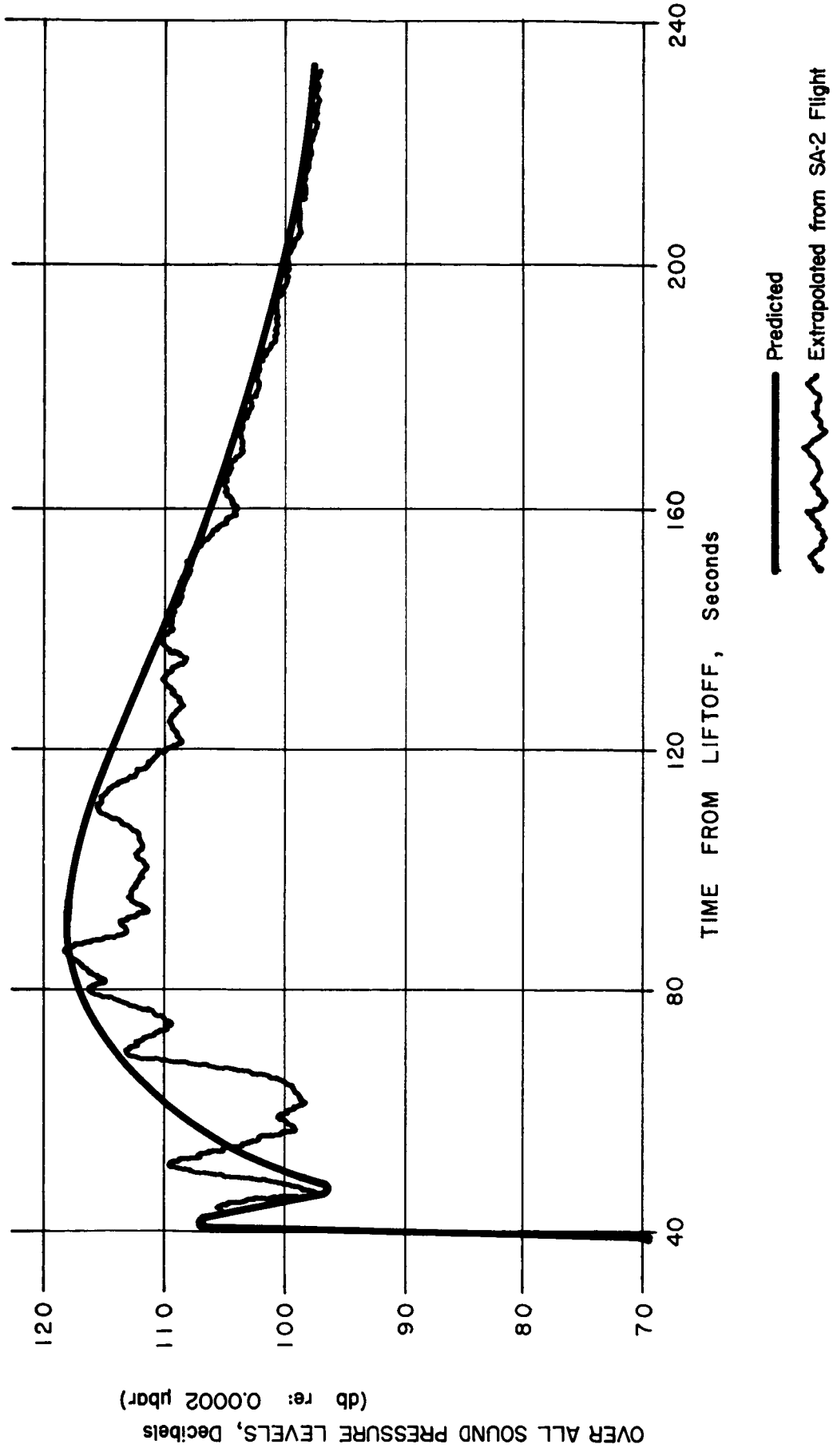

Fig. III-10 Post-Saturn Acoustic Time History in Titusville, Florida

2. Atmospheric Effects

The multilayered atmosphere method of analyzing the sound focusing problem was used in this study. The atmosphere is divided into horizontal layers whose boundary conditions are defined by meteorological data taken at different altitudes. The meteorological data used to calculate the velocity of sound profile include temperature, wind velocity, and wind direction. It is assumed that the velocity of sound varies linearly with altitude for a given azimuth.

This means that for a given layer the velocity of sound is not constant but changes at a constant rate.

When the velocity-of-sound profile has been calculated, the ray path for a given starting angle (θ_o) may be determined.

When the ray is passing through a layer, one of three things will occur. If the velocity gradient is zero, the ray will be undeflected; if the gradient is positive it will be bent back towards the earth; and if the gradient is negative, the ray will be deflected upwards. An atmosphere in which all of the layers have zero or negative gradients will never result in focusing on the surface of the earth.

Since focusing is determined by the velocity profile, and certain types of velocity-of-sound profiles occur frequently, a set of basic types has been established with the maximum sound pressure level increase obtainable for each type. These are shown in Fig. III-11.

An approximation of the possible sound pressure level increase due to concentration of the acoustical energy may be made by classifying the velocity of sound profile in one of the basic categories. The range at which the intensification occurs is calculated by tracing ray paths for different starting angles (θ_o) and determining where they converge. In the calculation a method is used that calculates only the landing points of the rays with various starting angles.

Category	Description		Amplification Factor
0	No Velocity Gradient		0
1	Single Negative Gradient	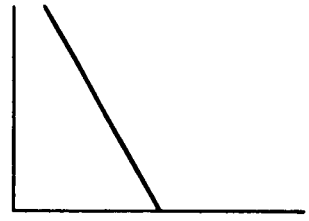	-5
2	Single Positive Gradient	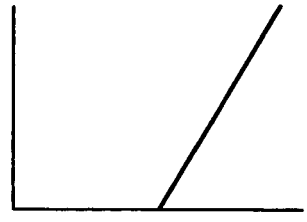	5
3	Zero Gradient Near Surface with Positive Gradient Above	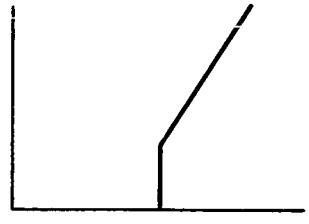	10
4	Weak Positive Gradient Near Surface with Strong Positive Gradient Above	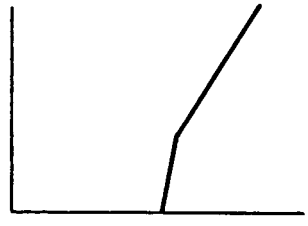	25
5	Negative Gradient Near Surface with Strong Positive Gradient Above	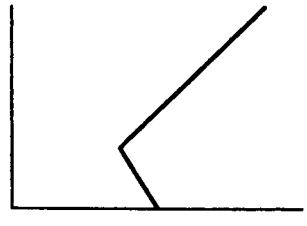	100

Fig. III-11 Acoustic Velocity Profile Categories

The limitation in the accuracy of this method is primarily a function of how well the earth's atmosphere resembles the model of the atmosphere as depicted by the meteorological data and our basic assumptions. If meteorological data are recorded at 500-ft intervals and there exists a region somewhere between the 1000- and 1500-ft boundaries that contained a wind only 5 mph higher than that measured at the 1500-ft level, the focal zone would be moved several miles closer to the source (Ref 9). Tedrick has postulated this to be the cause of a discrepancy that was noted between calculated focal zones and horn data. This limitation may be minimized by taking more data at closer intervals.

Another assumption that is not always valid in the physical atmosphere is that the wind is parallel to the earth's surface. This is usually a safe assumption to make but, when a front is passing through the region, strong up or downdrafts will be present. This limitation is a basic weakness of the system that requires data not now available. Currently no regular data are taken that include the vertical component of the wind.

Finally, it is impossible to measure the temperature and wind velocity and direction with unlimited precision. This introduces another uncertainty that may cause the physical atmosphere to be imperfectly represented by our model used to calculate the focal zones.

Typical meteorological readings available for MILA are taken at the surface, 500, 2000, 3500, 5000, 6600, 8300, and 10,000 ft above the surface.

The large intervals between data restrict the precision of the predictions, although this method provides the best method currently devised for determining acoustic focusing. Analysis of data from more years will give a higher degree of reliability to the predictions that have been made.

B. THEORY

The velocity of sound must be calculated at each boundary from the meteorological data. A good approximation to the velocity of sound in still air is obtained from the relation (Ref 13):

$$C(T)_i = 1052.03 + 1.106\ T_i. \qquad [III-8]$$

where $C(T)_i$ = velocity of sound in still air.

Wind must be added vectorially to the velocity of sound in still air yielding:

$$C_i = C(T)_i + C(WIND)_i$$

$$C_i = 1052.03 + 1.106\ T_i - V_i \cos\left(\theta - \alpha_i\right) \qquad [III-9]$$

where

C_i = speed of sound in the i^{th} layer,

T_i = temperature in the i^{th} layer,

V_i = velocity of wind in the i^{th} layer,

φ = azimuth for the velocity profile,

α = direction of the wind in the i^{th} layer.

When the velocity of sound is known at each boundary layer, the velocity gradient may be found. It is assumed to be constant and may therefore be calculated directly from the boundary conditions of the layer.

$$u_i = \frac{d\ C_i}{d\ Y_i} = \frac{C_i - C_{i-1}}{Y_i - Y_{i-1}} \qquad [III-10]$$

where

Y_i = altitude of the i boundary above the surface of the earth (ft).

The velocity of sound at any altitude then could be calculated as:

$$C = C_{i-1} + u_i \left(Y - Y_{i-1}\right) \qquad [III-11]$$

The ray paths are dependent upon the velocity profile and the starting angle (θ_o). The type of path the ray takes is determined by the relation:

$$\sin \theta_i = \sqrt{1-\left(\frac{C_i}{C_o}\right)^2 (\cos \theta_o)^2}. \qquad [III-12]$$

where C_o is the sound propagation velocity on the surface. If the radicand is negative or zero, the ray is refracted to earth in the i^{th} layer. If, however, the radicand is positive, the ray traverses the i^{th} layer.

The ray may be refracted back to earth only from a layer in which the velocity gradient (u_i) is positive. If the velocity gradient is negative or zero, the ray will be bent upwards if it is negative and will be undeflected if it is zero.

If the ray is not bent back in the i^{th} layer, we are interested in calculating the horizontal distance it travels in traversing that layer.

Either

$$C_i = C_{i-1} \text{ or } C_i \neq C_{i-1}$$

If $C_i = C_{i-1}$, then $\theta_i = \theta_{i-1}$ and

$$X_i = (Y_i - Y_{i-1}) \cot (\theta_{i-1}) \qquad [III-13]$$

and X_i = horizontal distance traveled by this ray in the i^{th} layer. If, however,

$$C_i \neq C_{i-1},$$

$$X_i = \frac{C_o \left[\sin(\theta_{i-1}) - \sin (\theta_i)\right]}{(u_i) \cos (\theta_o)}. \qquad [III-14]$$

If the ray reaches a maximum value in the k^{th} layer and is turned back it will return to earth symmetrical about this vertex. Therefore, the landing point of the ray which has a given starting angle θ_o will be given by the relations:

$$X = 2 \left[\sum_{i=1}^{k} X_i + \frac{C_o \left[\sin(\theta_{k-1})\right]}{(u_k) \cos (\theta_o)}\right], \qquad [III-15]$$

where the X_i's are horizontal distances in passing through the respective layers and are calculated by the appropriate relation given above in [III-13] or [III-14].

By then choosing a new starting angle and repeating the process, a series of rays will be traced and the landing point determined. By examining the landing points and the velocity profile, it is possible to determine if intensification of acoustical energy has occurred and at what range.

Assigning a value to the sound pressure level as a function of distance from the source under conditions of focusing is somewhat more difficult, and at present is more in the form of an art than an exact science. This is done by placing the velocity of sound profile in one of the basic categories and examining the density of rays at this point to determine the approximate sound pressure level.

The methods described above were used to analyze meteorological data from MILA. The data that were analyzed include all rawinsonde data we have for November 1956 to November 1958.

Both the velocity of sound profiles and the landing points of all rays refracted back to earth were calculated for each set of data. The percentage of time that focusing of Types 0 thru 5 occurred is shown in Fig. III-12 thru III-16. The maximum percentage of time that focusing could produce a maximum 15-db increase over the predicted level of 118 db is shown in Fig. III-17.

The results of this part of the study are quite conservative. The sound pressure levels shown in Fig. III-12 thru III-16 are the maximum that would occur for that focusing condition. The percentage of time when a maximum level of 133 db would occur, as shown in Fig. III-17, are representative of the general focusing considered.

Acoustic focusing studies conducted by NASA at the Mississippi Test Facility revealed the 15-db focusing condition to be excessive and 5 db to be the general case. It must be pointed out, however, that focusing conditions have occurred in the past which could produce higher sound pressure levels than 133 db. In order to evaluate these conditions, a more detailed study than was possible under this contract should be conducted. For the purpose of this study, a maximum sound pressure level of 135 db will be considered.

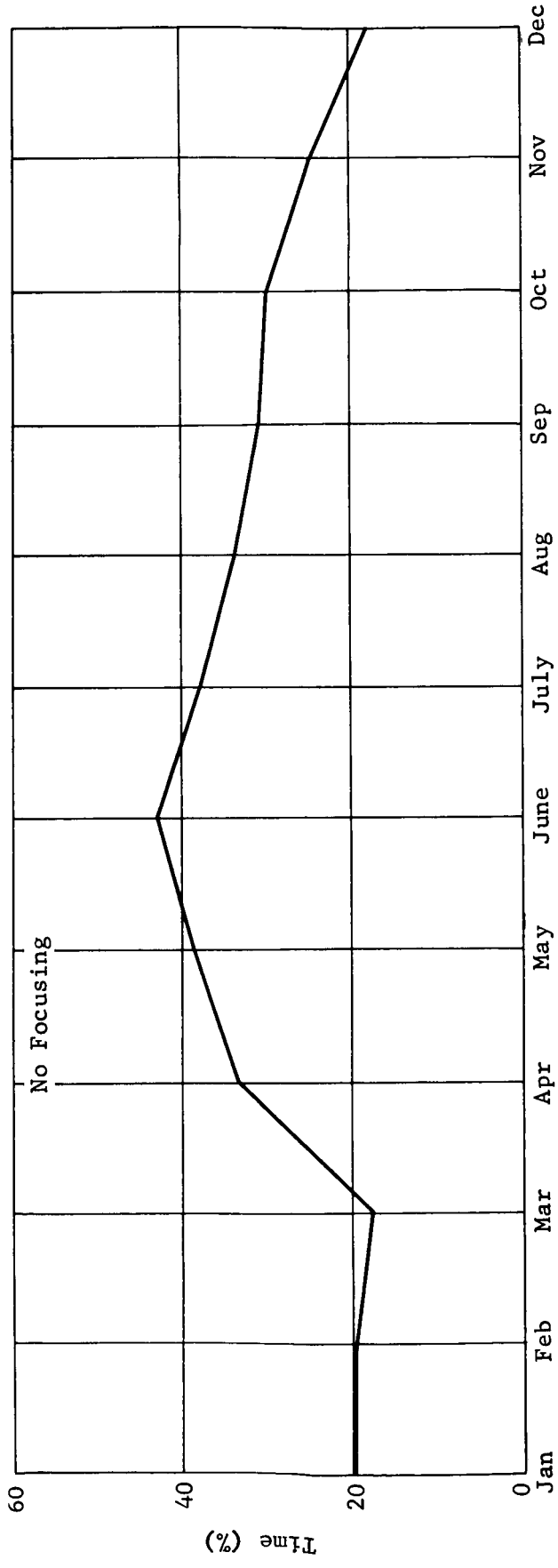

Fig. III-12 Percent of Time When no Focusing Occurred, 217-deg Azimuth (Titusville), Velocity Profile Types 0 and 1

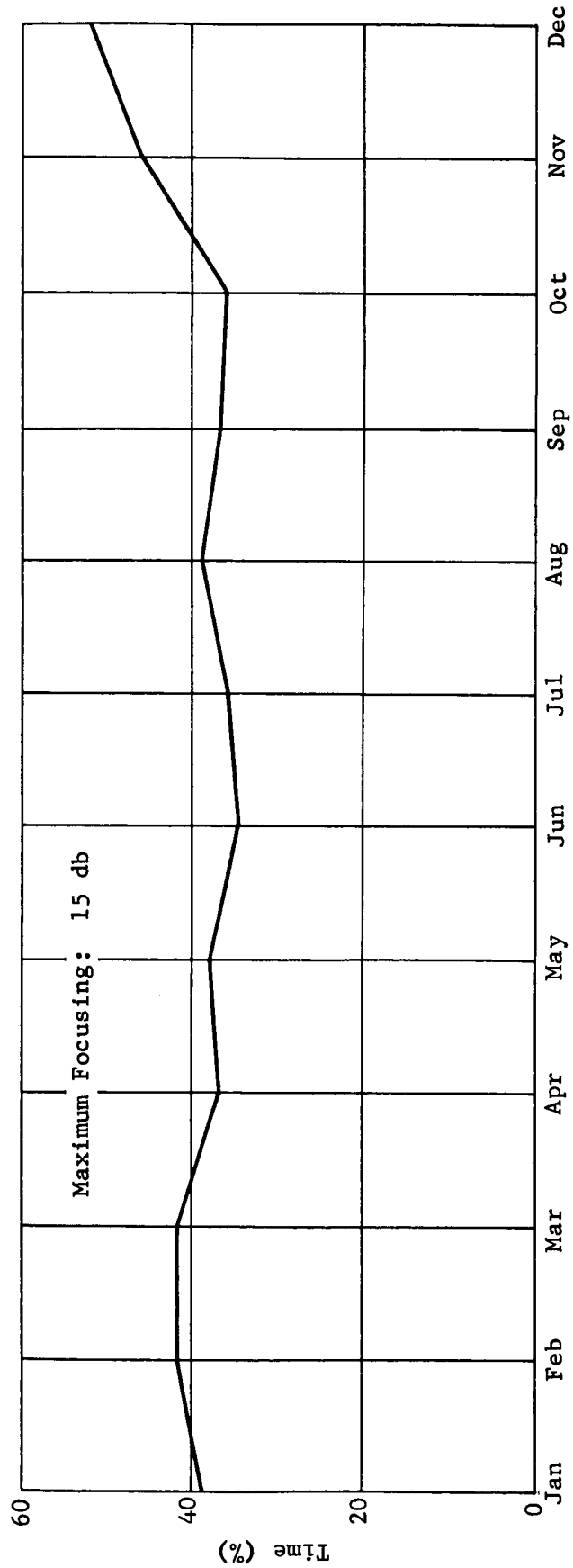

Fig. III-13 Percent of Time When Velocity Profile Type 2 Occurred, 217-deg Azimuth (Titusville)

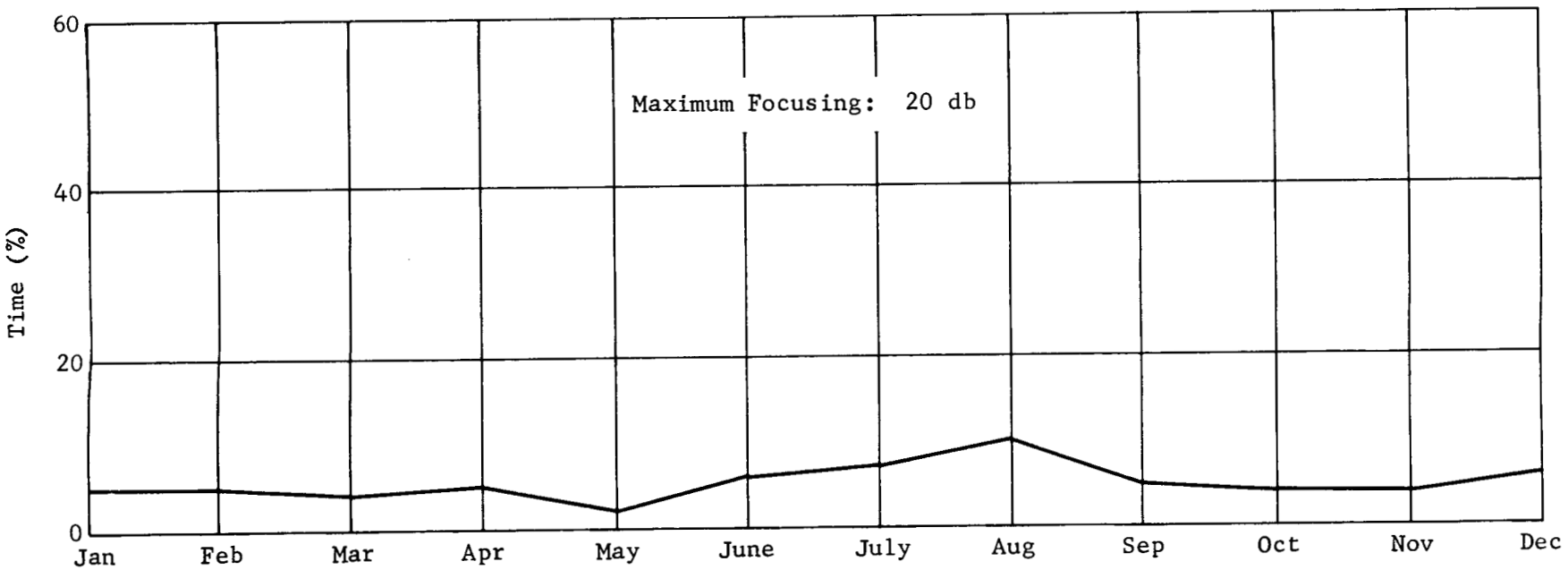

Fig. III-14 Percent of Time When Velocity Profile Type 3 Occurred, 217-deg Azimuth (Titusville)

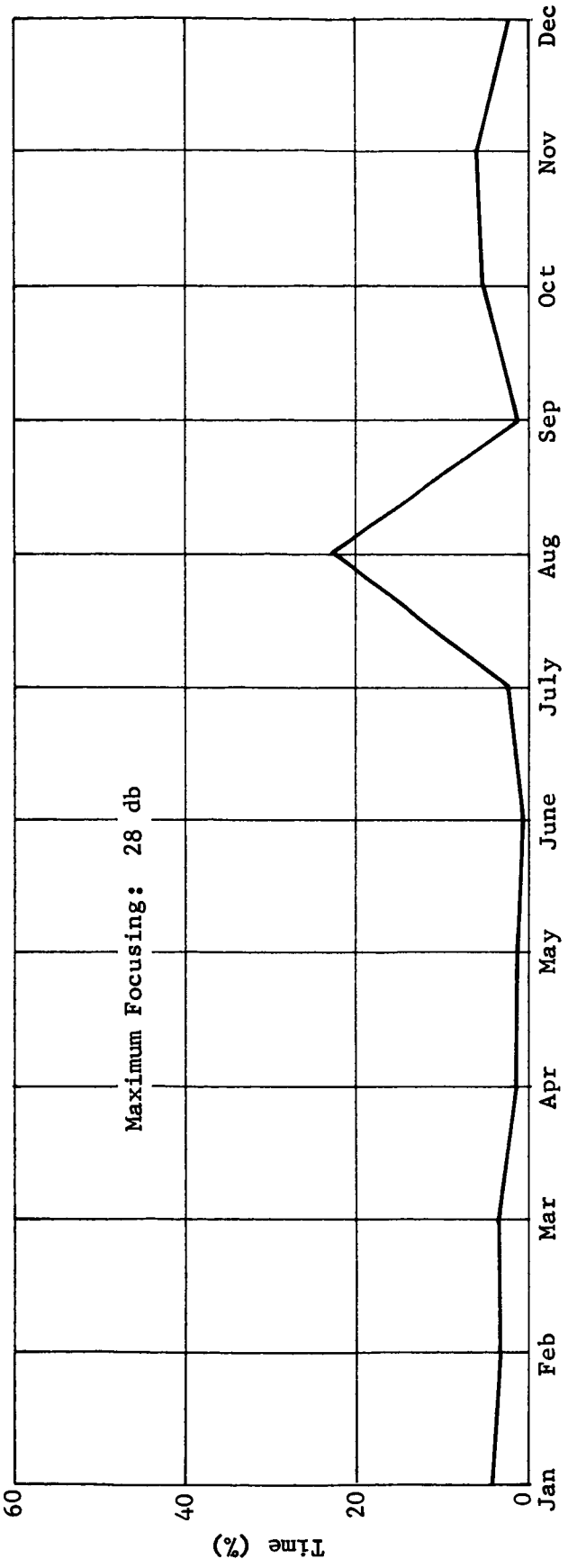

Fig. III-15 Percent of Time When Velocity Profile Type 4 Occurred, 217-deg Azimuth (Titusville)

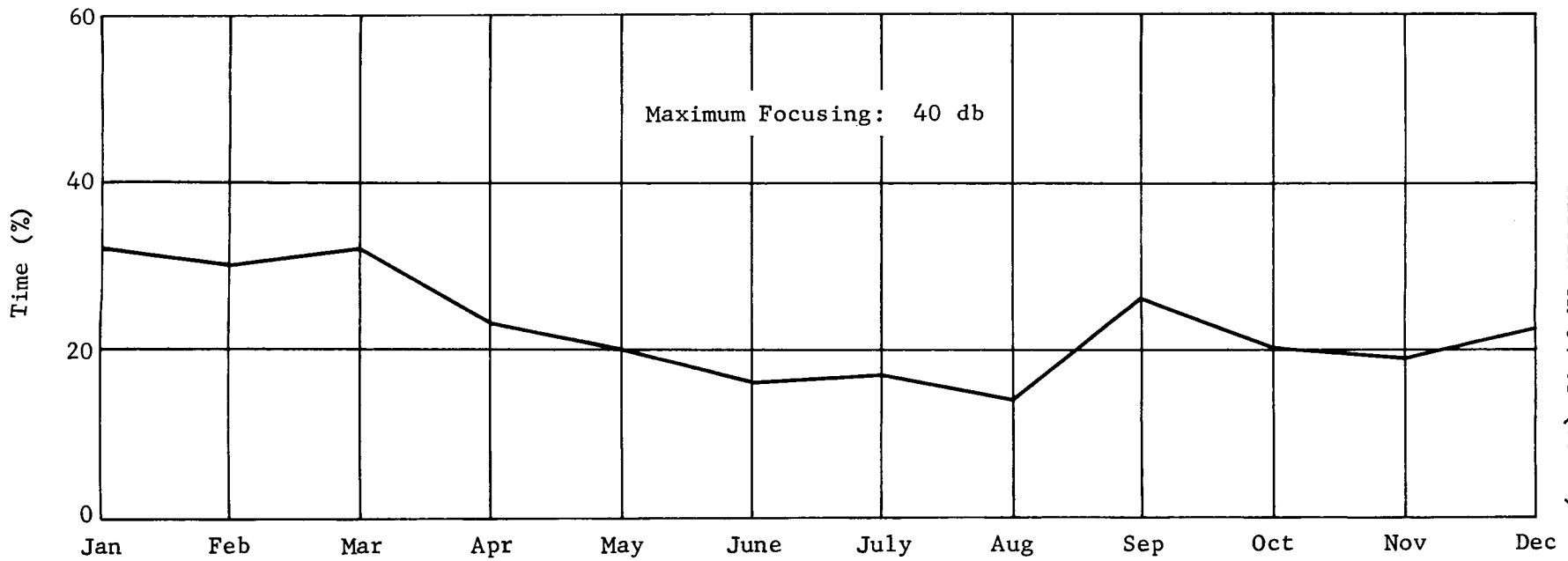

Fig. III-16 Percent of Time When Velocity Profile Type 5 Occurred, 217-deg Azimuth (Titusville)

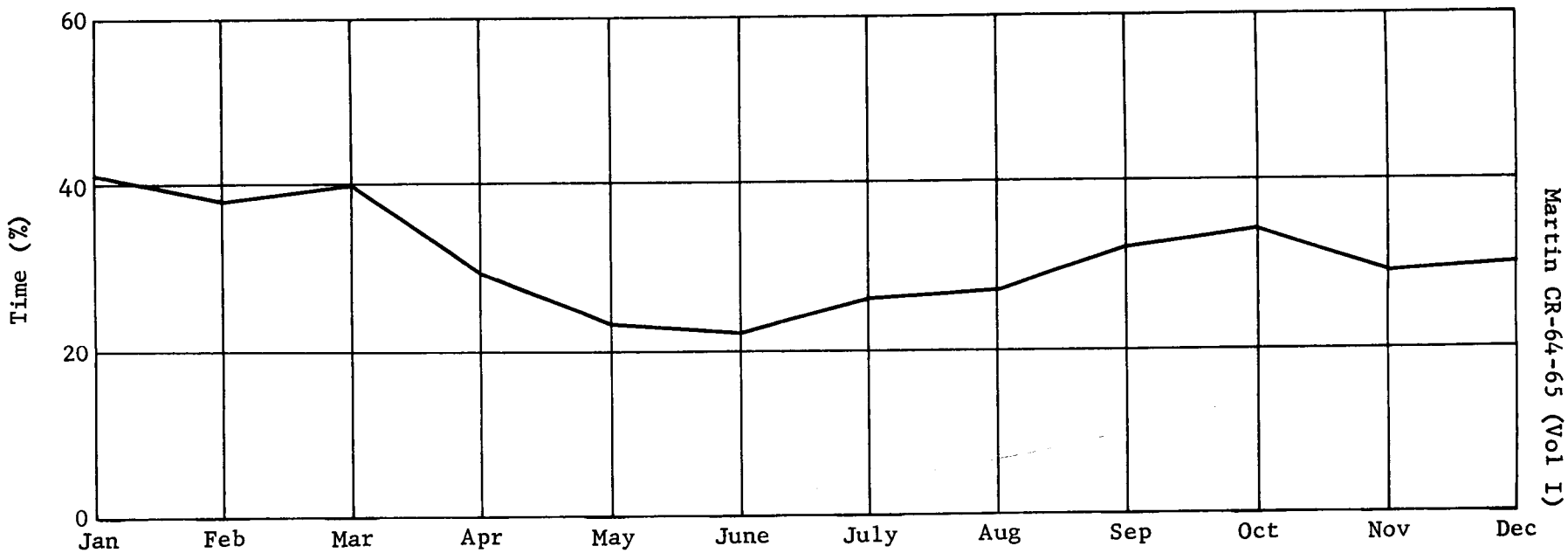

Fig. III-17 Maximum Time that Focusing Produces Sound Pressure Levels Exceeding 133 db in the Titusville Area

Data from Saturn flights SA-1 thru SA-6 were examined to determine the effect of focusing. These data were measured by Test Division, MSFC, and LVO, JFKSC, and are shown in Fig. III-18. Angular position was not considered since the noise field should be axisymmetric when the vehicle is in flight. It is obvious that the spread of data increases with increasing distance. This appears to be reasonable since those factors that affect noise propagation, i.e., temperature, humidity, wind, turbulence, ground absorption, etc, have more time to operate on the noise. Some of the spread may also be caused by differences in engine performance and errors in measurement. Thus, the spread of data should include all of the outside factors that affect wave propagation without identifying them individually. The mean value of the data was determined at distances where eight or more measured data points are available. The mean values agree closely with calculated values for Saturn I.

The mean line of Fig. III-18 is drawn as a best-fit curve to the calculated mean sound pressure levels at 5,000, 15,000, 30,000, 50,000, and 75,000 ft. At each of these distances, the mean and the standard deviation (s_n) of the sound pressure levels was calculated. Then, using tables that give the fraction of the infinite population that lies below the mean (these are one-sided tables) by a given number of standard deviations as a function of sample size, the 95% line of Fig. III-19 was calculated. This line says that for a distance of 18,000 ft from the pad, 95% of the sound pressure level data will be equal to or less than 120 db. In other words, considering all of the factors that contribute to the measured sound pressure level at 18,000 ft, fully 95% of the firings will produce sound pressure levels below 120 db. The mean line gives a separation distance for 120 db of only 9000 ft, but the data show that the sound pressure level can be expected to exceed 120 db on 50% of the firings. It is obvious from Fig. III-19 that the standard deviation, which is a measure of the "spread" of the data, increases with increasing distance.

For a separation distance of 10 mi (distance from Post-Saturn launch to Titusville), we find there is a spread of 12 db between the 50% line and 99% line. Assuming the launch conditions to be the same for Post-Saturn as for Saturn I, there is a 99% confidence that the sound pressure level would not exceed 130 db (118 db predicted plus a 12-db spread). Thus, the conclusion of no more than 15 db focusing as a criterion seems to be a safe assumption.

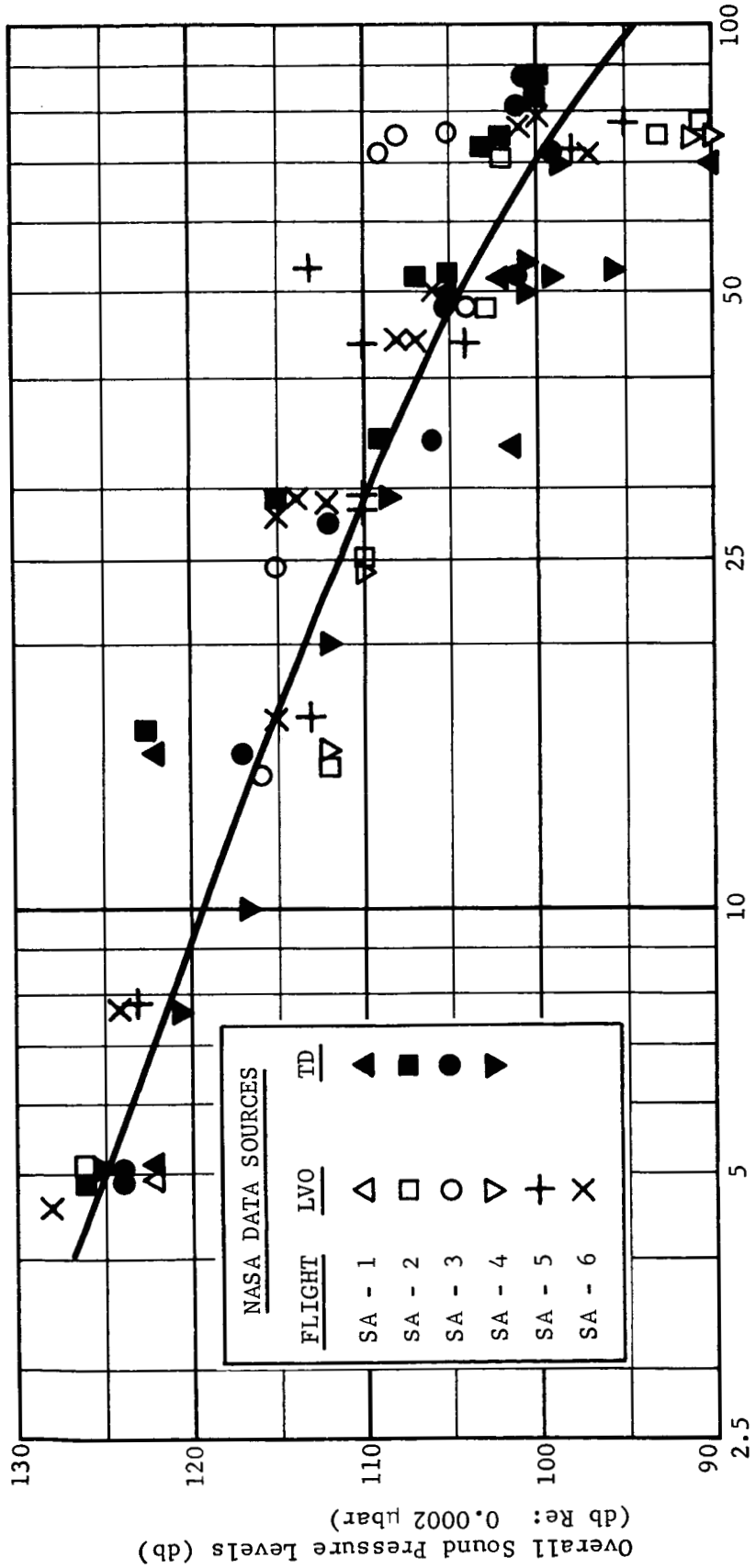

Fig. III-18 Maximum Noise Levels at Ground Elevations Resulting from SA Flights

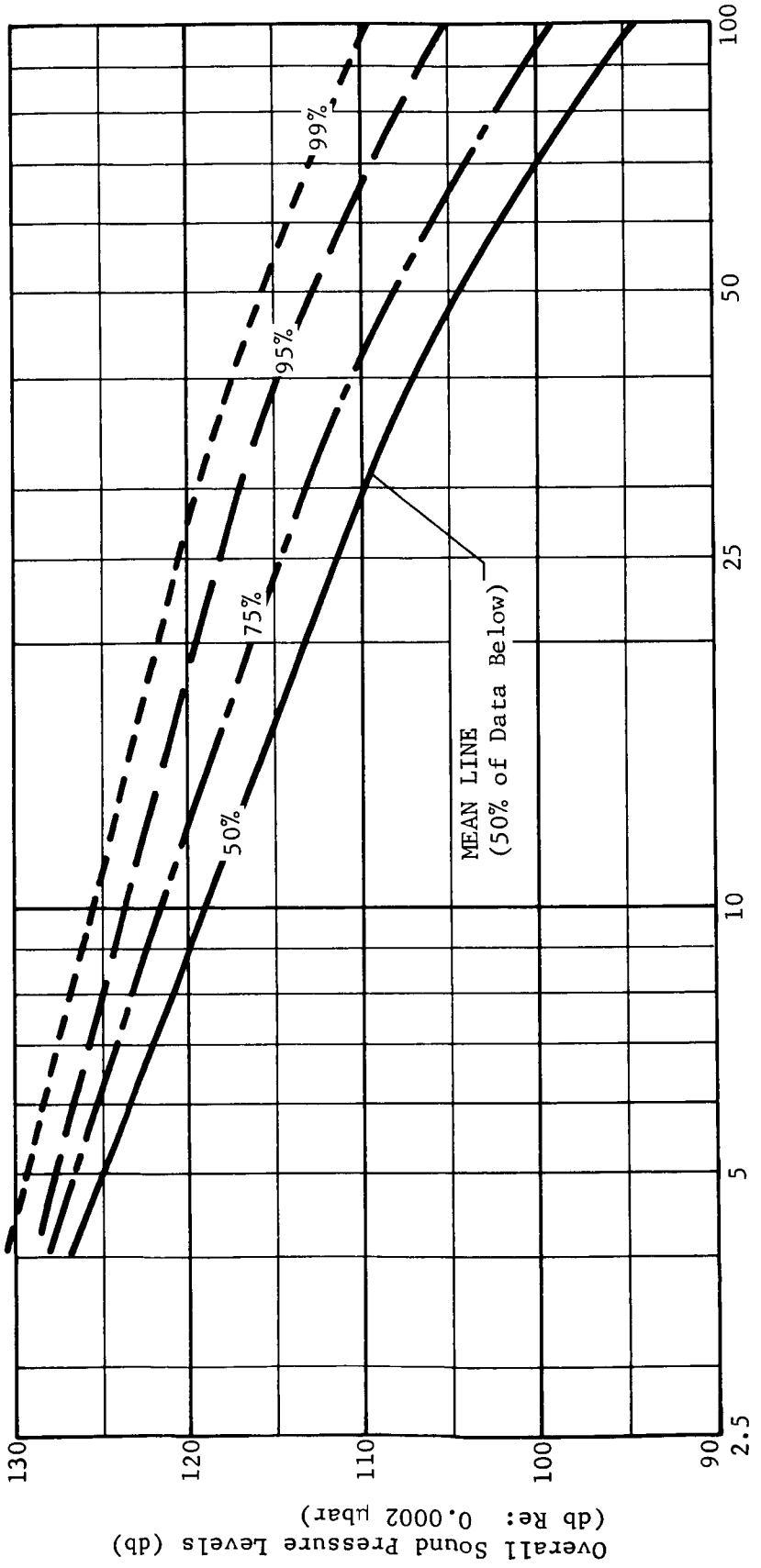

Fig. III-19 Maximum Noise Levels at Ground Elevations Resulting from Saturn I Flights (Mean-Line and Noted Population Lines)

C. DYNAMIC RESPONSE OF WINDOWS

The problem of dynamic response of glass windows to noise pressure is extremely complex. There exist a number of uncertain factors that may highly affect the result of analysis, such as edge conditions, damping factors, imperfections and irregularity of materials, and stress concentrations. Moreover, the problem is further complicated by the nonlinear response to sinusoidal as well as random excitations. It is therefore necessary to simplify the basic assumptions and methods of analysis and use experimental data to evaluate certain physical behavior of glass panels.

1. Basic Assumptions

The panel is assumed to be a single-degree-of-freedom system vibrating at a frequency equal to a model frequency of the plate. Total response of the panel can then be obtained by superposition of responses to each vibrating mode, commonly known as the method of model superposition.

Glass is assumed to be linearly elastic, homogeneous, and isotropic. Deflections and displacements of plate surface are taken as very small in comparison with plate thickness. With these assumptions, the ordinary linear theory of elastic plates can be applicable to the analysis.

Effects due to imperfection and irregularity of material and nonuniform bearing at edges are to be neglected in the course of analysis. However, note that these uncertainties may cause discrepancies between analytical and experimental results.

2. Method of Analysis

a. Dynamic Response of Plates

The basic equation of motion for an elastic system is:

$$m\ddot{x} + c\dot{x} + D(x) = F(K, \xi, \eta) \qquad \text{[III-16]}$$

where

m = mass,

c = damping constant,

D = linear differential operator of problem =

$$K\left(\frac{\partial^2}{\partial \xi^2} + \frac{\partial^2}{\partial \eta^2}\right) \text{ for plates,}$$

t = time, ξ, η = coordinates of the plate,

k = flexural constants of elastic plate.

In the case where the plate is assumed to vibrate in a similar manner as a single degree of freedom, the equation of motion can be simplified as

$$m\ddot{x} + c\dot{x} + kx = F(t).$$

Two types of acoustic loads are considered in analyzing the dynamic response of a glass panel, the harmonic variation of sound pressure and random loading.

Harmonic Variation - The forcing function of acoustic excitation is harmonic, having a sinusoidal relationship with time. The differential equation of motion for a single-degree-of-freedom system can then be expressed as:

$$m\ddot{x} + c\dot{x} + kx = F_o \sin \omega t.$$

where

ω = circular frequency of forcing function,

F_o = amplitude of pulsating force.

The solution of this differential equation is:

$$x = Xe^{-\xi\omega_n t} \sin\left[\sqrt{1-\xi^2}\left(\omega_n t - \varphi_1\right)\right] + \frac{F_o \sin(\omega t - \varphi)}{\sqrt{(k - m\omega^2) + (c\omega)^2}} \qquad \text{[III-17]}$$

where

$$X = \frac{F_o}{\sqrt{(k - m\omega^2)^2 + (c\omega)^2}},$$

and

$$\varphi = \arctan \frac{c\omega}{k - m\omega^2} .$$

These equations can also be written as

$$\frac{X}{X_o} = \frac{1}{\sqrt{\left[1-\left(\omega/\omega_n\right)^2\right]^2 + \left(2\xi\ \omega/\omega_n\right)^2}} \qquad \text{[III-18]}$$

$$\tan \varphi = \frac{2\xi\ \omega/\omega_n}{1-\left(\omega/\omega_n\right)^2} \qquad \text{[III-19]}$$

where

$X_o = F_o/k$ = static deflection,

$\omega_n = \sqrt{k/m}$ = natural frequency of undamped system,

$\xi = c/c_c$ = damping factor.

The ratio $\frac{X}{X_o}$ is called the magnification factor.

Random Excitation -

Let

μ_a = magnification factor $\frac{X_a}{X_o}$ at ω_a/ω_n,

e_a = rms excitation at ω_a/ω_n,

r_a = rms response.

The response to any given single excitation is response = excitation x magnification, or

$$r_a = e_a\ \mu_a .$$

For two separate excitations, the rms response would be

$$r_{a+b} = \sqrt{(e_a\ \mu_a)^2 + (e_b\ \mu_b)^2} \qquad [III-20]$$

and for several discrete frequency excitations, the rms response is:

$$r = \sqrt{\sum_n (\ell_n\ \mu_n)^2}. \qquad [III-21]$$

For a continuous spectrum of excitations

$$R = \sqrt{\int_o^\infty (\ell_u\ \mu_u)^2}\ d\omega. \qquad [III-22]$$

In this equation, e_ω is now a density function, the units of which must be

$$\text{rms } g\sqrt{\omega}.$$

b. Natural Frequencies of Plates

Calculation of natural frequencies of rectangular plates is based on the paper written by G. B. Warburton (Ref 10). The free transverse vibrations of rectangular plates were considered in Warburton's paper with all possible boundary conditions obtained by combining free, simply supported, and fixed edges. The Rayleigh method, assuming waveforms similar to those of beams, is used to derive an approximate frequency expression for all modes of vibration.

$$f = \frac{\lambda h \pi}{a^2}\left[\frac{Eg}{48\rho\ (1-\nu^2)}\right]^{\frac{1}{2}} \qquad [III-23]$$

in which

$$\lambda^2 = G_x^4 + G_y^4\frac{a^4}{b^4} + \frac{2a^2}{b^2}\left[\nu H_x\ H_y + (1-\nu)\ J_x\ J_y\right]$$

where

a, b = length of sides of rectangular plate,

f = frequency,

g = acceleration due to gravity,

h = thickness of plate,

E = modulus of elasticity,

ν = poisson's ratio,

ρ = weight per unit volume,

G_x, H_x, J_x = functions of m (number of nodal lines in x direction) and boundary conditions,

G_y, H_y, J_y = functions of n (number of nodal lines in y direction) and boundary conditions.

Expressions for G_x, H_x, J_x, G_y, H_y, and J_y are given in Warburton's paper for 15 various cases of boundary conditions which involve different combinations of free, simply-supported, and fixed edges.

c. Stresses in Plates

The deflection surface of a rectangular plate subject to a static uniform pressure can be used as an approximate configuration of the lowest natural mode of free vibration. The maximum deflection, usually at or near the center of the plate, depending on boundary conditions, is:

$$w_{max} = \lambda_1 \frac{qa^4}{D} \qquad [III-24]$$

where

q = uniform load intensity on plate,

a = length of edge of plate,

$$D = \frac{Eh^3}{12(1-\nu)} ,$$

λ_1 = a numerical coefficient varying with the length ratio of the sides.

The maximum bending moment in plate due to uniform pressure loading can also be expressed in the form of

$$M_{max} = \lambda_2 \, qa^2 \qquad [III-25]$$

from which the deflection bending moment relationship is written as

$$w_{max} = \frac{\lambda_1}{\lambda_2} \cdot \frac{a^2}{D} \cdot M_{max}. \qquad [III-26]$$

The maximum flexural stress in plate is

$$\sigma_{max} = \frac{6M_{max}}{h^2} \qquad [III-27]$$

$$\therefore w_{max} = \frac{a^2 h^2}{6D} \cdot \frac{\lambda_1}{\lambda_2} \cdot \sigma_{max}. \qquad [III-28]$$

For steady-state vibration without damping of a single-degree-of-freedom system, the acceleration can be expressed in terms of displacement as:

$$\ddot{x} = -\omega^2 x = -4\pi^2 f^2 x, \qquad [III-29]$$

where

ω = circular frequency (rad/sec),

f = frequency (cps).

If only the lowest mode of vibration is considered and the plate is taken as a single-degree-of-freedom system, then

$$X_{max} = w_{max}$$

and

$$\ddot{x}_{max} = -4\pi^2 f^2 \frac{a^2 h^2}{6D} \cdot \frac{\lambda_1}{\lambda_2} \tau_{max}. \qquad [III-30]$$

The following physical constants of window glass are used for purpose of analysis (Ref 11):

$E = 10{,}000{,}000$ psi,

$\nu = 0.23$,

$\sigma_{ultimate} = 5000$ psi,

$\rho = 0.0913$ lb/in.^{3}.

The limit of acceleration for glass breakage is therefore:

$$\ddot{x}_{max} = 8\pi^2 f^2 \sigma_{ult} \frac{(1-\nu^2)}{E} \cdot \left(\frac{\lambda_1}{\lambda_2}\right) \cdot \left(\frac{a^2}{h}\right) \text{ in./sec}^2. \qquad [III-31]$$

The terms $\frac{\lambda_1}{\lambda_2}$ and $\frac{a^2}{h}$ are functions of plate geometry. For a given size of window glass, the limit of response acceleration varies directly with the square of its frequency. A curve showing relationship between limiting value of peak acceleration and frequency can be plotted for a window glass of known size and boundary condition. Comparing this curve with the acceleration frequency spectrum obtained by field acoustic tests with assigned sound-pressure level, one can tell the possibility of glass breakage for that acoustic environment.

Conversely, stress in plate can be calculated from accelerometer readings of tests, using the same stress acceleration as before and assuming that the lowest mode of vibration is dominant. Thus, the stress becomes:

$$\sigma = \frac{1}{8\pi^2 f^2} \cdot \frac{E}{(1-\nu^2)} \cdot \left(\frac{\lambda_2}{\lambda_1}\right) \cdot \left(\frac{h}{a^2}\right) \cdot \ddot{x} \text{ psi}. \qquad [III-32]$$

The stress in a plate can be calculated from the following stress equation (Ref 12); using measured strain data

$$\sigma_1 = \frac{E}{(1 - \nu^2)} (e_1 + \nu e_2), \qquad \text{[III-33]}$$

where the subscripts 1 and 2 refer to principal stress directions. At the center of the window, only one direction must be measured because of the symmetry of the stress field.

d. Relationship between Random and Sinusoidal Excitation

The rms response of a simple structure to a narrow-band random excitation of a known rms level is equivalent to the response produced by sinusoidal excitation of the same rms level. If it is assumed that the peak-to-rms value of the stress time history is 3, the use of a sinusoidal excitation that has a peak amplitude equal to three times the rms value of the random excitation should cause no failures that would not be caused by the random excitation (Ref 13). Thus, a narrow-band acoustic excitation, p_r (p will be assumed to be an rms value unless otherwise noted), may be simulated by a sinusoidal excitation, p_s, as follows:

$$p_s = \frac{3}{\sqrt{2}} p_r. \qquad \text{[III-34]}$$

The definition of what limits may be placed on the bandwidth of a narrow-band random excitation (as well as a narrow-band random response) is difficult. Thus, one may wish to explore the feasibility of simulating a broad-band excitation by the use of sinusoidal excitation. Miles (Ref 14) has estimated the stress response of a linear single-degree-of-freedom system with low damping ($S \ll 1$) to random loads as follows:

$$\sigma_r^2 = \left(\frac{\pi}{4\xi}\right) \left[\frac{\omega_o f(\omega_o)}{F_o^2}\right]^{1/2} S_o^2, \qquad \text{[III-35]}$$

where

S_o = stress produced by a static load F_o,

$\omega_o f$ = power spectral density at the dominant mode of oscillation.

Assuming a unit loading, F_o,

$$\sigma_r = \left(\frac{\pi}{4\xi}\right)\left[\omega_o f(\omega_o)\right] S_o. \qquad \text{[III-36]}$$

If $\omega_o f$ is the power spectral density of the acoustic pressure,

$$\sigma_r = \frac{p_r(f_o)}{2}\left(\frac{\pi f_o}{\xi}\right)^{1/2} S_o. \qquad \text{[III-37]}$$

The stress response of a single-degree-of-freedom system, at its natural frequency is:

$$\sigma_s = p_s Q S_o. \qquad \text{[III-38]}$$

Thus, by limiting the peak value of the excitation and response to 3 times the rms value and requiring that the peak response be equivalent for both sinusoidal and random excitation, the equivalent stress for sinusoidal and random excitation can be estimated:

$$\sqrt{2}p_s Q = 3\left[\frac{p_r(f_o)}{2}\left(\frac{\pi f_o}{\xi}\right)\right]^{1/2},$$

$$p_s = \frac{3}{\sqrt{2}}\left[\frac{p_r(f_o)}{2}\left(\pi\xi f_o\right)\right]^{1/2}. \qquad \text{[III-39]}$$

e. Sources of Error

Discrepancy between calculated stress and actual stress is sometimes inevitable. Sources of error can be summarized as follows:

1) The actual edge condition is different from the idealized condition, which is made convenient for mathematical solution. The degree of fixity at the supporting edge is always uncertain and, therefore, statistical data should be relied on. The edge of frame is generally assumed to be rigid but, in case of high loading, the edge may deflect slightly;

2) The damping characteristic of window glasses is not completely known. The effect of caulking, aging, and method of framing are all important factors of variations in damping;

3) Nonlinear characteristics in window glass vibration are significant, particularly under high pressure, large deflection, and low frequency. All these critical conditions occur near the point of breakage;

4) The ultimate strength of window glass has a wide range of variety for different batches and ages. However, glass breakage due to high sound-pressure levels can be predicted from extensive test results.

D. ANALYSIS OF DATA

As previously mentioned, the primary objective of this study was to determine the rocket engine noise damage criterion to community dwellings. Such a criterion had been proposed by Reiger, Mays, and Edge (Ref 15) and by NASA-MSFC (Ref 16). These criteria are shown in Fig. III-20. The primary difference between these two criteria is that Reiger, Mays, and Edge included the effect of resonance on the fragility, while NASA-MSFC did not. Further window data obtained by Freynik (Ref 12) of NASA-Langley tended to substantiate the Reiger, Mays, and Edge criterion.

The NASA-Langley data were obtained under closely controlled conditions. The window units were securely fastened to the rigid mouth of the test enclosure. Thus, the window vibrated as a plate with fixed and rigid support conditions. A reproduction of these data is shown in Fig. III-21. To complete a criterion for communities, however, one must include the field effects, such as edge conditions, age, etc. The data obtained in these tests were acquired to evaluate such field conditions.

Data were acquired in Florida and Denver. It was necessary to use a sinusoidal siren for field tests because of power limitations. Random acoustic tests were included to correlate random and sinusoidal response. It was also found that strain gage measurements over a broad frequency range were impractical because of the low-voltage output, and acceleration measurements were, therefore, substituted. A sufficient number of strain measurements to establish the stress-acceleration relationship was also required. Over 3500 data points were taken, some of which were unusable. Analysis of these data included scatter, accuracy, repeatability, linearity, and failure prediction.

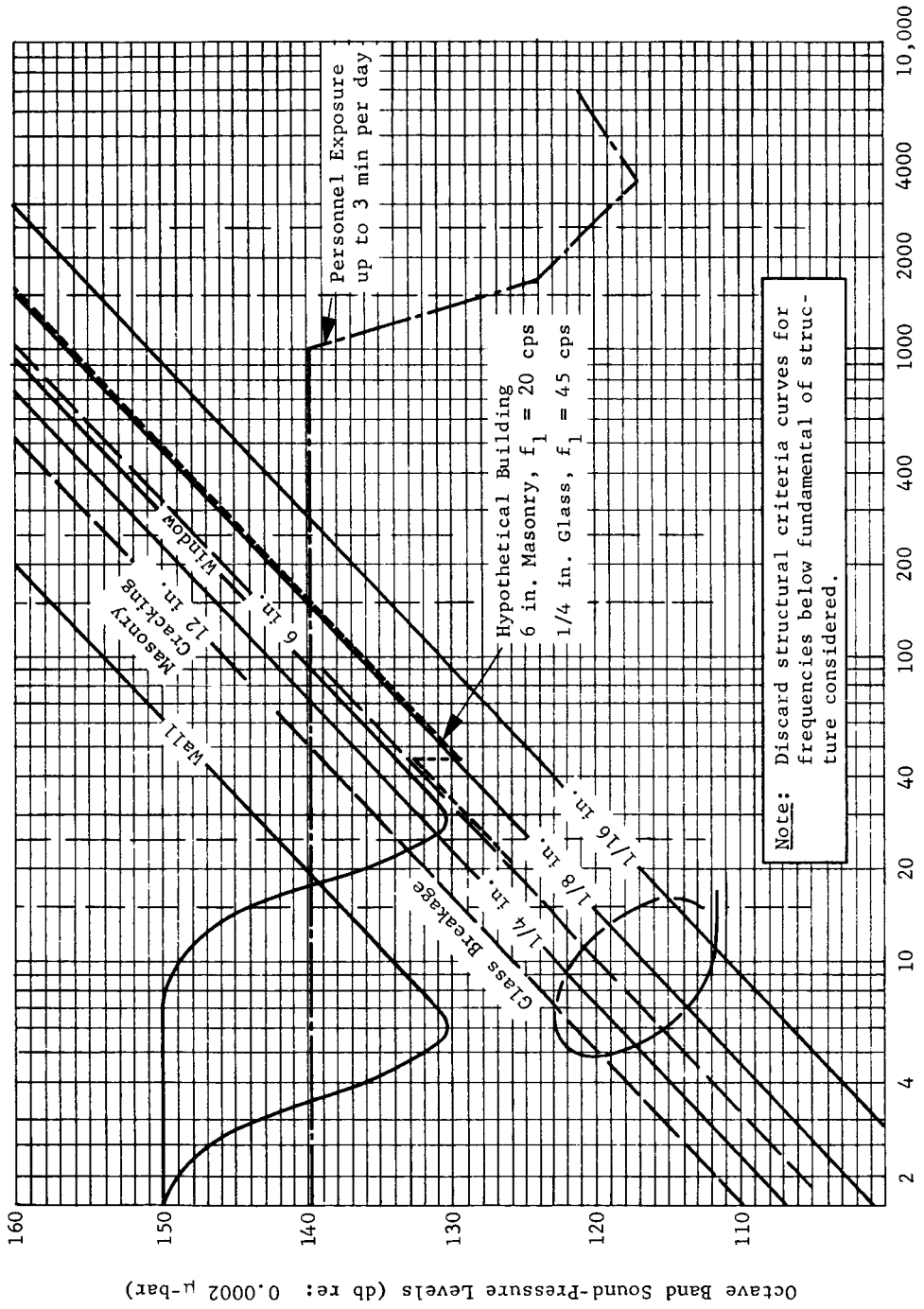

Fig. III-20 Noise Exposure Criteria for Building Structures and Unprotected Personnel

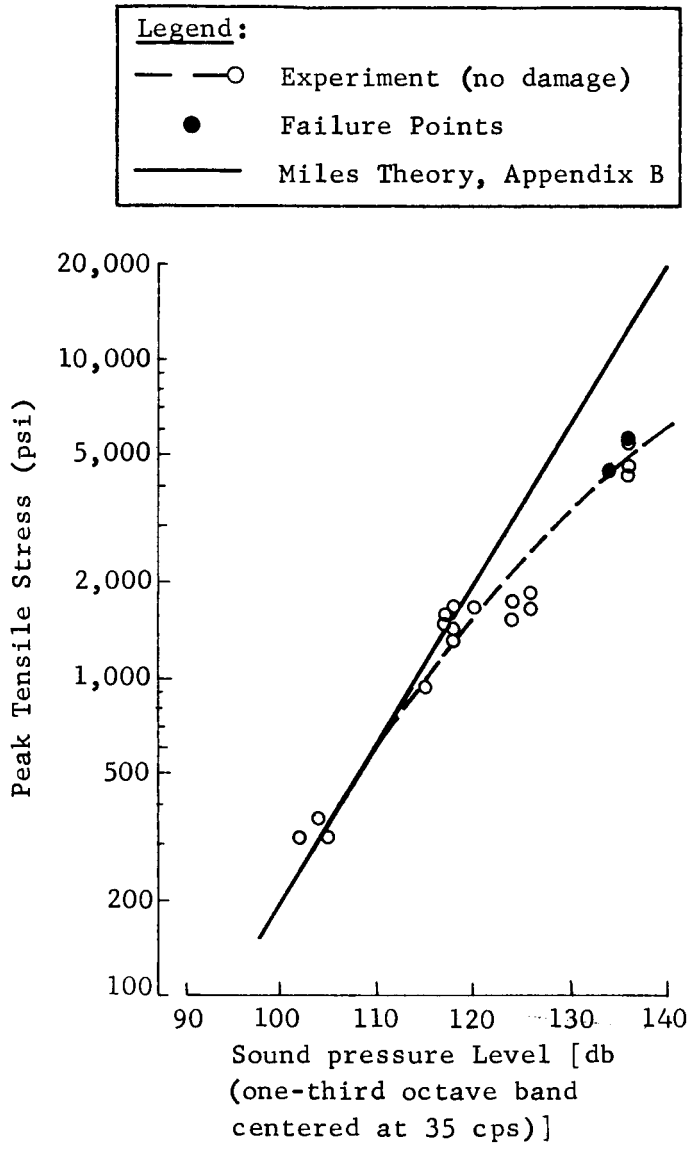

Fig. III-21 Total Peak Outer-Fiber Tensile Stress at the Center of Window Due to Random Noise Input

From Ref. 18

The scatter of data acquired from the center accelerometers on each window, for both random and sinusoidal excitation, is shown in Fig. II-11 and II-18 of Chap. II. The spread of data show good repeatability, considering the variety of windows tested. Of particular significance is the predominance of the peak response in the 20- to 30-cps frequency region. These data do not agree with the calculated values of fundamental frequencies shown in Table III-1. The calculation of fundamental frequencies of the window panes was based on the assumption of fixed boundary conditions. It was found, however, that wood composition walls with windows exhibited a high vibration response to acoustic excitation. Thus, the total vibration response of a window mounted in a wooden wall is the sum of the vibration of the window and wall as a system. Those plate glass windows that were mounted in block walls tended to respond in the manner of a plate with fixed edges. The similarity of the response of Window 7 (a 22x32-in. plate window in a block wall) to the windows tested by NASA-Langley is also shown in Fig. III-22.

The tensile stress in the wood wall window is less than that of a block wall window for the same acoustic excitation. This phenomenon will be discussed in more detail later in this report.

Many of the windows in Florida were loosely mounted. The looseness resulted from improper mounting, poor design, or aging. Some windows were tightly mounted on one or more edges and loose on the remaining edges. Occasional jalousy and awning windows "banged" against adjoining panes under acoustic loading. Section windows could, in some cases, be deflected without significant bending of the glass. Near the failure sound-pressure levels, some wood and aluminum frames incurred structural failure before actual glass failure. It would not be possible to accurately define all boundary conditions. During the Florida tests, an attempt was made to test a cross section of windows to produce a data spread that included the extremes in boundary conditions. The data appear to lie between the case of windows mounted in block walls and windows mounted in wood walls.

Table III-1 Fundamental Frequencies

Run	Calculated (cps)	Measured (cps)
1	35	39
2	67	35
3	72	32
4	123	33
5	10	31
6	12	26
7	23	42
8	97	25
9	82	35
10	93	40
12	51	20
13	None	27*
14	54	45
15	18	60
16	15	40
17	13	60
18		25
19		22
20		25, 31

*Wood Wall

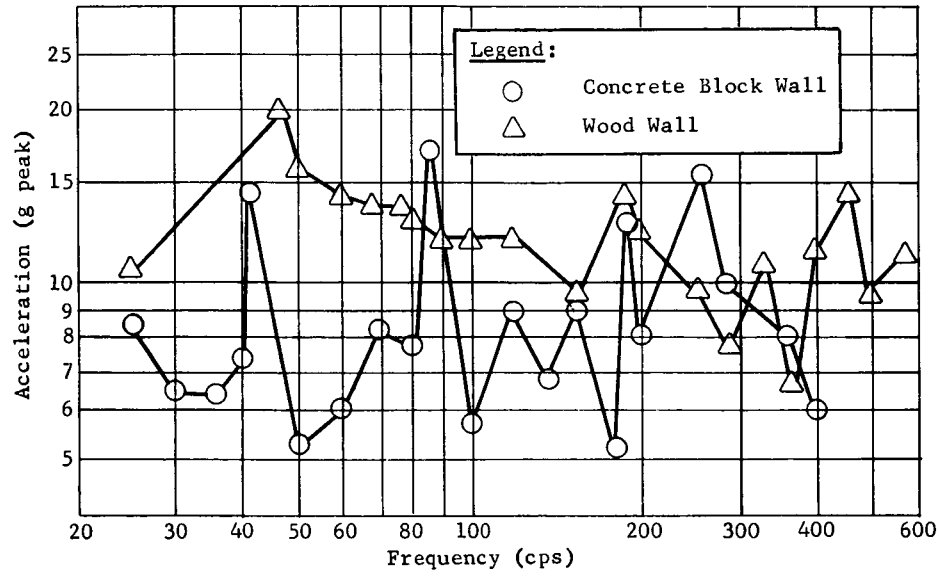

(a) Comparison of Vibration Response of Plate Window Mounted in Wood Wall and Plate Window Mounted in Concrete Block Wall

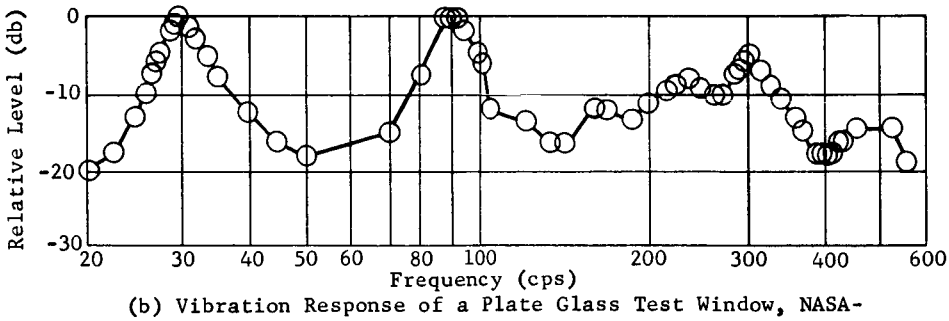

(b) Vibration Response of a Plate Glass Test Window, NASA-Langley (Ref 18)

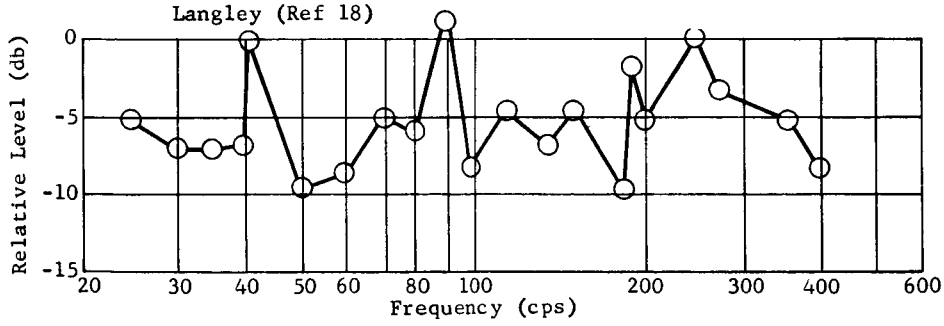

(c) Vibration Response of Plate Glass Window in Concrete Block Wall, Florida Test Window 7

Fig. III-22 Vibration Response of Various Plate Glass Windows

Stress data points vs sound-pressure level are shown in Fig. III-23. Stress was computed from strain data by Eq [III-33]. The data from the random tests were plotted directly. The equivalent random excitation level for the sinusoidal tests was determined from Eq [III-39], corrected for bandwidth, and plotted as equivalent random 1/3-octave sound-pressure level. These data appear to lie on a line that has the same slope as the calculated values shown in Fig. III-21. The bandwidth correction depended on the frequency at which maximum stress occurred. The peak frequency, however, occurred within such a narrow band of frequencies that the use of a bandwidth correction for the 31-cps filter for all data would have produced an error of less than 1 db. During the sinusoidal tests at Denver, acceleration levels were measured for various sound-pressure levels at the peak resonant frequency. The acoustic level was raised from 135 db until failure occurred. These data are shown as acceleration in g peak vs rms sound-pressure level in Fig. III-24. The window response exhibited a linear behavior below 135 to 137 db. Above these levels, nonlinearity became apparent. Strain data acquired during the 135-db excitation provided a single-point correlation of stress and acceleration. Since the slope of the data was approximately the same as the stress data below 135 db, it was assumed that the stress-acceleration relationship would hold for other sound-pressure levels. The acceleration levels of Fig. III-24 were plotted in terms of stress in Fig. III-25. Strain data from the left window were incorrect and the stress levels were not included. The data from Fig. III-25 were plotted with the NASA-Langley data in Fig. III-26. The shape of these two curves is similar but the data from this test program are displaced approximately 10 db to the right. As previously mentioned, the NASA-Langley data were taken from a window pane that closely resembled a plate with clamped edges and rigid supports. Good agreement between calculated values and measured values were found in the linear region. At higher sound pressure levels, however, the vibration response became increasingly nonlinear. Except for plate windows in masonry walls, the windows that were tested in this study did not produce stresses of the magnitude that were produced in the NASA-Langley tests. There are two possible explanations for this difference. First, windows that were mounted in wood walls did not have rigid supports. The wooden walls themselves were also subjected to acoustically induced vibration. If the wall and window were vibrating in phase, the window pane and the wall would experience the same harmonic motion and the stress in the window would therefore be less. In addition, most of the windows were louvered, awning, double hung, or some type that did not resemble a homogenous plate. Some of these edge conditions were sufficiently free and the supports sufficiently limber that comparatively lower

stresses were produced at the center of the pane. This conclusion seemed to be valid because of the similar shape of the two curves of Fig. III-26. It appeared that the vibration response of the plate window with fixed, rigid edge conditions was generally lower for the same sound pressure level than the other windows that were tested, but that when equal stress was induced in the individual panes at higher sound pressure levels, the stress response curve of each pane was similar. Thus, the most fragile window would appear to be a plate glass with clamped edges and rigid supports, such as a 1/8-in. plate glass in a masonry wall. Data acquired on the NASA test wall at JFKSC during the SA-6 flight is also shown in Fig. III-26. These points show good agreement with other data.

Thus far, we have determined the stress response and fragility level at only the fundamental frequency. The fragility level at other frequencies may be determined by making two simplifying assumptions. First, the failure stress is assumed to be the same at all frequencies. The yield strength of glass has been shown to increase with the rate of loading. Thus, this assumption should provide conservative estimates. A yield strength of 5000 psi was found from both these tests and the NASA-Langley tests, and will therefore be used. Second, the sound pressure-stress relationship is assumed to be the same at all frequencies as at resonance. An examination of the random test data showed this assumption to be approximately true in the linear range, as indicated in Fig. III-27. The stress-acceleration relationship was established at resonance and could be determined for other frequencies from Eq [III-32]. The sound pressure level (ΔSPL) required to increase the stress to 5000 psi was determined from Fig. III-26. The sum of the ΔSPL and the test level yielded the approximate sound pressure level that would induce failure at that frequency. This procedure was followed for all data and the results plotted in Fig. III-28.

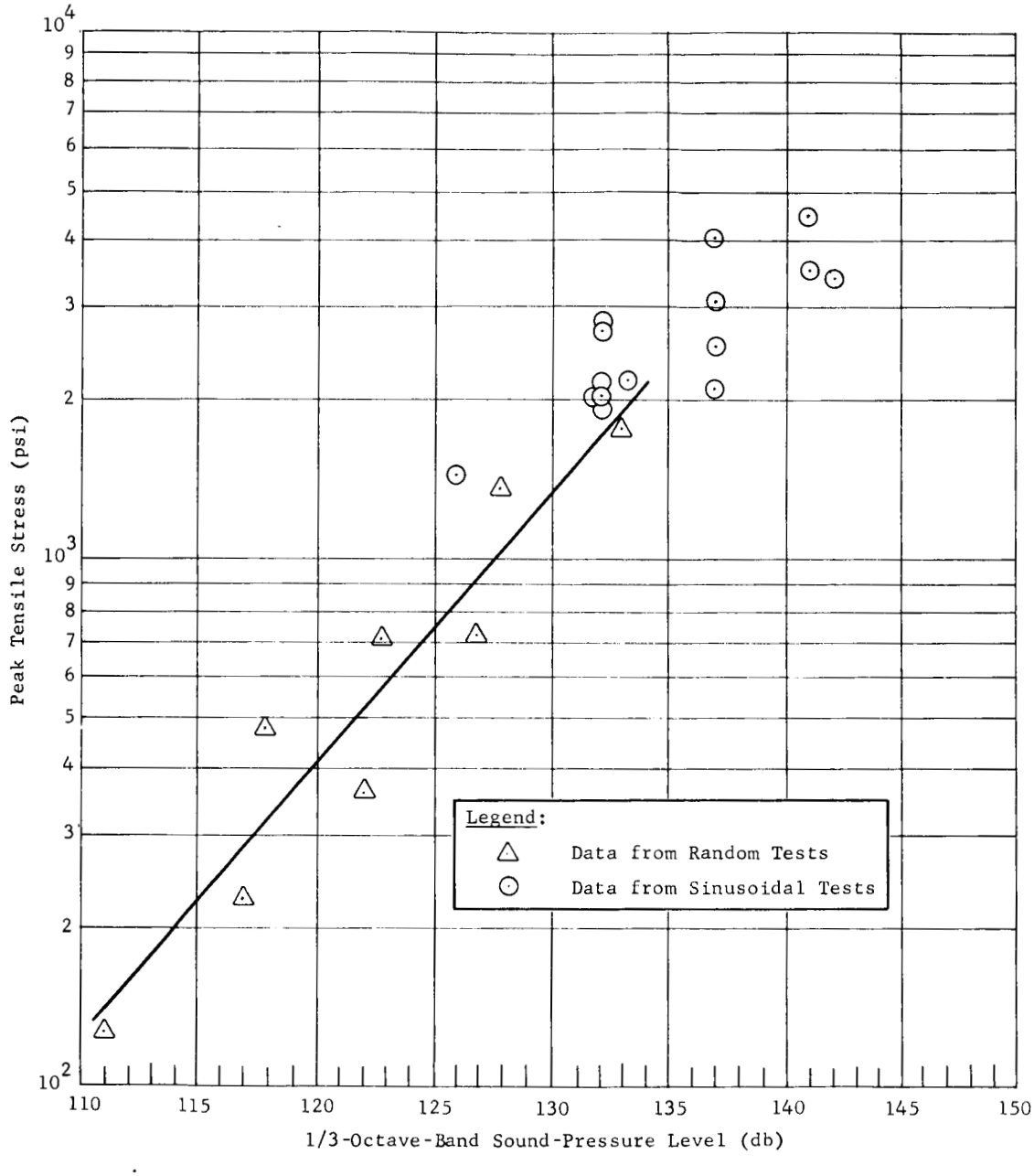

Fig. III-23 Peak Tensile Stress vs 1/3-Octave-Band Sound-Pressure Level at the Peak Vibration Frequency (Data Obtained from Strain Measurements)

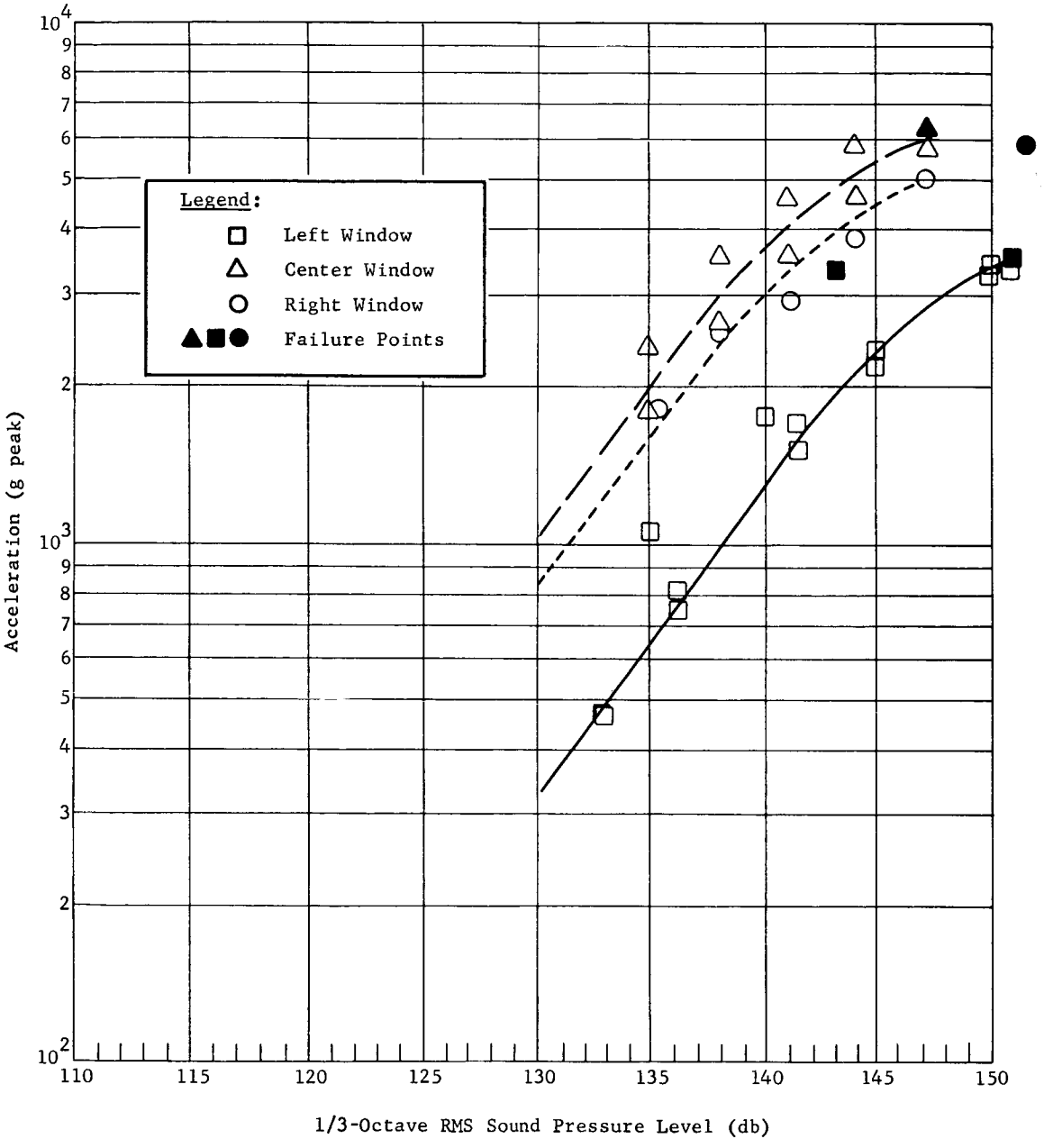

Fig. III-24 Acceleration Levels at Increasing Sound Pressure Levels at Peak Vibration Frequencies of 25 to 31 cps (Data Obtained during Denver Sinusoidal Tests)

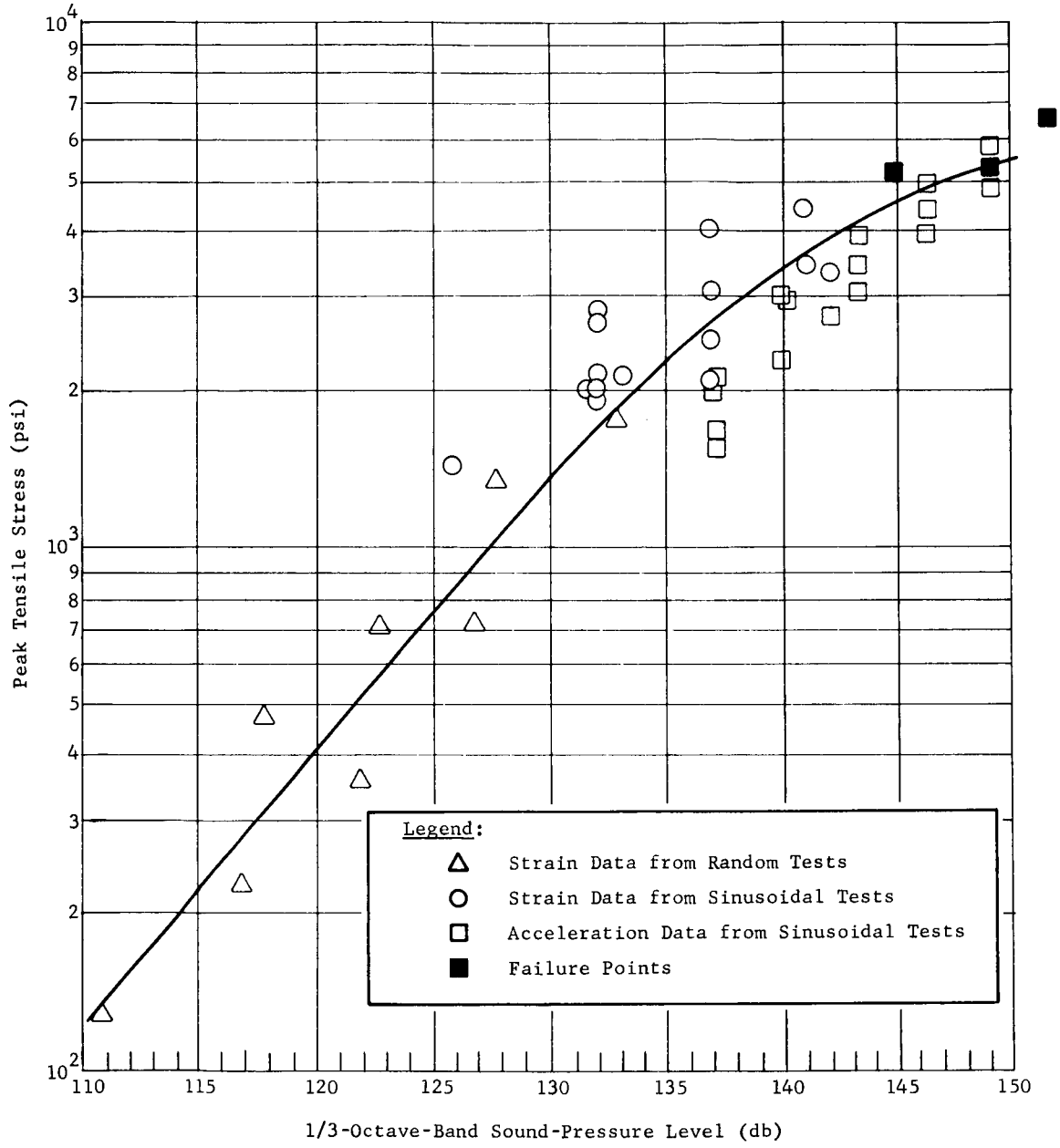

Fig. III-25 Peak Tensile Stress vs 1/3-Octave-Band Sound-Pressure Level at Peak Frequencies of 25 to 31 cps

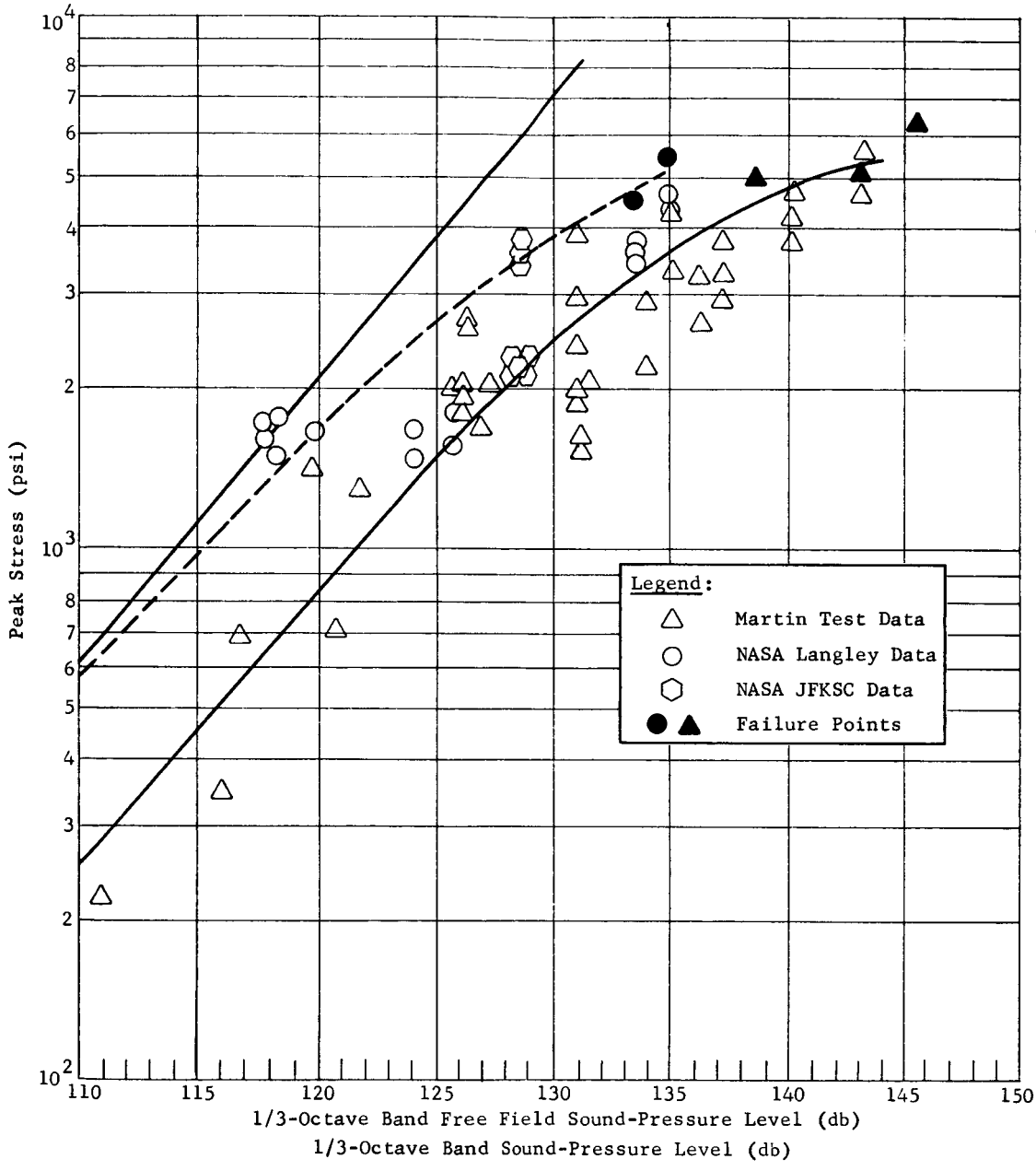

Fig. III-26 Stress vs Free Field Sound-Pressure Level Comparing Data from Three Sources

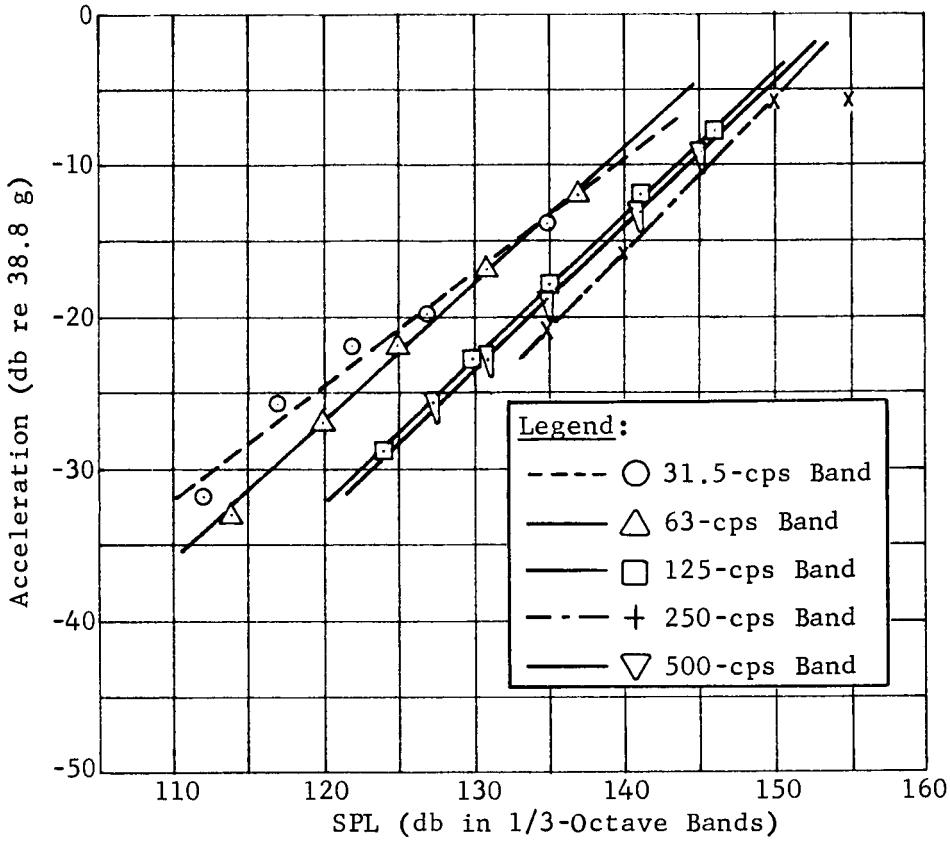

Fig. III-27 Acceleration with Increasing Sound-Pressure Levels from Random Tests, Window 3, Runs 1 thru 5, Accelerometer 4

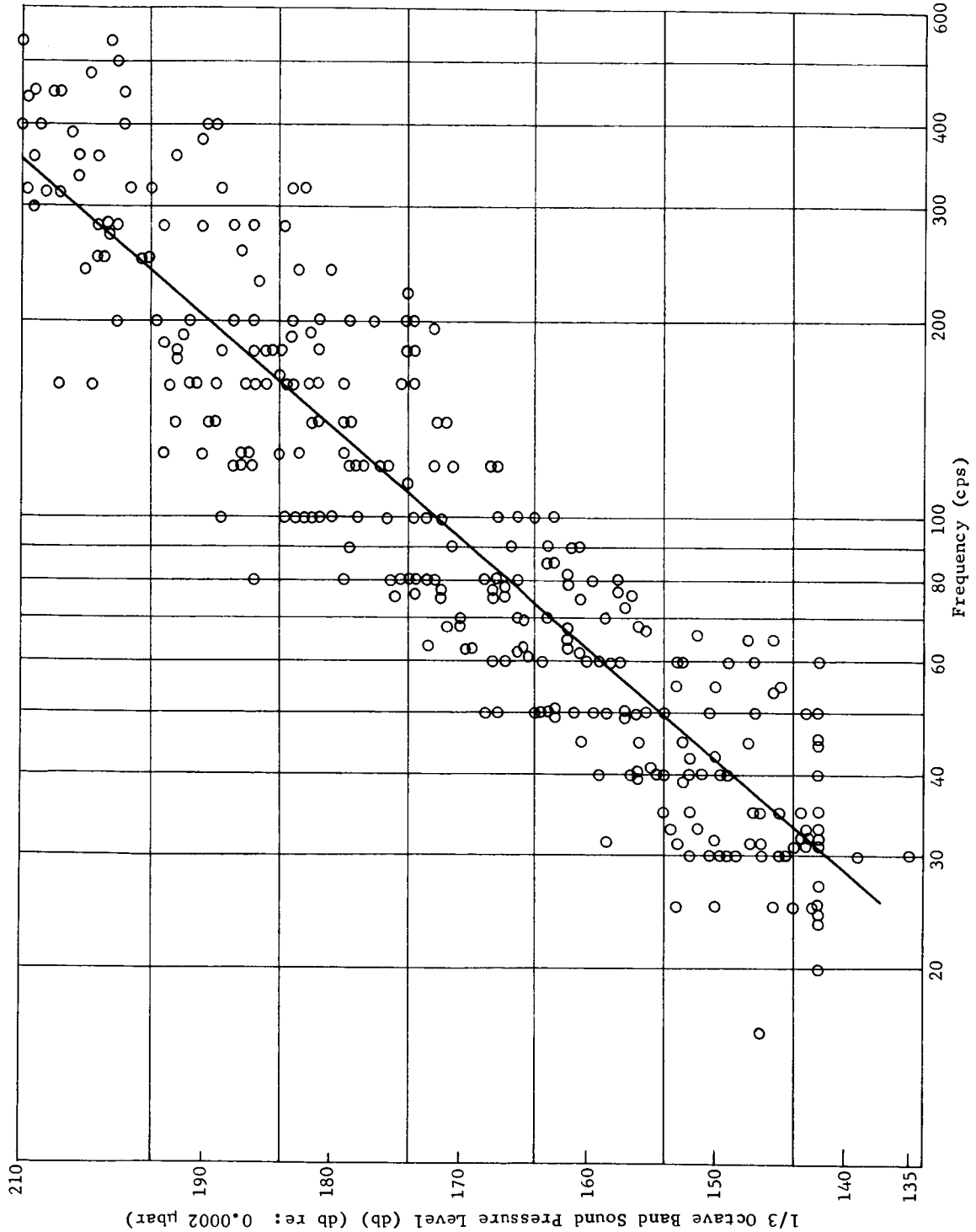

Fig. III-28 Predicted Fragility of Window Units, Denver and Florida Data

IV. ROCKET ENGINE NOISE DAMAGE CRITERIA

A. CONSIDERATIONS

Recently, design specifications for large space booster launch facility structures and equipment have included rocket engine noise damage criteria. These criteria are generally achieved through a balance of structural and location parameters. For example, it may be desirable to locate an equipment building in an area of the lowest noise to reduce structural cost, but such a move might increase the cost of signal transmission to the launch stand. Thus, a tradeoff between costs would yield the optimum design. Such a tradeoff is possible because the engineer has control of not only the location and design, but also the quality of design, materials, and construction. Since the performance requirements and fragility levels are known, a well-defined confidence level may be attached to the criteria. In deriving a damage criteria for communities, however, the parameters are not so accurately known. First, the type and quality of structures are not as well defined or controlled, and surveys of a sample of structures are necessary to define the structure category. In addition, the construction of new buildings is not closely controlled. Second, the choice of a confidence limit, or safety factor, is not a fixed parameter but a variable that must be chosen by those ultimately responsible for any damage that might occur.

The following factors will be considered in the selection of a rocket engine noise damage criteria:

1) Structural fragility;

2) Confidence limits;

3) Safety factor;

4) Types of structures.

Each of these factors will be considered separately to provide the reader with his choice in determining the effect on the criteria. Sections B thru D will be devoted to windows alone, while Section E will cover wall structures.

B. STRUCTURAL FRAGILITY

From the previous tests, we have determined the fragility of a number of window units. These data are shown in Fig. III-28. It was assumed that this sample was representative of those windows in communities near MILA that will be subjected to large space booster launch noise. A survey of the communities was conducted to verify this assumption. The conditions governing the fragility of these window units vary over a wide range. Some of the conditions are:

1) The vibration response of windows mounted in wooden walls did not agree with calculated values. In general, the fundamental mode of the window corresponded with the fundamental frequency of the window-wall system;

2) The first mode of the wood walls in the horizontal direction was governed by the distance between studs. Thus, the lowest vibration mode of most wood walls occurred in a narrow frequency band, centered around 30 cps;

3) The vibration response of plate glass windows installed in masonry walls most nearly duplicated the calculated values using plate theory;

4) The edge conditions of windows that were louvered, awning, wood sash, four-pane, etc, varied widely from window to window. As a result, the measured values of the fundamental frequency varied widely from calculated values;

5) During the tests at Denver, the window failures were accompanied by simultaneous failure of some frames (described in Chap. II);

6) Some windows, such as louvered windows, had a tendency to bang against adjoining panes. The pane thickness of louvered windows was generally thicker, which had a tendency to offset the stresses induced by the impact.

The conclusion drawn from the preceding conditions is that the many variables involved make precise definition of window fragility unfeasible. It would appear, therefore, that the approach taken in this study is the most practical at this time. All data will be considered as a group and not individually, and the fragility levels of Fig. III-28 will be considered in terms of their distribution and used to formulate a fragility criterion.

The effect of aging on the yield strength of windows has been studied by Seiders and McKinley (Ref 17). Some of their findings are discussed. Glass strength is affected by condition of surface, rate of loading, and size. The last of these factors was included in the testing and now the chief concern is with the effect of surface conditions. Seiders and McKinley listed those conditions that cause surface flaws:

1) Atmosphere - water vapor and sand abrasion;

2) Production flaws - batch irregularities and polishing defects;

3) Packaging flaws - scratches, water spots, scum, and strain.

The tests in Ref 17 have shown that surface flaws can reduce strength over 50%. Such a decrease in yield strength could result in a decrease in the fragility level of 10 db. Thus, further evaluation is required. The type of cut which produced the large reduction in strength was made by a cutting wheel. Shallow surface scratches had little weakening effect. Abrasion tests caused surface scratches and a reduction in thickness. Both scratch and abrasion tests were designed to simulate packaging environments. The air blasting tests with 70 grit carborundum were perhaps more indicative of the Florida environment where blowing sand and dust can cause surface damage. Thus, the damaged windows can be divided into two categories: those damaged during packaging and installation and those damaged from wind erosion. Because of the high velocity hurricane winds (the building code specifies design for 120 mph), older windows whose strength has been reduced by surface damage, may fail during hurricane winds. Regier, et al. (Ref 15) found 1/8-in. window glass failures ranging from 30 psf to 150 psf while Bowles and Sugarman (Ref 18) found a mean of 108 psf for 40 panels. The Bowles and Sugarman data are shown in Fig. IV-1a. The extremes proposed by Regier, et al. are imposed on this graph. It would appear that any sizable reduction in breaking strength would result in window breakage during hurricane winds. Thus, older windows would as a group, tend to have fewer imperfections

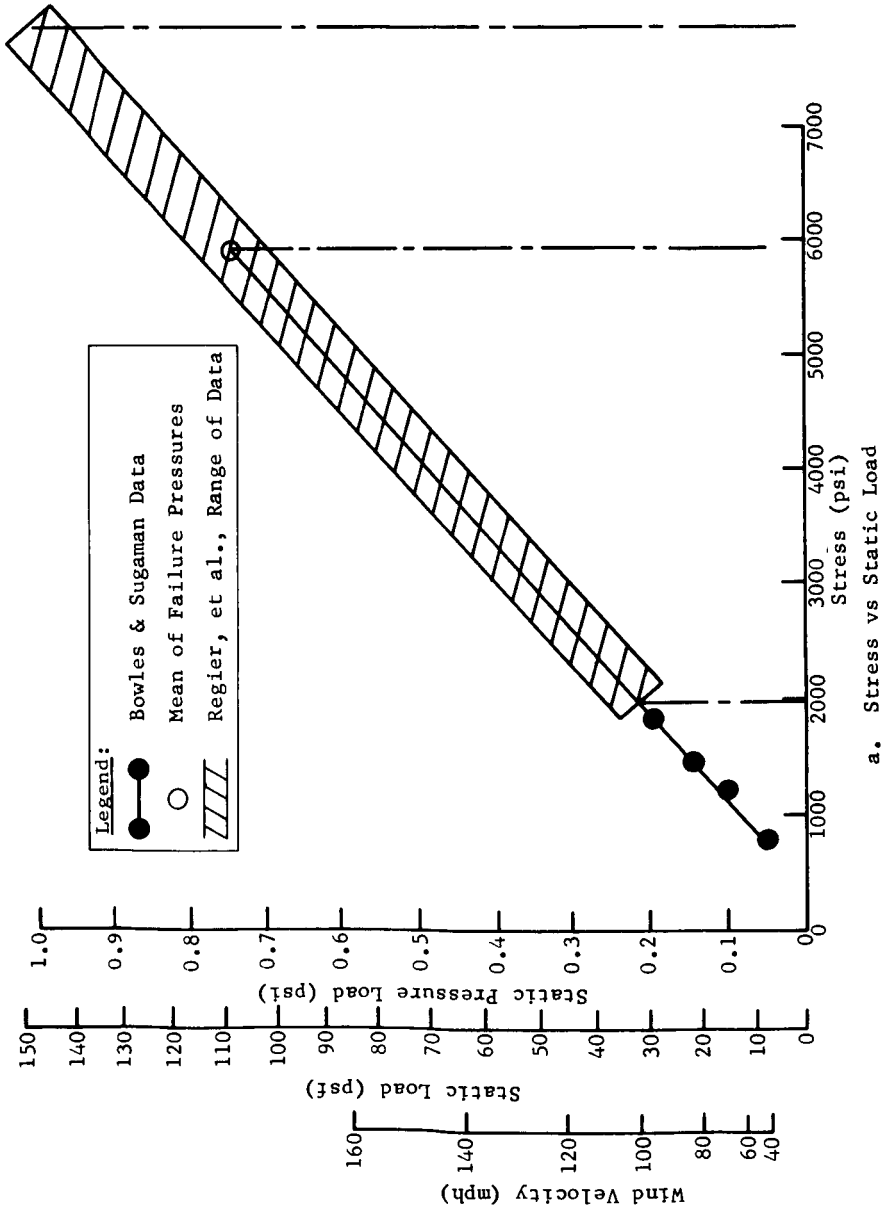

a. Stress vs Static Load

b. Relationship between Mean Bursting Pressure and Thickness of Plate and Sheet Glass Panels (Ref 18)

Fig. IV-1 Effect of State Pressure Loading on Glass

which would lower their breaking strength. Wind erosion tends to reduce glass thickness. From Fig. IV-1b, it can be seen that a reduction in thickness of 25% on a 1/8-in. plate would result in decrease in fragility level of less than 3 db. It would appear, therefore, that window breakage might be more severe for new construction than old. It would be impractical to account for all possible cases. Considering the small percentage of new construction to older construction (that surviving one hurricane season), and considering further the small percentage of windows with reduced breaking strength, it would appear that breakage from surface imperfection weaknesses would be negligible.

C. CONFIDENCE LIMITS

The testing of windows with a wide variety of age, edge conditions, and window composition has produced a large variation of window stress for a given input sound pressure level. This is illustrated in Fig. III-26 where, for example, at 131 db input at the resonant frequency the measured stress for all windows varied from 1600 to 4000 psi. In other words, at any given sound pressure level some windows will react to produce a large glass stress, while others will exhibit a relatively low stress. This indicates that a single fragility curve will not adequately describe the response of the entire window population. Referring again to Fig. III-26, it can be seen that the mean stress at a sound pressure level of 131 db is about 2800 psi and that the maximum stress measured was 4000 psi. These results, however, do not rule out the possibility of a window configuration existing (not measured in these tests) which would result in a window stress of 5000 psi at this sound pressure level input. For this reason the measured stress data have been analyzed to determine the statistical characteristics which would be useful in establishing the fragility curves. Assuming a normal distribution of the stress the standard deviation (s_n) was calculated from the data of Fig. III-26. Consulting tables of areas of the normal curve (Ref 19) (actually a t table for small samples) we find that if we go 1.86 standard deviations above the mean stress, then 95% of the population will lie below this point; that is from 1.86 s_n to minus infinity. This means (referring to the lower curve of Fig. III-26) that a sound pressure level of 135 db produces a mean stress of ~3600 psi and that 95% of the population lies below 3600 + 1.86 s_n where s_n equals 750 psi. Therefore 5% of the stress population will equal

or exceed 5000 psi. It can also be seen that 50% of the stresses will exceed 5000 psi when the sound pressure level equals 141 db since this is on the approximate mean line. Proceeding in this manner and using the approximate mean line data of Fig. III-28, Fig. IV-2 results. We read for example that if the incident free field sound pressure level reaches 132 db at 30 cps, then 1% of the windows in the population will have a stress equal to or exceeding 5000 psi and will fail. In a similar manner, if the incident sound pressure level in the 30 cps band equals 136.5 db, then 10% of the windows will be stressed to 5000 psi. The 50% failure line comes directly from the approximate mean line of Fig. III-28 with the line at 30 cps fixed by the measured failure point of Fig. III-26. The stress distribution is assumed to be the same for frequencies off resonance as that at resonance. The curves of Fig. IV-2 below resonance are dotted because only a few data points were available and the accuracy of fixing the line is poor. The plateau at 150 db at low frequencies is the damage level where acoustic peak pressures equal static-failure pressures (Ref 15). Figure IV-2 is the window damage criteria.

D. SAFETY FACTOR

The safety factor of window panes has been defined by McKinley and is shown in Figure IV-3a. The safety factor is shown in terms of decibels in Fig. IV-3b. The use of the safety factor is very simple. The safety factor is chosen and found in terms of a decibel. Then the criteria are lowered by a corresponding number of decibels. For example, a safety factor of 5 would lower the criteria by 7 db.

E. WALL DAMAGE CRITERIA

The fragility of walls, particularly wood walls with exterior stucco or interior plaster, is much more difficult to determine than fragility of windows. While the fracture of windows from acoustic loading is not necessarily time dependent, the failure of plaster is. A conventional stress strain curve for plaster would be difficult to draw. As a plaster wall becomes stressed, some of the fibers fail and the strength is reduced. The age of plaster will also affect its resistance. New plaster is highly elastic while older plaster becomes quite brittle. Older plaster, however,

may be covered with sufficient coats of paint to give it a higher tensile strength. None of the test houses contained plaster walls that had not been previously damaged so test data points could be acquired. Some response measurements were made, however, and will be utilized to allow a comparison with data taken by others.

Building damage from sonic booms was discussed by Mays and Edge (Ref 20). An example of their experience is shown in Fig. IV-4. The rocket engine noise would be comparable to an overall sound pressure level of approximately 130 db.

The Bureau of Mines has conducted several studies of building damage from blasting. The results of these tests were used to formulate damage criteria (Ref 21) shown in Fig. IV-5. Although these criteria were formulated from seismic excitation, they can be used for acoustic excitation since the damage was expressed in terms of displacement. Measured displacements acquired from wood walls during the Florida tests are superimposed on Fig. IV-5. Sinusoidal acoustic energy at 135 db was used. Data below 50 cps was not usable. Generally, the data were approximately the same as the data points acquired through the Bureau of Mines' tests. The damage criterion for acoustic excitation was determined in the following manner. First, a damage criterion line following the "Crandell Line of V = 3.3 in./sec" was chosen for this study. Next, a best fit line was drawn through the Martin data. The distance between the best fit line and the criterion line could then be determined. Since the excitation level that produced the Martin data was known, the excitation level would produce a velocity of 3.3 in./sec could be determined. This level is shown as the lower part of the plaster criterion of Fig. IV-6. The upper line of the criterion was determined by the distance between the 3.3 in./sec and 7.6 in./sec line of Fig. IV-5. The criterion was not extended below 10 cps since the Bureau of Mines data do not extend into this region. The wallboard criteria were derived from the Denver test data. Since only two data points were taken, a safety factor of 5 was employed. Overpressure from wind gusts in terms of equivalent sound pressure levels was placed on Fig. IV-6. Note that a wind gust with a frequency near the fundamental frequency of the wall could produce displacements in excess of the criterion.

The wall damage criterion was not based on many data points and may not, therefore, be as accurate as the window criterion. The Acoustic Group at NASA Langley is planning extensive tests on plaster walls in the near future. It is suggested that the data from these tests be used, when available, to revise the wall criteria suggested by this study.

Figure IV-4 shows that the number of complaints from wall damage exceeds that of window damage. This would be expected since the wall criterion is lower than the window criterion. The type of complaints usually received were from minor damage, of very weak walls. Such complaints may not be as intense in Titusville since the hurricane winds have a tendency to separate out the weak structures.

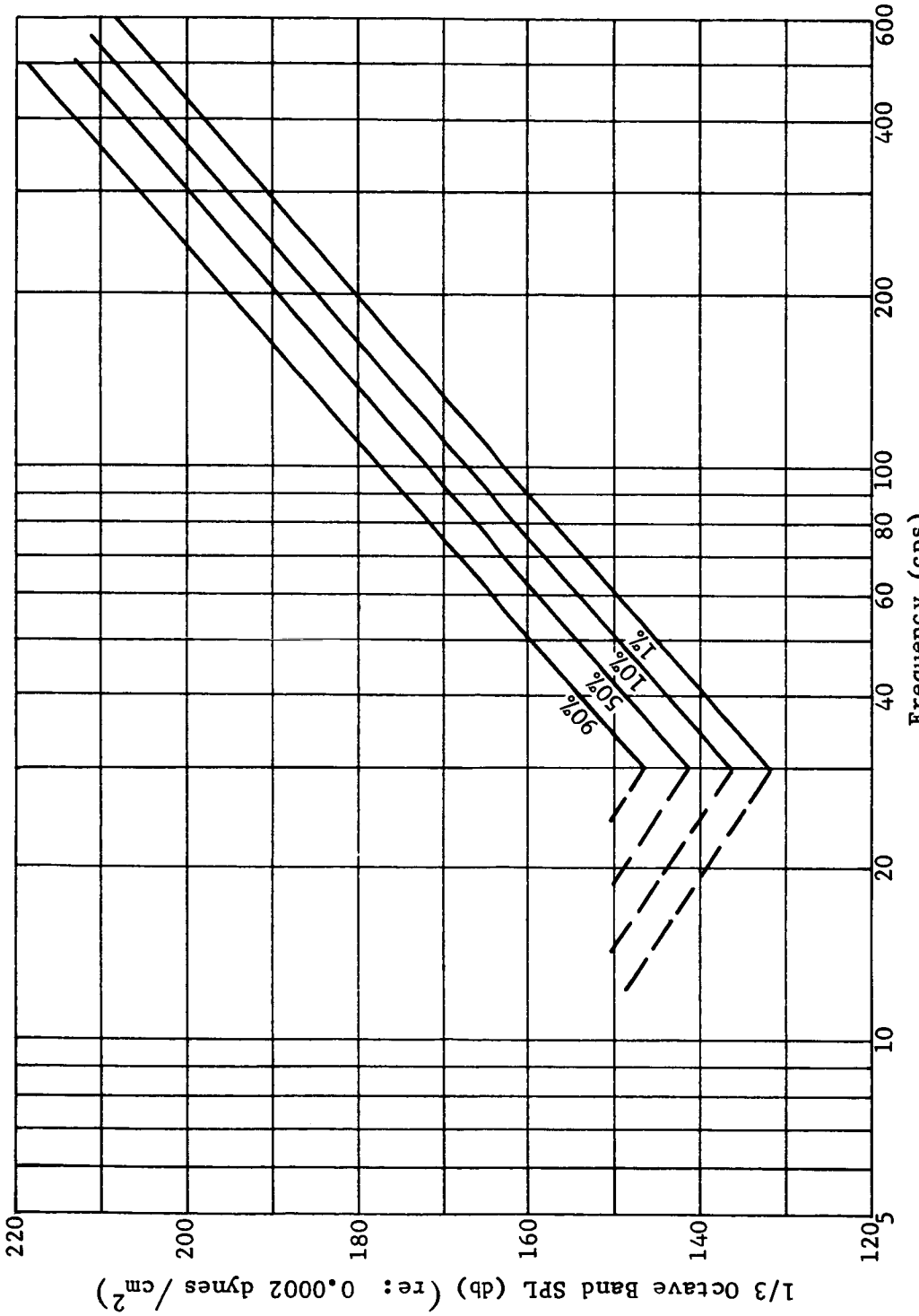

Fig. IV-2 Recommended Damage Criteria for Windows Excited by Rocket Engine Noise

Safety Factor	Probable Number of Lights* Which Will Break at Initial Occurrence of Design Load (of each 1,000 loaded)
1	500
2	22
2.5	8
3	4
4	1.3
5	0.7
8	0.2
10	0.150

*Rectangular lights adequately supported on four edges in a weathertight rabbet, assuming statistically normal strength distribution and a coefficient of variation of 25%.

a. Relationship of Safety Factors to the Statistical Probability of Failure

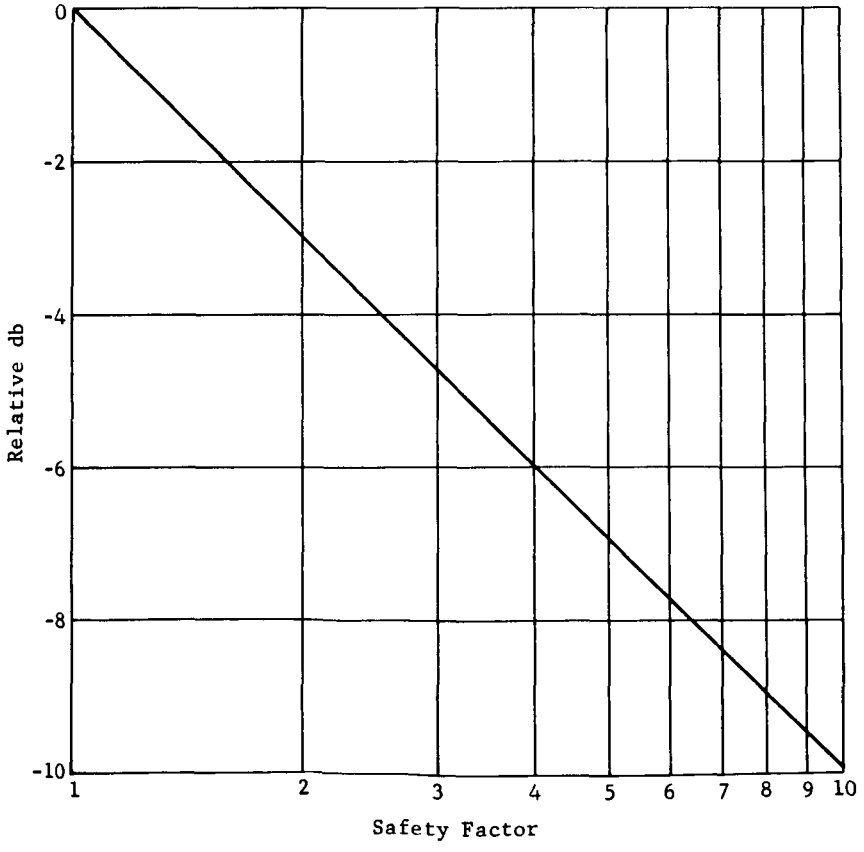

b. Relationship between Safety Factor and db

Fig. IV-3 Safety Factors

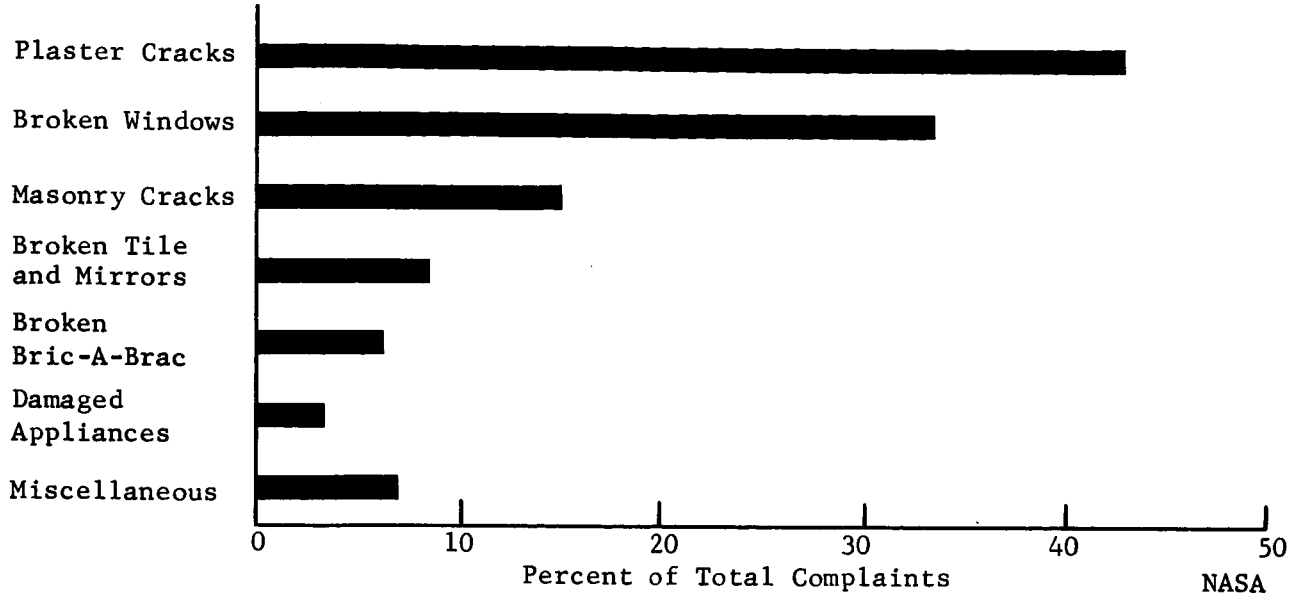

a. Breakdown of about 3,000 Complaints due to Sonic Booms Recorded in Air Force Files

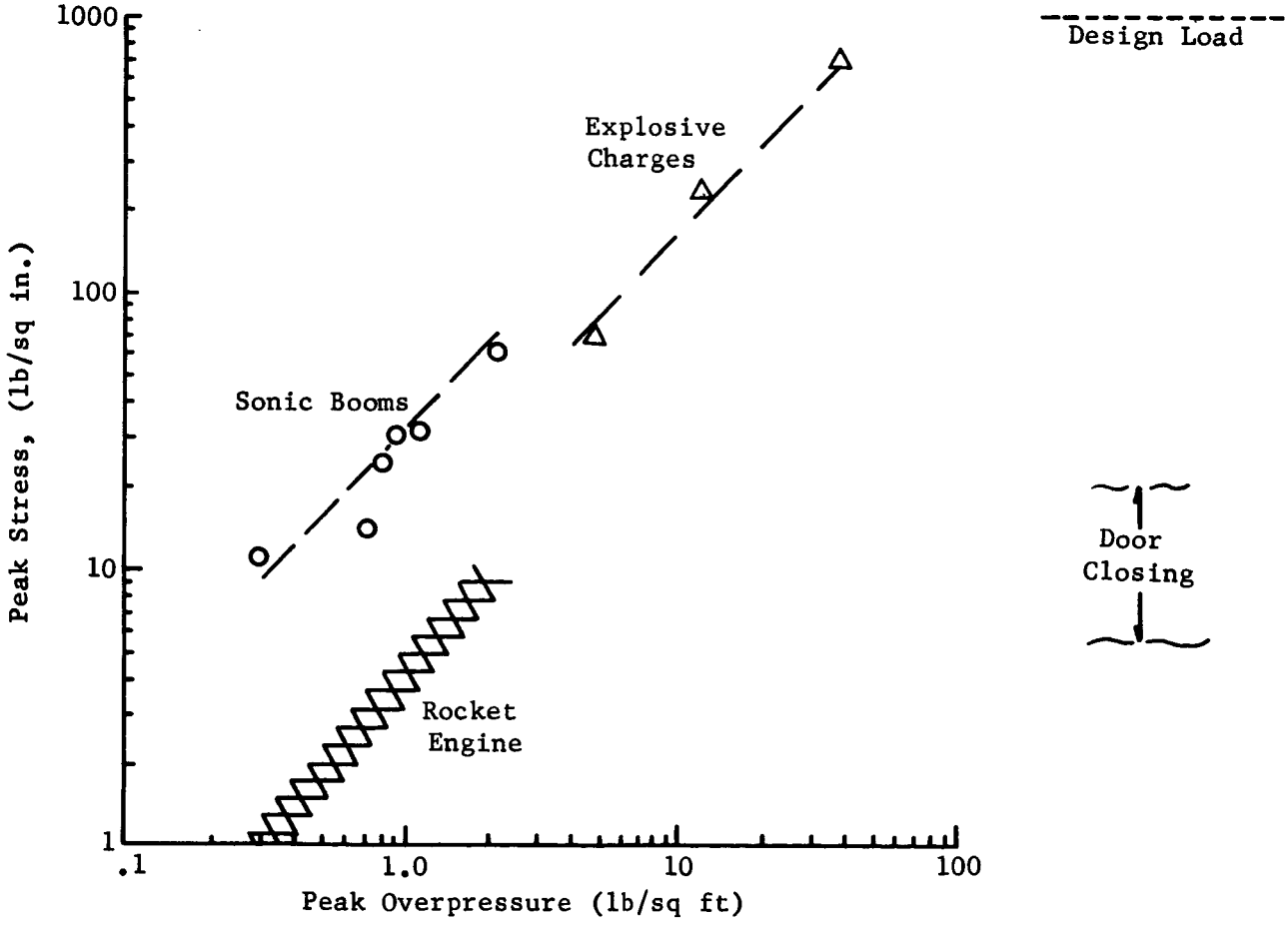

b. Peak Vertical Stud Stresses as a Function of Peak Overpressure for Various Types of Excitation

Fig. IV-4 Examples of Structural Damage from Various Types of Loading (Ref 20)

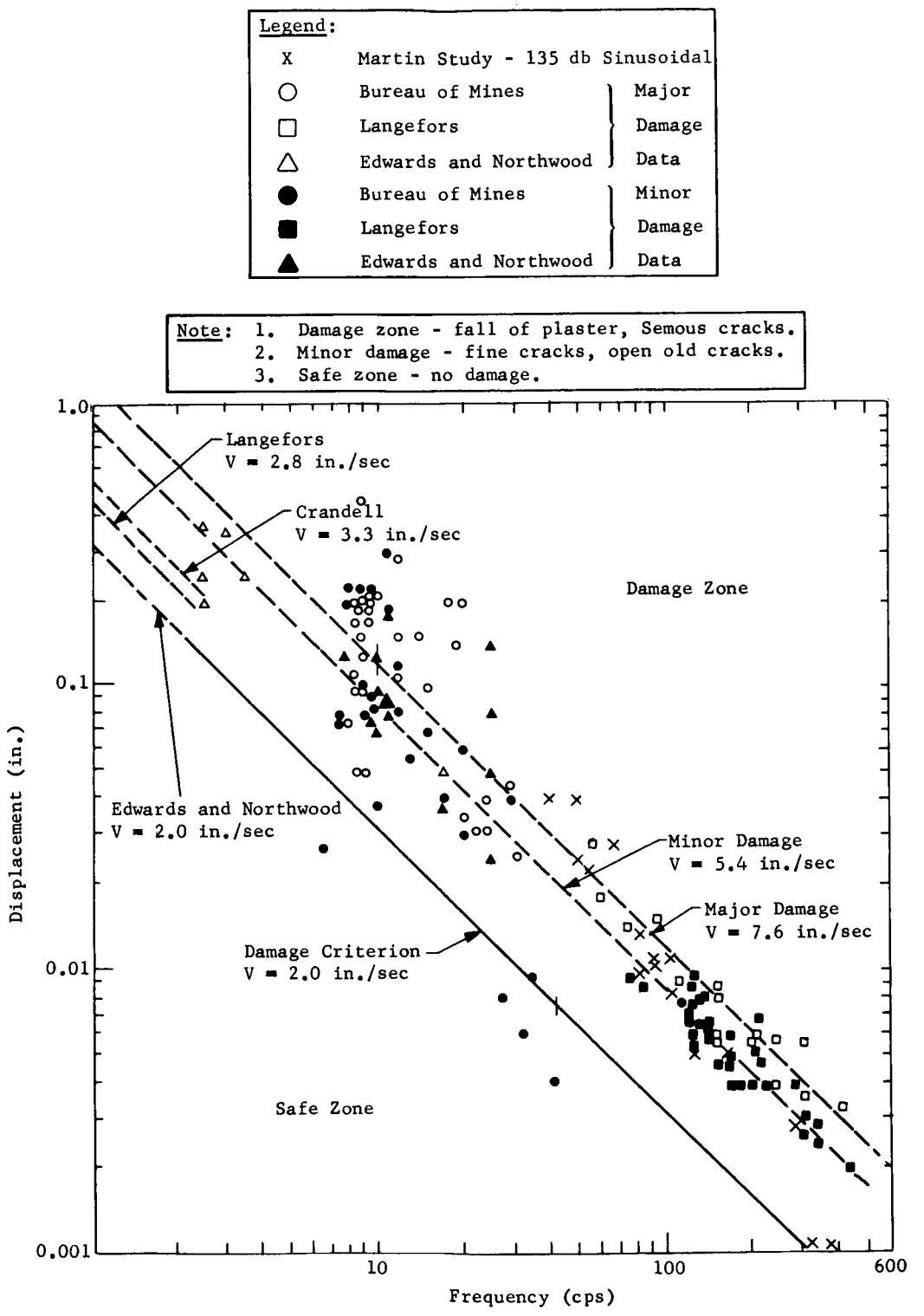

Fig. IV-5 Recommended Damage Criteria (Ref 21) with Martin Test Data, Florida Tests

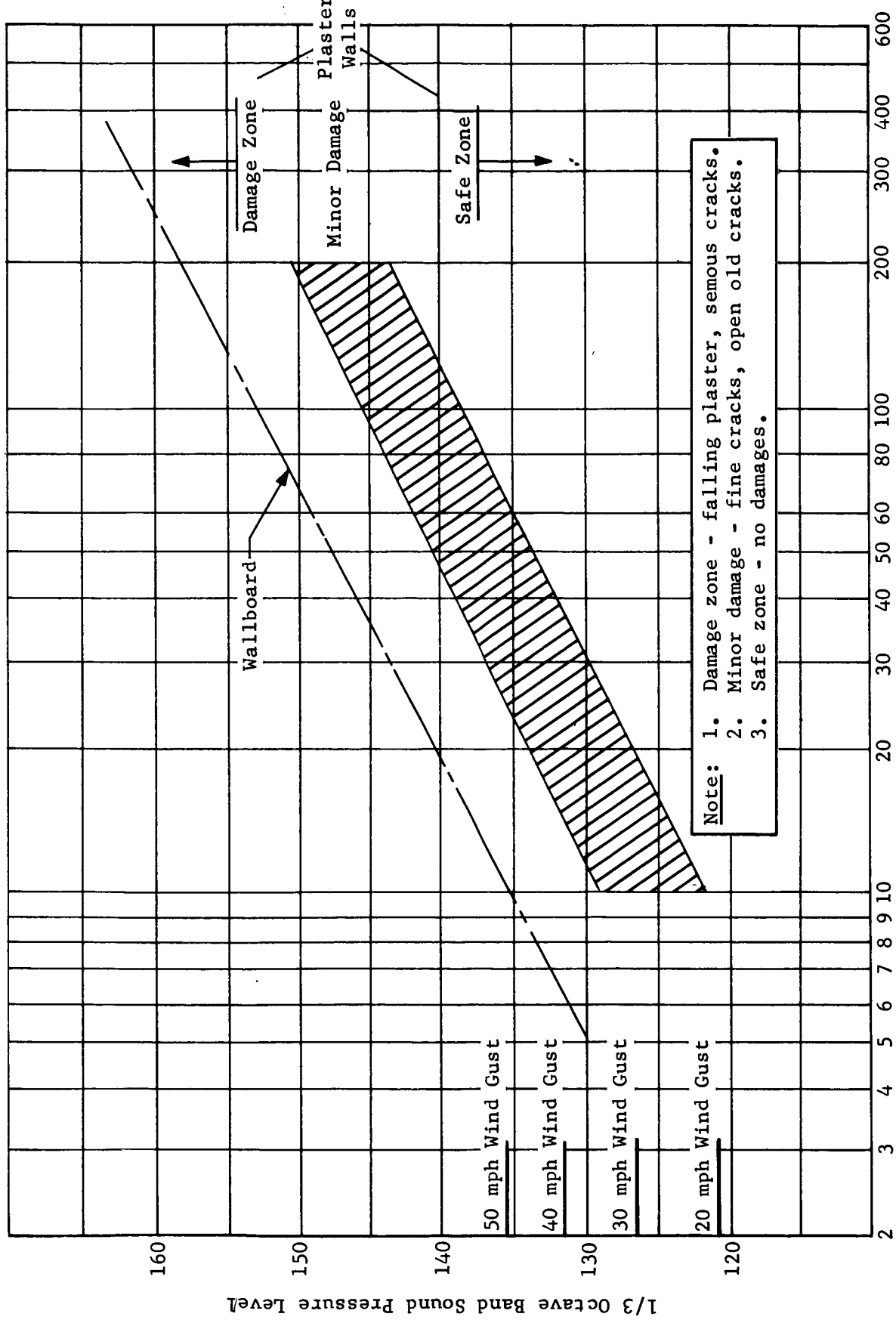

Fig. IV-6 Tentative Damage Criteria Wood Composition Walls

V. CONCLUSIONS

During this study rocket engine noise damage thresholds of community buildings near the Merritt Island Launch Area have been determined. This study has (1) estimated the noise levels produced by Post-Saturn class boosters; (2) examined the atmospheric focusing problem; (3) determined the damage criteria of windows in community dwellings; (4) surveyed the community dwellings; (5) determined the damage criteria for buildings; and (6) determined a safety factor for these criteria. The noise level predictions are summarized in Fig. V-1, where an overall sound pressure level of 118 db is shown in the Titusville area under normal weather conditions, and 133 db is shown under certain focusing conditions. The damage criteria are summarized in Fig. V-2.

In conclusion, the noise damage problem in the Titusville area does not appear to be significant for the 30×10^6-lb thrust booster, now being considered for Post-Saturn, or Saturn V. Under focusing conditions, some minor plaster damage might be expected. Under more severe focusing conditions, some major damage might occur. Note, however, that some damage claims will result from displeasure over the presence of the noise, ill-feelings against NASA, poor construction which would probably fail during the next hurricane, etc, even though the noise level is below the criteria.

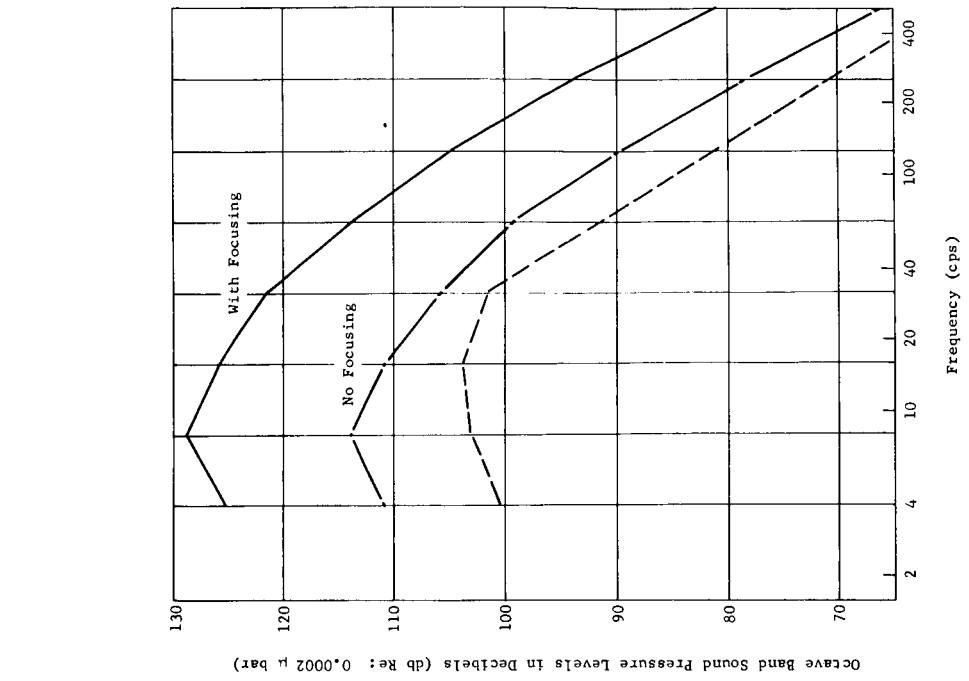

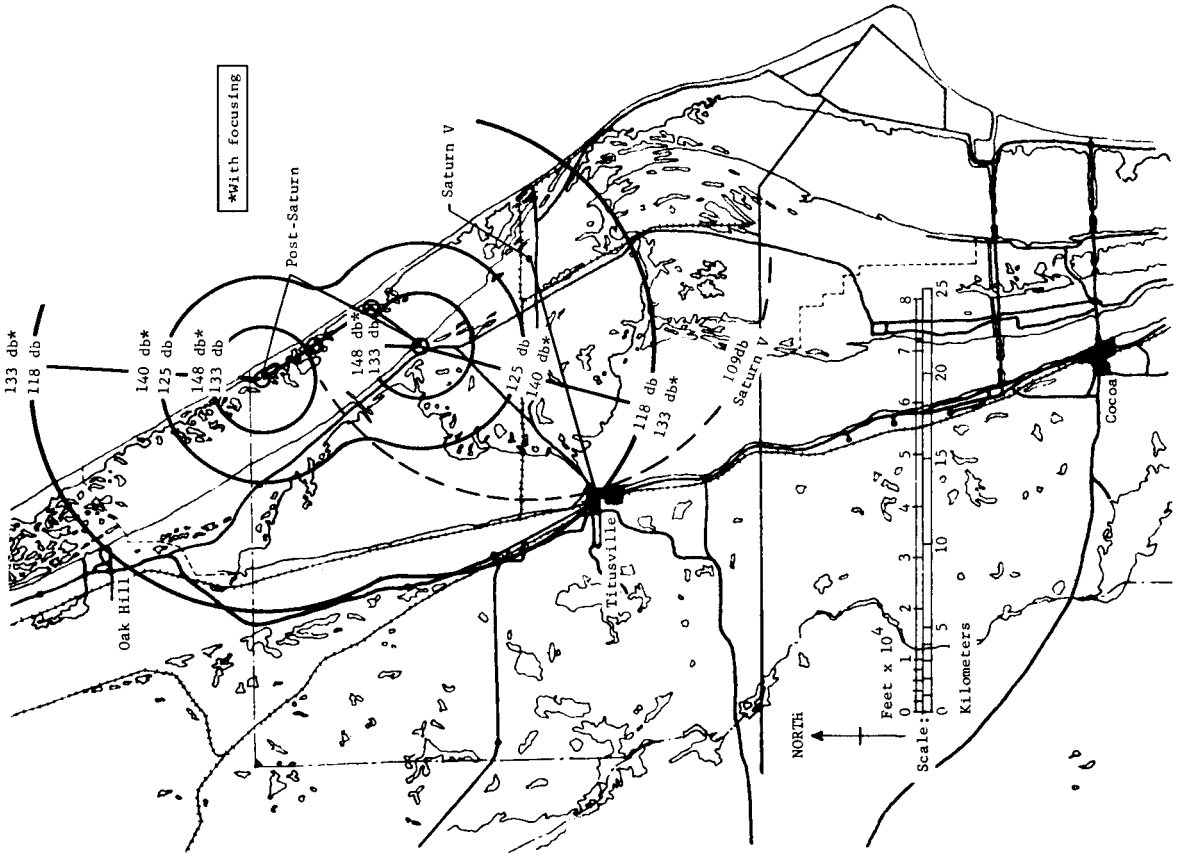

Fig. V-1 Predicted Post-Saturn and Saturn V Sound Pressure Levels

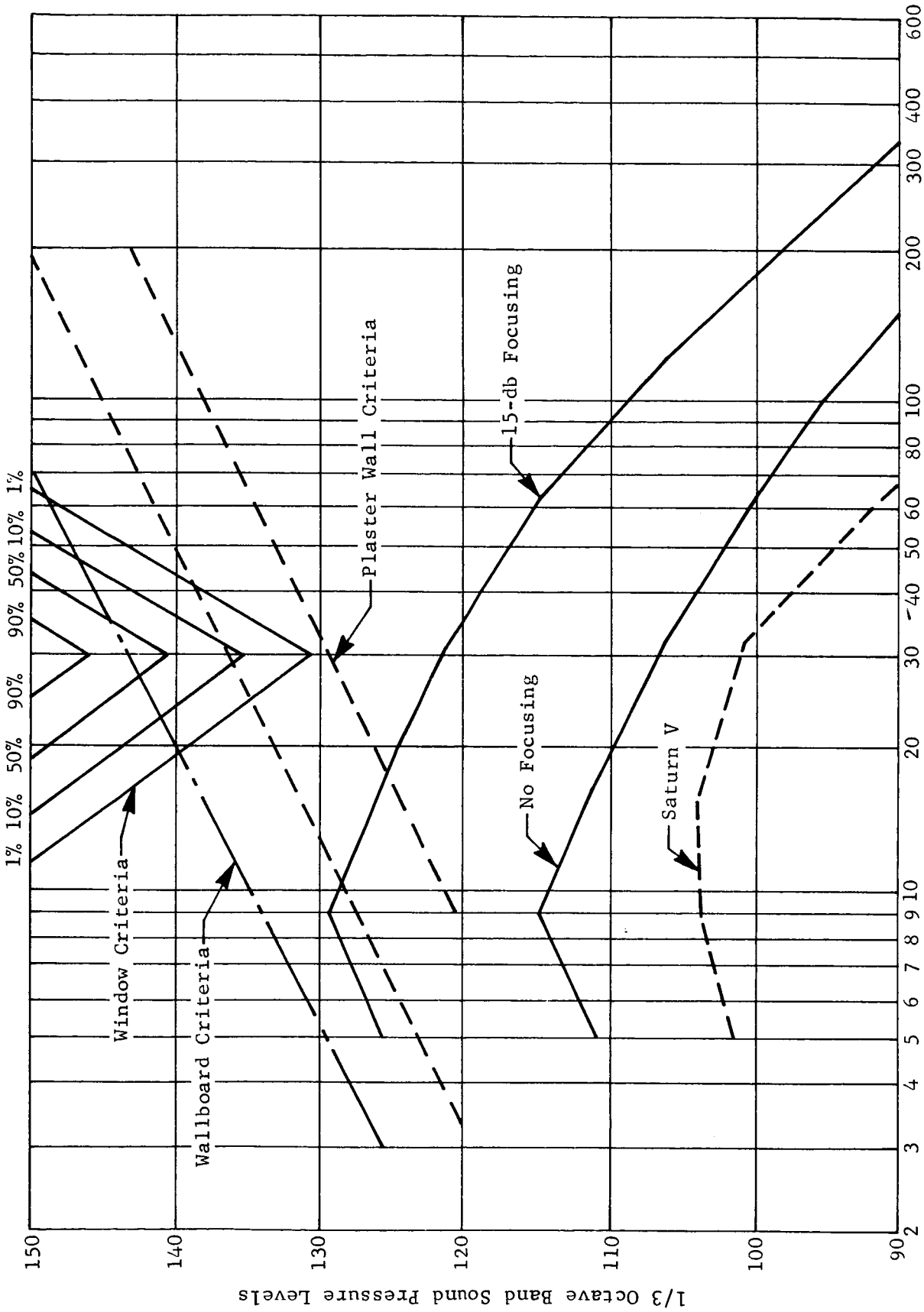

Fig. V-2 Rocket Engine Noise Damage Criterion with Predicted Post-Saturn and Saturn V Noise Levels in Titusville, Florida

VI. REFERENCES

1. V. Chohotov and A. Powell: On the Prediction of Acoustic Environment from Rockets. GM-TR-190. Ramo Wooldridge Corp., June 1957.

2. VonGierke, J. N. Cole et al.: Noise Radiation from Fourteen Types of Rockets in the 1,000 to 130,000 Pound Thrust Range. WADC TR-57-354. December 1957.

3. J. N. Cole et al.: Acoustic and Vibration Studies at Cape Canaveral Missile Test Annex, Atlantic Missile Range. ASD TR-61-608(1). December 1962.

4. R. Tedrick: Far Field Acoustic Levels Resulting from Titan Launches. MTP-Test-62-3. National Aeronautics and Space Administration, January 1962.

5. R. Tedrick and Wade Dorland: Results of Acoustical Survey of SA-2 Launch. MTP-Test-62-5. National Aeronautics and Space Administration, August 1962.

6. N. Cumings et al.: Results of Acoustical Survey of SA-3 Launch. MTP-Test-63-2. National Aeronautics and Space Administration, February 1963.

7. C. Thornton and R. Tedrick: Results of the Far-Field Acoustical Survey of SA-4 Launch. MTP-Test-63-5. National Aeronautics and Space Administration, May 1963.

8. G. A. Wilhold et al.: A Technique for Predicting Far-Field Acoustic Environments Due to a Moving Rocket Sound Source. TND-1832. National Aeronautics and Space Administration.

9. R. N. Tedrick: Acoustic Focal Zones Around Saturn Static Tests. MTP-Test-61-21. National Aeronautics and Space Administration, December 1961.

10. G. B. Warburton: "The Virbation of Rectangular Plates." Proceedings of the Institute of Mechanical Engineers, 1964.

11. R. W. McKinley: "The Response of Glass to Sonic Booms." ASTM 67th Annual Meeting, 25 June 1964.

12. H. S. Freynik, Jr: The Nonlinear Response of Windows to Random Noise. TN D-2025. National Aeronautics and Space Administration, December 1963.

13. I. Vigness: "Field Measurements and Testing." Random Vibration, Vol. II, Ch 8, J. Wiley and Son, 1963.

14. J. Miles: "On Structural Fatigue Under Random Loading." Jour. Aero. Sc. No. 11, November 1954, p 573 thru 762.

15. A. Regier, W. Mays & P. Edge, Jr.: "Noise Problems Associated with Launching Large Space Vehicles." Sound, Vol. I, No. 6, November 1962, p 7 thru 12.

16. Personal communication with Paul V. King, NASA-JFKSC.

17. G. D. Seiders and R. W. McKinley: "Effect of Surface Conditions on Glass Strength." To be published.

18. R. Bowles and B. Sugarman: "The Strength and Deflection Characteristics of Large Rectangular Glass Panels under Uniform Pressure." Glass Technology, Vol. 3, No. 5, October 1962.

19. W. J. Dixon and F. J. Massey, Jr.: Introduction to Statistical Analysis. McGraw-Hill Book Company, New York, New York, 1951.

20. W. H. Mays and P. Mp Edge, Jr.: Response of Ground Buildings to Sonic Booms. ASTM Symposium, Chicago, Illinois, June 25, 1954.

21. W. I. Duvall and D. E. Fogelson,: Review of Criteria for Estimating Damage to Residences, from Blasting Vibrations. RI 5968. Bureau of Mines, 1962.

DISTRIBUTION

Copies	To
1 thru 25 plus 1 reproducible	J. F. Kennedy Space Center National Aeronautics and Space Administration Cocoa Beach, Florida 32931 Attn: LO-GH6
Remaining Copies	Martin Company Denver Division Denver, Colorado 80201 Attn: Libraries Section